ANTIMICROBIAL ACTIVITY AND DEGRADATION EFFECT OF GREEN IRON NANOPARTICLES SYNTHESIZED USING *Galinsoga parviflora* (Cav.), *Conyza bonariensis* (L.) AND *Bidens pilosa* (L.) LEAVES

SAMMY INDIRE WANAKAI

MASTER OF SCIENCE

(Chemistry)

JOMO KENYATTA UNIVERSITY

OF

AGRICULTURE AND TECHNOLOGY

2023

Antimicrobial Activity and Degradation Effect of Green Iron Nanoparticles Synthesized Using *Galinsoga parviflora* (Cav.), *Conyza bonariensis* (L.) and *Bidens pilosa* (L.) Leaves

Sammy Indire Wanakai

A Thesis Submitted in Partial Fulfilment of the Requirements for the Degree of Master of Science in Chemistry of the Jomo Kenyatta University of Agriculture and Technology

2023

DECLARATION

This thesis is my original work and has not been presented for a degree in any other University

Signature: …… Date……..

Sammy Indire Wanakai

This thesis has been submitted for examination with our approval as University Supervisors

Signature: …… Date……..

Prof. Patrick Gachoki Kareru, PhD

JKUAT, Kenya

Signature: …… Date……..

Dr. David Sujee Makhanu, PhD

KARATINA UNIVERSITY, Kenya

DEDICATION

To my grandfathers Mr. Jafred Wasike Mutembete, and Julius Barasa Mutembete, and grandmother Mrs. Sarah Nasambu Wasike, my uncles Stephen Wasike and John Wasike, my cousins Wycliffee, Evans, and Eliud, Brother Wilson Wanakai and sisters, Lucy Wanakai, Dorice Wanakai, Pauline Wanakai and my father Michael Wanakai Wasike and mother, Ebby Alivitsa Anzigale Wanakai, my wife Nancy Nabukwangwa and our dear son Modiglian Myles Michael Indire.

ACKNOWLEDGEMENT

I am very grateful and thankful to my Lord God Almighty for granting me an opportunity to study. I also sincerely appreciate my Supervisors Prof. Patrick Kareru and Dr. David Sujee for their efforts in guidance, mentorship and encouragements throught my study and research work. You always took me as your son during these entire moment and encouraged me to keep the pace when I felt discouraged. May God bless and grand you the desires of your hearts. My gratitude also goes to the chairperson chemistry department–JKUAT Dr. Jackson Kiptoo for giving me a chance to exercise my skills in supporting the department. You always trusted me and gave me tasks that sharpened me in the field of academia. The entire chemistry department–JKUAT, I sincerely acknowledge the support offered to me in studying and using the University facilities laboratories during my research period. The GOK Chemistry Laboratory family; Dr. Edwin Madivoli, Dr. Rechab Sylvester, Ernest Gachui, and Augustine Nyabola, Brian Otemba and Dennis. You guys are amazing people. Kudos. May Godbless you. Last but not least, my sincere gratitude goes to my family. My grandfather Japheth, My father and mother Mr. Michael Wanakai Wasike and Ebby Alivitsa Anzigale Wanakai who with love and patience provided fees, upkeep and stood with me during the tough moments throught the study. God keep you. To my sisters, Lucy, Dorice Pauline and Bro Wilson thanks all for your love, prayers, financial and moral support. To my dear wife Nancy our son Modiglian Myles, you always suffered my absence at home and my late coming just to see this course accomplished. May God bless you.

TABLE OF CONTENTS

LIST OF TABLES

LIST OF FIGURES

LIST OF APPENDICES

LIST OF PLATES

ABBREVIATIONS AND ACRONYMS

BpNPs	*B. pilosa* nanoparticles
CbNPs	*C. bonariensis* nanoparticles
DMSO	Dimethyl sulfoxide
FTIR	Fourier Transform Infrared
GAE	Gallic Acid Equivalent
GpNPs	*G. parviflora* nanoparticles
MB	Methylene Blue
NP (s)	Nanoparticle (s)
Rif.	Rifampicin
RE	Rutin Equivalent
SEM	Scanning Electron Microscope
TB	Tuberculosis
UV-Vis	Ultra violet Visible spectroscopy
XRD	X-Ray diffraction
XRF	X-ray fluorescence

ABSTRACT

Infectious bacterial diseases remain a major global problem due to antibiotic resistance caused by the misuse of antibiotic drugs. Green nanoparticles have rare and unique applicability in various fields: medicine, nutrition, agriculture and environmental wastewater treatment. This study aimed to synthesize iron nanoparticles by reacting a 0.1 M Iron Chloride ($FeCl_3$) solution with aqueous leaf extracts from *Galinsoga parviflora* (*G. parviflora*), *Conyza bonariensis* (*C. bonariensis*) and *Bidens pilosa* (*B. pilosa*), and determining their antimicrobial effects against *Staphylococcus aureus* (*S. aureus*), *Bacillus subtilis* (*B. subtilis*), *Escherichia coli* (*E. coli*), *Pseudomonas arureginosa* (*P. aureginosa*) and *Candida albicans* (*C. albicans*). The degradation effects of Rifampicin and Methylene blue (MB) dye were also determined. Secondary metabolites from the plants' leaf extracts were screened for the presence of flavonoids, polyphenols, and phytosterols. *C. bonariensis* had the highest concentration of flavonoids (45.50±0.59 mg (Rutin Equivalent/Dry weight) while *B. pilosa* had the highest concentration of reducing polyphenol compounds at 126.27±0.01 mg (Gallic Acid Equivalent/Dry weight). Characterization of the green nanoparticles was done using several techniques: Ultraviolet–Visible (UV-Vis) spectroscopy, Fourier Transform Infrared (FTIR) spectroscopy, X-ray Fluorescence (XRF), X-ray Diffraction (XRD), and Scanning Electron Microscope (SEM). The sizes of *B. pilosa* nanoparticles (BpNPs), *G. parviflora* nanoparticles (GpNPs), and *C. bonariensis* nanoparticles (CbNPs) ranged from 60–90 nm and the mean sizes were 84, 51, and 78 nm, respectively. The formation of green iron nanoparticles was further confirmed by the absorption shifts in the UV–Vis and FTIR spectra. The green iron nanoparticles exhibited antimicrobial activity effects against *S. aureus, B. subtilis, E. coli, P. aureginosa* and *C. albicans* compared to the ampicillin standard. The percentage degradation efficiency of Methylene blue and Rifampicin increased with an increase in temperature, dosage and pH change with efficiencies of over 90%. Sunlight–assisted degradation of Rifampicin and Methylene blue by nanoparticles with H_2O_2 was over 93% in less than 20 minutes. The results from this study demonstrated that green iron nanoparticles had antimicrobial and degradation properties that can be exploited in the field of medicine and environmental degradation of dyes, such as Methylene blue.

CHAPTER ONE

INTRODUCTION

1.1 Background to the Study

Wound infections and other infections are an emerging global medical problem. Open wounds present a potential risk for serious bacterial infections that lead to chronic wounds, perpetual disabilities and death (WHO, 2022a). Wound infections happen due to bacterial entry through the skin, which stops healing and produces signs and symptoms (WHO, 2010). The most important therapeutic challenge in disease infection is multidrug–resistant bacteria with the most commonly reported *S. aureus* such as methicillin-resistant *S. aureus* (MRSA), which affect the early phases of wound healing, while *E. coli* and *P. aeruginosa* infect deeper skin layers leading to chronic wounds (Mihai *et al*., 2019). This causes huge economic burdens, morbidity as well as mortality rates. In addition, other bacterial, fungal, viral and parasitic infections as well as inflammation, cold, digestive problems, pain and many other health disorders and diseases have been reported in humans and these polymicrobial infections demand bacterial, viral, fungal, and parasitic investigations (Aftab *et al*., 2015; Wink, 2015). This has increased the utilization of pharmaceutical products across the globe which can diagnose, treat, as well as prevent the occurrence of various diseases thus improving the quality of millions of lives (Kansal *et al*., 2014). Pharmaceutical products can be natural or synthetic bioactive substances that are found in prescription drugs, over–the–counter therapeutics as well as veterinary drugs (Kansal *et al.*, 2014; Malakootian *et al*., 2020; Patel *et al*., 2019; Yang *et al.*, 2017).

1.1.1 Pharmaceuticals in Wastewater

Pharmaceutical residues and their metabolites have been detected in aquatic ecosystems which are introduced into water bodies through excretion by humans and animals after incomplete metabolism, improper households and hospital discharge of expired medicines, improper sewage treatment, and manufacturers' disposals (Leal *et al*., 2010; Mirzaei *et al*., 2017). The presence of these pharmaceutical drug compounds

in surface and underground water portrays an environmental challenge and have posed a major public health concern to the quality of life of both humans and animals and is a leading cause of drug resistance (Anjum *et al*., 2016; Kairigo *et al.*, 2020; Kansal *et al*., 2014). High drug prevalence in wastewater bodies has been linked to the increased population in urban areas, poor housing, improper waste disposal mechanisms and poor drainage facilities leading to environmental pollution through the release of human and animal excretion into the environment and more so, water treatment methods are not designed to adequately handle pharmaceuticals (Cecilia *et al*., 2020; Teixeira *et al*., 2016). In addition, most pharmaceuticals are not fully metabolized in the body and hence are excreted from the body together with human and animal waste. The pharmaceuticals are in low concentrations of nanograms to micrograms per litre which leads to poor detection limits, analysis as well as degradation process which pose a great threat to the environment and more so humans through developing antibiotic resistance (Das *et al*., 2018; Leal *et al*., 2010). Therefore, when they infiltrate into the water or soil ecosystem through various routes, they cause short and long-term adverse effects (Bagheri *et al*., 2016; Das *et al*., 2018; Smýkalová *et al*., 2019; Yang *et al*., 2017). When they enter the ecosystem, pharmaceuticals can be treated as ecological factors influencing the evolution of the environmental structure. Their chemical nature cause structural changes and mutations in microbial organisms. The mechanism involves enzymatic degradation of antimicrobial drugs and alteration of microbial proteins that are antimicrobial targets that disrupt of the endocrine processes leading to antibiotic resistance (Chang and Jianzhong, 2010). Hence, the use of drinking water containing pharmaceutical drugs and continuous consumption of the drugs, makes the disease–causing microbes develop mutation and become resistant to them making drugs less effective disrupting the endocrine operations, and can be toxic to the aquatic life as well (Demirezen *et al*., 2019; Rivera-Utrilla *et al*., 2013).

1.1.2 Antibiotic Drug Resistance

Rifampicin and isoniazid have been used as anti–tuberculous (TB) drugs globally. However, *Mycobacterium tuberculosis* the TB–causing strain has developed multidrug resistant leading to poor diagnosis, poor treatment strategies and high mortality rates

(Handa *et al*., 2018; Kurbatova *et al*., 2012; Masenga *et al*., 2017; Mvelase *et al.*, 2019; Sharma *et al*., 2014). This arising TB resistance has globally arisen due to poor management of drug sensitivity and drug resistance to TB. It is reported that Rifampicin–resistant and multidrug–resistant TB are treatable but very expensive since it requires a long duration of treatment and involves potentially toxic drugs (Handa *et al*., 2018). Besides, pathogens present in water becoming resistant to the drugs and with any kind of infection to the body, the antibiotics are not able to destroy the microbes (Halm-Lemeille and Gomez, 2016; Malakootian *et al*., 2020; Mullerpattan *et al*., 2017). It has been reported that plant extracts have antimicrobial activity against most pathogens due to the presence of various compounds with diverse structures in the same extract where the mode of action depends on the most active natural products (Hameed *et al*., 2019). The plant extracts also can potentially be used as reducing and capping agents for the preparation of metal nanoparticles with antimicrobial, anti–infection, or catalytic properties providing a facile biosynthetic method and good utilization of plant parts and agricultural waste (Igwe and Nwamezie, 2018; Katata-Seru *et al*., 2018; Sudhasree *et al*., 2014; Veeramanikandan *et al*., 2017; Yuan *et al*., 2017).

1.2 Problem Statement

Infectious diseases caused by bacteria have remained a major global health problem for many years, due to environmental pollution and pathogenic bacterial, fungal, viral, and parasitic resistance to currently available antibiotics in the market during the last decade (Guguloth, 2015). Pharmaceuticals present in drinking water contribute to reported cases of health disorders. Pharmaceuticals are disposed carelessly to the environment thus distorting the normal conditions leading to diseases and resistance to antibiotics through mutagenic reactions. Currently, multiresistant *S. aureus* and *Mycobacterium tuberculosis* are among the common cause of infections with high rates of morbidity and mortality worldwide (Silva *et al*., 2014; WHO, 2022b). It challenges the control of infectious diseases, jeopardizes progress on health outcomes by increasing morbidity and mortality and imposes huge costs on societies (Leung, *et al.*, 2011).

Resistance can be intrinsic to a bacterium, or acquired through mutations or by the incorporation of new genes. The increasing prevalence of infections caused by *S. aureus* strains during the last two decades throughout the world has been associated with the widespread occurrence of specific strains of *S. aureus* internationally (Silva *et al*., 2014). Rifampicin the anti-TB drug has been reported as the most powerful drug used to treat TB infection. However, in 2022, the World Health Organization reported over 420,000 new cases of Resistance-TB (WHO, 2022b). This health challenge has greatly increased the utilization of pharmaceuticals and their products across the globe for diagnosis, treatment, and prevention of the occurrence of various diseases.

1.3 Justification of the Study

Therapeutic agents with novel structures and modes of action should be developed to combat the threat originating from resistant strains. Considering the emergence of pathogenic bacteria multidrug–resistant strains, the discovery of new antimicrobial compounds is highly important. Plants have a great and exceptional ability to produce cytotoxic agents. Various studies have documented the importance of plant extracts. Traditionally, plants have always provided a source of hope for various novel drug compounds, for human health and well-being, such as plant herbal mixtures. Phytochemicals not only protect the plant but have great physiological properties in humans and animals which include antibacterial, antiviral, and antifungal.

Traditional medicine was accepted as an alternative form of health care, due to the popular use of plant extracts as remedies for many infections, the emergence of microbial resistance to the synthetic antibiotics, investigations on medicinal plants, and the search for substances with antimicrobial activity in plants is frequent (Parimelazhagan, 2016). Further research on phytochemical constituents and screening is needed to develop pharmaceuticals from plants. While some plant extracts have been used as antibiotics, more research is needed on their antimicrobial and antifungal properties. Inorganic compounds play critical roles and it has been established that many organic compounds used in medicine are activated or bio-transformed by metal ion metabolism. Transition metals exhibit different oxidation states and can interact with several negatively charged molecules. The mechanisms of

action and the roles of these metal compounds in cellular regulation and signaling in health and diseases are of principal interest. There are few reports on the antifungal and antibacterial activity of transitional metal complexes in the literature. These complexes have been shown to possess antimicrobial activity against pathogenic fungi and bacteria. Secondary metabolites, including tannins, terpenoids, alkaloids, and flavonoids, possess antimicrobial properties in plants. Their structures have diverse functional groups, forming coordinate bonds with metal ions, resulting in novel compounds. The threat of antimicrobial resistance and the insubordinate nature of infections call for the development of alternative strategies to treat bacterial diseases. Nanoparticles have been considered one of the emerging and most promising platforms in this respect. The inclusion of transition metals increases the planarity of the compounds present and thus enhances the bioactive properties of the extracts.

Disease infection is linked to environmental pollution due to increased population in the urban areas, poor housing, improper waste disposal mechanisms from industries, poor drainage facilities and poorly designed water treatment methods threatening health standards. This influences the utilization of pharmaceuticals and their products for diagnosis, and treatment of various diseases to improve health status (Kansal *et al.*, 2014). These may find their way back to drinking water when disposed from homes and hospitals or after incomplete metabolism thus leading to cases of drug resistance as the pathogens undergo mutation while in the body (Anjum *et al.*, 2016; Kairigo *et al.*, 2020; Kansal *et al.*, 2014). Hence, there is a need to detect and remove pollutants in water before use. Unfortunately, the methods employed in wastewater treatment require high energy, generate toxic sludge and there is incomplete pollutant removal. Hence the need to search for more efficient methods where nanotechnology has found its way as remediate (Anjum *et al*., 2016; Ferroudja *et al*., 2013; Gupta *et al*., 2011; Shahryari-ghoshekandi & Ramin, 2014; Zare *et al*., 2013).

1.4 Hypothesis

The synthesized iron nanoparticles have neither antimicrobial nor degradation effect against selected microbes, Methylene blue and Rifampicin antibiotics.

1.5 Objectives

1.5.1 General Objective

To evaluate the antimicrobial and degradation effect of green iron nanoparticles synthesized using *G. parviflora, C. bonariensis* and *B. pilosa* leaf extracts.

1.5.2 Specific Objectives

1. To extract plant phytochemicals from *G. parviflora, C. bonariensis* and *B. pilosa* leaves.
2. To synthesize green iron nanoparticles using the plant phytochemicals and characterize them using UV-Vis, FTIR, XRF, XRD, and SEM.
3. To determine the antimicrobial effects of the synthesized iron nanoparticles against *S. aureus, B. subtilis, E. coli, P. aureginosa* and *C. albicans*.
4. To determine the degradation effects of the synthesized iron nanoparticles against Rifampicin and Methylene blue.

CHAPTER TWO

LITERATURE REVIEW

2.1 Therapeutic Agents from Plants

The United Nations World Health Organization estimates that about eighty percent of the world's population utilizes herbal medicine for primary health care (Kigen *et al*., 2013). Plants and their products have been relied on by humans for fulfilling their day–to–day needs since the ancient past. The use of plants in the treatment of various body ailments was and is still very common in many human civilizations such as the Chinese and Indian medical systems still in practice. Human beings have relied on natural drugs, mostly from fungi, plants and animals (Singh, 2017). The knowledge of plants as medical and health references is still the main therapeutic source for a large number of global communities and ethnic groups (Catarinense, *et al*., 2013).

The treatment of body infections and health disorders with herbal medicine usually involves several active natural compounds mostly of low molecular weight and of great structural diversity (Wink, 2015), which include primary metabolites and secondary metabolites that have defensive mechanisms that offer protection from various diseases. In addition, these drugs do not have any cases of drug resistance that have been widely reported therefore, long term use of these natural remedies will prevent environmental pollution. Medicinal plants have phytochemical constituents that are present in the roots, stems, stalks and leaves, and are useful for healing as well as curing human diseases. Primary constituents include proteins and common sugars while secondary compounds include terpenoids, alkaloids and phenolic compounds (Maobe *et al*., 2013; Zamin *et al*., 2013). Terpenoids exhibit various important pharmacological activities such as anti-inflammatory, anticancer, anti-malarial, anti-viral and anti-bacterial activities (Masyita *et al*., 2022). The bioactivities of these compounds are explained by their structural nature which may contain different types of substituents at different positions, leading to a large variety of pharmacological properties (Donfack *et al*., 2014). The presence of substituents such as hydroxyl and carbonyl groups on the ring structure opens up the possibility of forming coordinated

bonds with metal ions through the reduction and stabilization of the metal ion by donating electrons thus forming green metallic nanoparticles *(Ferum et al., 2017; Iravani, 2016; Kaushik and Joshi, 2015; Makarov et al., 2014; Yadi et al., 2018).*

2.1.1 *Galinsoga parviflora* (Gallant Soldier)

G. parviflora **(Plate 2.1)** is a small annual herb in the family Asteraceae, that grows all over in fertile soils up to 80 cm, with discrete yellow and white flowers.

Plate 2.1: *G. parviflora* Plant with Leaves, Flowers and Seeds

G. parviflora is used in many communities specifically by Luhya Bukusu sub-tribe as vegetables, food to domestic animals such as rabbit, goat, sheep and cow. *G. parviflora* leaves and flowers have been analyzed and its leaves have been found to show significant presence of flavonoids, tannins, quinines and cellulose while flowers contain significant amount of flavonoids, carbohydrates, tannins, quinins, glycosides, celluloses and steroids. Various compounds such as sitosterols, stimasterols, 3,4-dimethoxycinnamic acid, phytol, fumaric acid, and triacontanol have been extracted from *G. parviflora* leaves using ethanol **(Figure 2.1)** (Ranjitha and Suganthi, 2017).

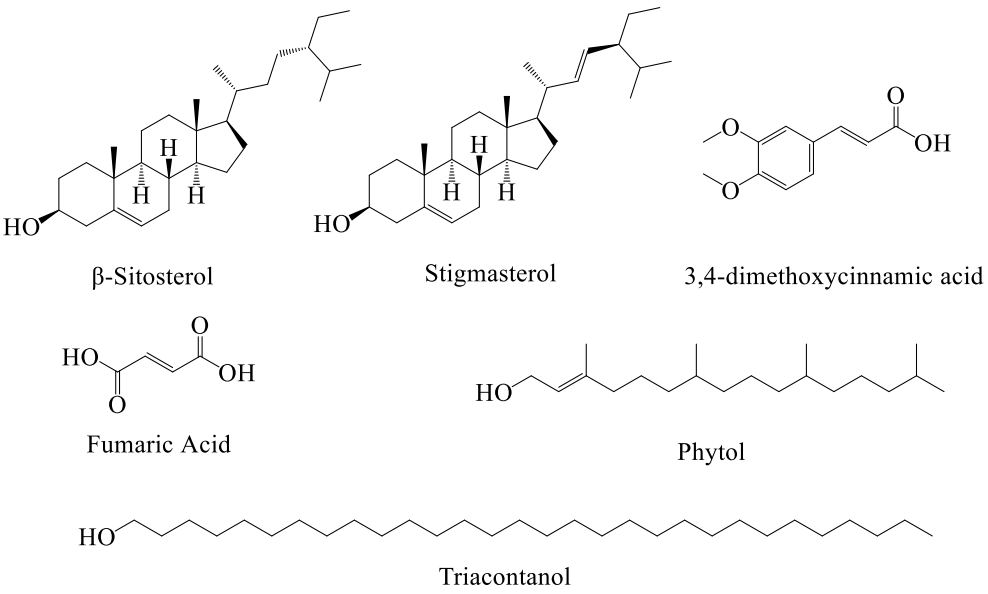

Figure 2.1: Some structures of ethanol extract of *G. parviflora*

Flavonoids and tannins are responsible for wound healing properties and have many therapeutic uses due to their anti-fungal, anti-inflammatory, and antioxidant properties while tannins are free radical scavengers (de Sousa Araújo *et al*., 2008; Ranjitha and Suganthi, 2017). Aqueous ethanoic extracts of *G. parviflora* have been found to contain *β*-sitosterol, triacontanol, stigmasterol, and others **(Figure 2.1)** which have been found to exhibit substantial antimicrobial activity against *B. subtilis*, *E. coli*, *P. aeruginosa*, *A. niger*, and *C. albicans* (Mostafa *et al*.,2013).

2.1.2 *Bidens pilosa* (Black Jack)

B. pilosa **(Plate 2.2)** is an annual, erect, ruderal, invasive herb widely distributed in many tropical and subtropical countries that grows easily up to 1.5 m in height and its leaves offer food as vegetables and medicine for humans and animals (Bartolome *et al*., 2013; Catarinense *et al*., 2013). The Bukusu Luhya subtribe call it Kamakoye and use it as vegetables and squeeze the juice for wound healing purpose.

Plate 2.2: *B. pilosa* with its flowers, seeds and leaves

B. pilosa has a long ethnomedicinal history of being used to treat malaria, skin infections, stomach and liver problems. It has been utilized as a source of natural antimicrobials, anti-inflammatory, hepatoprotective, and cytotoxic agents against various cancer cells (Garima *et al*., 2017). *B. pilosa* phytochemical screening revealed the presence of phenylpropanoids, polyacetylenes, polyphenols, triterpenes, saponins, and alkaloids (Dang *et al*., 2016). The plant's pharmaceutical properties appear to be linked to bioactive phytochemical compounds which inhibit the growth of pathogenic microorganisms and have anti-inflammatory effects. Phytochemicals isolated from *B. pilosa* leaves have been found to contain usable amounts of phenolic compounds **(Figure 2.2)** which have free radical scavenging potential (Dang *et al*., 2016; Garima *et al*., 2017; Idris *et al*., 2023).

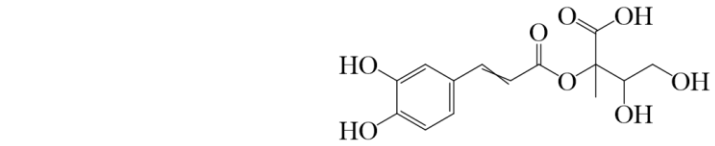

2-[[3-(3,4-dihydroxy-phenyl)-1-oxo-2-propenyl]oxy]-3,4-dihydroxy-2-methyl-butanoic acid

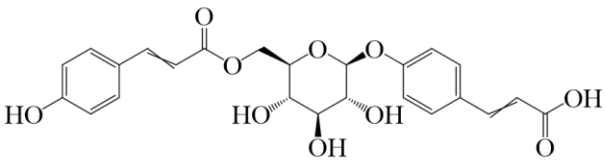

3-[4-[[6-O-[3-(4-hydroxyphenyl)-1-oxo-2-propen-1-yl]-β-D-glucopyranosyl]-oxy]-phenyl]-2-propenoic acid

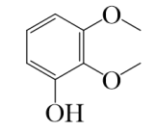

Dimethoxyphenol

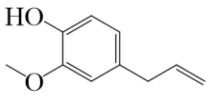

2-methoxy-4(2-propen-1-yl)-phenol

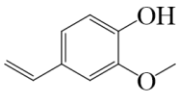

4-ethenyl-2-methoxy-phenol

Figure 2.2: Structures of some phenolic compounds of *B. pilosa*

Some porphyrin rings **(Figure 2.3)** containing carboxylic acids and esters parts have also been isolated from *B. pilosa* leaves and have been reported to have pharmacological activity (Bartolome *et al*., 2013).

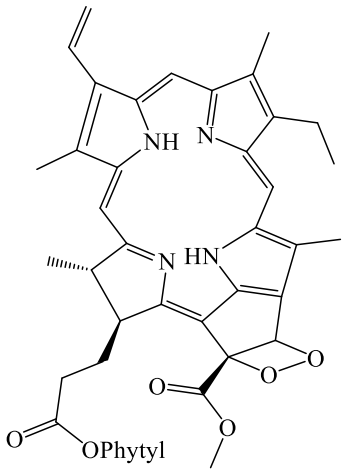

Bidenphytin A

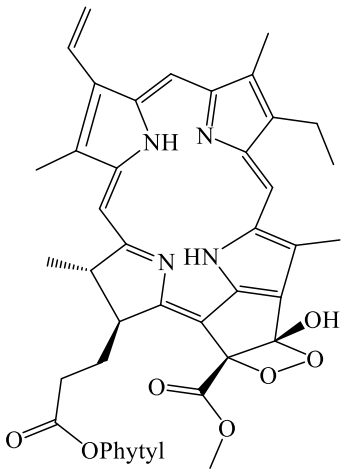

Bidenphytin B

Figure 2.3: Porphyrins isolated from the leaves of *B. pilosa*

Flavonoids **(Figure 2.4)** have also been extracted from *B. pilosa* leaves. These bioactive compounds such as tannins, steroids, saponins, contain important functional groups such the OH and keto groups which influence their pharmacological properties.

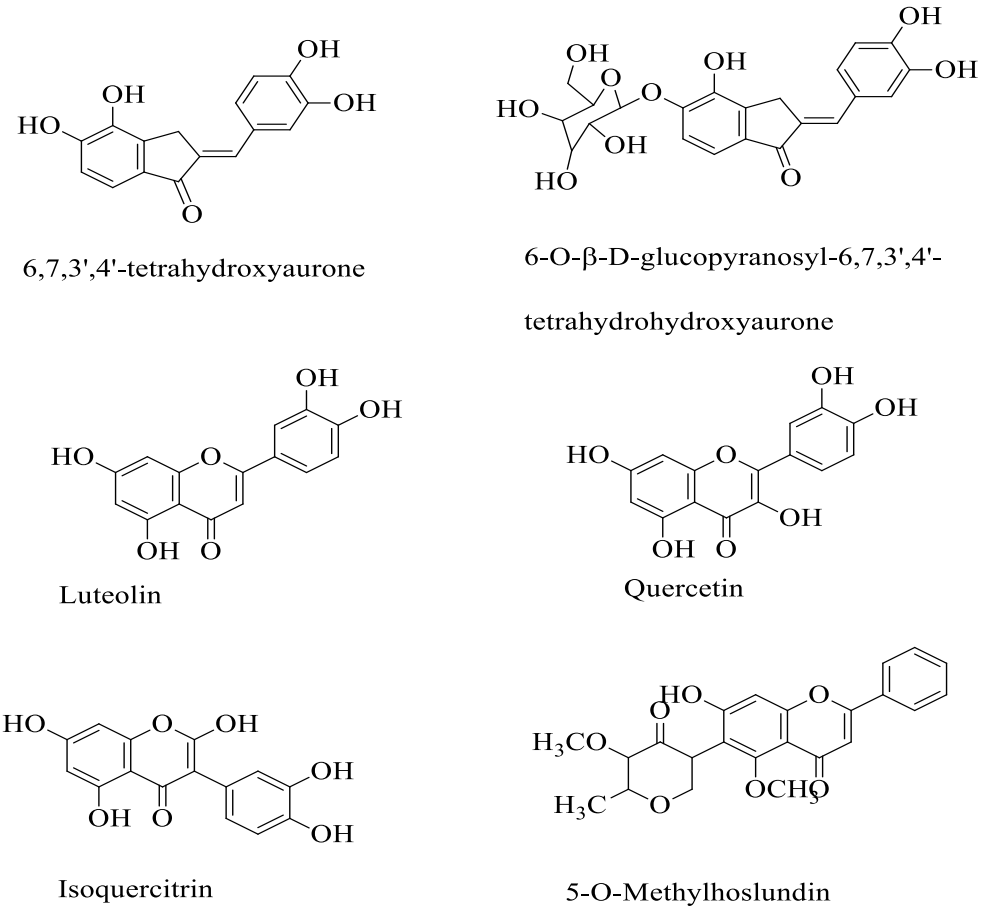

Figure 2.4: Some of the Flavonoids extracted from *B. pilosa*

Porphyrins and flavonoids such as Luteolin, Quercetin, Isoquercetin, 5-O-methylhoslundin, 6-O-beta-D-glucopyranosyl-6, 7, 3', 4'-tetrahydrohydroxyaurone and 6, 7, 3', 4'-tetrahydroxyaurone influence the plants' pharmacological activities as well as facilitating the synthesis of nanoparticles through reduction and stabilization of metal precursors (Bairwa *et al*., 2010; Bartolome *et al*., 2013; Cortés-Rojas *et al*., 2013; Madivoli *et al*., 2019).

2.1.3 *Conyza bonariensis* (Hairy Fleabane)

C. bonariensis, an Asteraceae family annual or short-lived perennial weed with green leaves and hairy seeds **(Plate 2.3)** is utilized as a medicinal herb by many communities**.**

Plate 2.3: *C. bonariensis* leaves and seed

It is widely used as a folk medicine in the treatment of rheumatism, gout, cystitis, nephritis, dysmenorrhea, tooth pain, and headache; and also has anti-ulcerogenic and anticoagulant activity and is used to treat a number of skin disorders (Girma and Jiru, 2021). The Bukusu Luhya sub-tribe call it Nalusambu. It is mainly used for wound healing, where the leaves are squeezed and applied on the wound surface. Besides, *C. bonariensis* leaves has been reported to contain alkenes **(Figure 2.5)**.

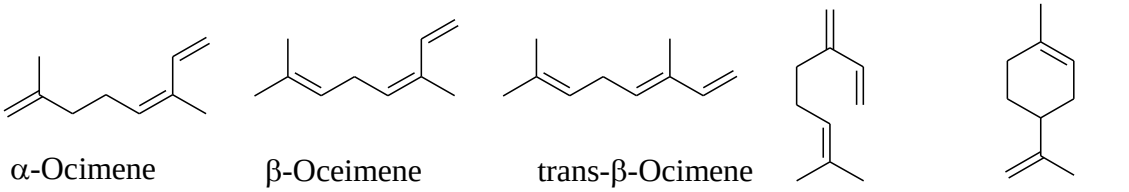

Figure 2.5: Some Compounds Extracted from *C. bonariensis*

Further, phytochemicals extracted from the aerial parts of *C. bonariensis* have been reported to contain essential oils which include monoterpene hydrocarbons; limonene, *trans*-ocimene and sesquiterpene hydrocarbon *trans*-β-farnesene, alkaloids, phenolic

acids and flavonoids (do Amaral *et al*., 2018). The essential oils indicated a minimum inhibitory concentration against *E. coli* 12.5%, while that of *Salmonella typhi* 6.25%. These indicated the antibacterial activity of *C. bonariensis* (Musembei and Joyce, 2017). *C. bonariensis* has been reported to have wide and popular use in folk medicine in the treatment of hemorrhoids, rheumatism, cystitis, dysmenorrhea, tooth pain and diarrhea. Biologically, *C. bonariensis* has been reported to have molluscicidal activity against Biomphalaria snails, antipyretic effects, anti-inflammatory activity and antimicrobial activity (Chhetri *et al*., 2015; Ncc and A, 2010; Thabit *et al*., 2014).

Plants contain biomolecules such as carbohydrates, proteins, and coenzymes that have the potential to reduce metal salts into nanoparticles (Ebrahiminezhad *et al*., 2018). *B. pilosa, C. bonariensis*, and *G. parviflora* have been reported to contain high amounts of metabolites such as polyphenols, flavonoids, esters, sugars, and carboxylic acids which can be utilized in the reduction and stabilization of metal ions to form metallic nanoparticles (Bartolome *et al*., 2013; Girma and Jiru, 2021; Mostafa *et al*., 2013; Thabit *et al*., 2014).

2.2 Nanoparticles as Antimicrobial Agents

Nanoparticles are microscopic particles with a size dimension of 1–100 nm (Darezereshki *et al*, 2010). Metallic nanoparticles have been effectively applied in numerous fields, such as health care, synthetic biology, and cellular transportation (Shaik *et al*., 2017). The use of metallic nanoparticles developed from various metal precursors and plant extracts has been reported in various studies as antimicrobial agents and has gained much interest (Irshad, 2017; Muthukumar and Matheswaran, 2015; Nagar and Devra, 2018). They are being widely applied in biomedical applications for the diagnosis and treatment of various diseases as antiplasmodial (Govindarajan and Benelli, 2017; Joseph and Sreelekha, 2014), anticancer, mosquitocidal, antimicrobial (Benelli, 2016; Dinesh *et al*., 2015), synthetic biology and cellular transportation, (Izadiyan *et al*., 2018; Shaik *et al.*, 2017) and cosmetic industry as sunscreen lotions due to their antioxidant activity (Hasan and Hasan, 2015).

Silver nanoparticles have been reported to have unique morphologies, stability, and controlled geometry and this has greatly awarded them great attention (Shaik *et al*., 2017). Green synthesized iron oxide nanoparticles using *Acacia nilotica* pods have been reported to have moderate antimicrobial activity (Kanagasubbulakshmi and Kadirvelu, 2017). Kanagasubbulakshmi and Kadirvelu, 2017 reported an inhibitory zone of 8 and 10 mm of iron oxide nanoparticles against *S. aureus* and *E. coli,* respectively. Cytotoxicity of synthesized iron oxide nanoparticles using *Juglans regia* green husk extract has also been reported to cause 50% growth inhibition of tumor cells (Izadiyan *et al*., 2018).

Nanoparticles are a few hundred nanometres smaller than comparable large biological molecules such as enzymes, receptors and antibodies (Seigneuric *et al.*, 2010). The unique physical and chemical properties of metal nanoparticles may lead to effective interactions between themselves, bacterial cell membrane and other biological entities (Karaman *et al*., 2017; Seigneuric *et al*., 2010). The antimicrobial activity of nanoparticles is not well understood, however, various mechanisms have been suggested. The nanoparticles have been reported to cause oxidative stress to the cell of gram-negative bacteria by generating excess Reactive Oxygen Species (Slavin *et al*., 2017) as well as the release of antimicrobial metal ions from the surface of the nanoparticle. The nanoparticles also have a membrane–damaging abrasiveness which inherently gives them antimicrobial properties (Fernando *et al*., 2018).

2.2.1 Disease Causing Microbes

Disease-causing microbes, including bacteria, viruses, fungi, and parasites, are the root cause of numerous infectious diseases worldwide. These microorganisms possess unique mechanisms that enable them to invade and colonize the human body, leading to various health issues (Zachary, 2020). Bacteria, such as *E. coli* and *S. aureus*, can produce toxins and damage tissues. Viruses, such as influenza and HIV, hijack host cells to replicate and spread. Fungi like Candida and Aspergillus can cause opportunistic infections in immunocompromised individuals. Parasites, including Plasmodium and Trypanosoma, cause diseases like malaria and Chagas disease. Understanding the pathogenic mechanisms of these microbes is crucial for developing

effective prevention strategies, diagnostics, and treatments (Badiee and Hashemizadeh, 2014). This study involved the antimicrobial activity of the synthesized iron nanoparticles against *S. aureus, B. subtilis*, *E. coli*, *P. aureginosa* and *C. albicans.*

2.2.1.1 *Staphylococcus aureus*

S. aureus is a Gram-positive bacterium found on skin and mucous membranes. It is a major pathogen of public health importance that causes a variety of infections. It is associated with the skin, skin glands, and mucous membranes of almost all warm blooded animals, and it colonizes approximately 30% of the human population.skin. It is reported to cause infections and serious conditions like pneumonia and septicemia, often resistant to antibiotics (Cheun *et al*., 2021; Tadesse *et al*., 2018). Resistance to commonly used antimicrobials has limited treatment options for infections caused by this pathogen. *S. aureus* is a normal flora and has ability to infiltrate the host immune system via various virulence factors, and also has rapid acquisition of a multidrug resistance phenotype, making it one of the most notorious organisms among gram positive bacterial pathogens (Tadesse *et al*., 2018).

2.2.1.2 *Basillus subtilis*

B. subtilis is also Gram-positive, soil-dwelling bacterium with industrial uses. As a soil bacterium, it is subjected to frequent environmental changes. *B. subtilis*, for example, is continuously exposed to osmotic stress due to the interchanging periods of flooding and drying of the upper layers of the soil. It uses a step-by-step response strategy to maintain turgor, minimize cellular damage, and proliferate under hypo- and hyperosmotic conditions. Notably, cellular adaptations to osmotic stress cause a slower growth rate, which contributes to increased antibiotic tolerance (Morawska and Kuipers, 2022).

2.2.1.3 *Escherichia coli*

Another bacteria is *E. coli* which is Gram-negative and is present in the intestines of humans and animals. While most strains are harmless, some can cause foodborne

illnesses and urinary tract infections. These may come as a result of fecal contaminants in the water supply in the form of water contamination, potentially resulting in the transmission of enteric pathogens such as *E. coli*. These pathogens are typically found in human and animal feces and may enter domestic water supplies and further into food via leaching or other means such as improperly treated sewage (Mahmud *et al*., 2019).

2.2.1.4 *Pseudomonas aureginosa*

P. aeruginosa is also a Gram-negative bacterium commonly found in soil and water. It can cause severe infections, especially in immunocompromised individuals, and is known for its antibiotic resistance. This pathogen's large genome, which gives it the metabolic flexibility to quickly adapt to changes in its environment, and its large weapons of cell-associated and secreted virulence factors, which protect it from recognition and attack by the host's immune responses, are what makse it so successful in colonizing diverse environments within its host. What is concerning about *P. aeruginosa* is it's high intrinsic and acquired resistance to many available antibiotics, emphasizing the need and impetus for the development of novel strategies to combat this organism (Wood *et al*., 2023).

2.2.1.5 *Candida albicans*

C. albicans is an opportunistic and polymorphic yeast-like fungus naturally occurring in the human body. It infects humans through mucosal, disseminated, and invasive infections that can cause candidiasis, an infection commonly affecting the mouth, vagina, and skin, especially in immunocompromised individuals or those on prolonged antibiotic use (Dantas *et al*., 2016). One of the key virulence factors in *C. albicans* is the transition from the yeast to the hyphal form, which contributes to macrophage evasion, tissue invasion, and biofilm formation. Nontoxic small molecules that inhibit *C. albicans* yeast-to-hypha conversion and hyphal growth could be a valuable source of information for understanding pathogenic fungal morphogenesis, identifying drug targets, and serving as templates for the development of novel antifungal agents (Vediyappan *et al*., 2013).

2.2.2 Antimicrobial Activity

The antimicrobial activity of nanoparticles has gained significant attention in recent years. Numerous studies have demonstrated the potential of nanoparticles as effective antimicrobial agents against various microorganisms. These nanoparticles, including silver, gold, zinc oxide, and copper nanoparticles, exhibit broad-spectrum activity due to their unique physicochemical properties (Fernando *et al*., 2018). They can disrupt microbial cell membranes, inhibit enzymatic activities, generate Reactive Oxygen Species, and induce DNA damage. Additionally, nanoparticles can be functionalized or combined with other agents to enhance their antimicrobial efficacy. Despite the promising results, further research is needed to elucidate the mechanisms of action, optimize nanoparticle synthesis, assess toxicity, and evaluate their effectiveness in real-world applications (Slavin *et al*., 2017; Fernando *et al*., 2018).

2.3 Environmental Remediation

2.3.1 Removal of Pharmaceuticals in Water

It is established that household, sewage and wastewater effluents are the major sources of dyes and pharmaceuticals in surface and drinking water, and various ways of removing them have been reported. In developing countries, wastewater treatment plants are not well equipped to handle emerging pollutants and various methods have been developed to transform them into less toxic forms and remove them from the environment (Smýkalová *et al*., 2019). However, their removal efficiency depends on their physical and chemical properties. Conventionally, activated sludge processes and biological treatment (biofiltration) have been applied. These methods have not been feasible in the removal of these organic contaminants since they produce by-products that are harmful to living microorganisms and more so humans (Bhamare and Kulkarni, 2019; Leal *et al.,* 2010). Therefore, it is needful to develop more efficient ways that can be used to treat the broadly used harmful pharmaceuticals in water, transform them into less toxic and more biodegradable forms and remove them from the surrounding.

Recently, various methods involving Oxidation Processes have been proposed to be efficient for the removal of harmful organic compounds in aquatic environments; these include activated carbon adsorption, membrane filtration, advanced oxidation processes (AOPs) which involve Fenton and photo Fenton oxidation, ozonation, photolysis, sonolysis and heterogeneous photocatalysis (Das *et al.*, 2018; Yargeau and Danylo, 2015). Activated sludge and chemical coagulants have been employed but have proved hazardous due to the poisonous by-products (Bhamare and Kulkarni, 2019; Leal *et al*., 2010).

Advanced Oxidation Processes are the most powerful and recommended methods for the complete elimination of organic contaminants in most polluted water since they mineralize contaminants into carbon dioxide, water, and biodegradable and less harmful compounds (Kansal *et al*., 2014; Teixeira *et al*., 2016). This usually involves the use of metallic nanoparticles and hydrogen peroxide or ozone. Metallic nanoparticles synthesized using titanium, iron, platinum, zinc and zirconium have been employed as semiconductor photo catalysts in the degradation of organic dyes and pharmaceuticals through filtration, adsorption, photocatalysis and Fenton methods with hydrogen peroxide as an oxidizing agent that generates hydroxyl radicals which attack and oxidize the organic pollutants (Aksu Demirezen *et al*., 2019; Bhamare and Kulkarni, 2019; Das *et al*., 2018; De Andrade *et al*., 2018; Kansal *et al*., 2014; Malakootian *et al*., 2020; Mbiri *et al*., 2018; Teixeira *et al*., 2016; Cai *et al.*, 2019).

Zidovudine an antiretroviral agent for treatment of AIDs have been degraded catalytically by barium Doped zinc oxide nanoparticles where the process is depended on the amount of the catalyst (Bhamare and Kulkarni, 2019). Titanium oxide nanoparticles have also been used to catalytically degrade levofloxacin, ciprofloxacin and meloxicam with over 80% (percentage) degradation within 60 minute (Kansal *et al*., 2014; Malakootian *et al*., 2020; Nadim *et al*., 2015; Nasuhoglu *et al*., 2012). Rifampicin was removed from an aqueous solution through adsorption using recyclable iron nanoparticles which gave a removal efficiency of 61.5% in about 60 minute.

Metallic nanoparticles can be synthesized using various physical and chemical methods such as milling, sodium borohydride and solvothermal methods. Physical methods include evaporation-condensation and laser ablation while chemical methods involve the reduction of metal-containing salts/precursors with an appropriate solvent (S *et al*., 2014). Physically and chemically synthesized nanoparticles have proved inefficient due to the toxic by-products that cause undesired environmental effects, and the nanoparticles produced, especially iron nanoparticles tend to agglomerate due to the Van der Waals and magnetic interactions (Cai *et al*., 2013; Huang *et al*., 2017; Ibrahem *et al*., 2012; Saif *et al*., 2016). Green synthesized nanoparticles have proved the best due to their low toxicity, low cost, active sites, and they are environment friendly.

2.3.2 Degradation of Organic Dyes

Previous studies have shown that iron nanoparticles produced from plants have been used to catalyze the degradation of organic dyes such as bromothymol blue, Methylene blue, aniline and Rhoda mine B (Groiss *et al*., 2017; Sravanthi *et al*., 2018). The iron nanoparticles have shown much efficiency in the oxidation of organic dyes. This is because iron has two stable oxidation states (+2 and +3) which influence the efficiency of iron nanoparticles as photocatalysts (Saif *et al*., 2016). It is suggested that the mechanism for photocatalytic degradation involves oxidation of the dye by hydrogen peroxide, catalyzed by iron and hydroxides present in the nanoparticles through a Fenton–like mechanism. This involves corrosion of the surface of the iron nanoparticles in an acidic environment producing ferrous ions that generate hydroxyl radicals. The radicals attack the dye molecules thus degrading them (Groiss *et al*., 2017; Makarov *et al*., 2014).

2.4 Synthesis of Nanoparticles

2.4.1 Nanomaterials

Nanomaterials are manufactured materials that have unbound nanoparticles with sizes in the range of 1–100 nm. Nanomaterials can be classified as dendrimers, carbon–based, metal–based and composites. Dendrimers are branched materials that form a

chain between polymer and molecular chemistry through chemical manipulation. They are mainly applied in medicine as anticancer drugs and gene therapy (Biao *et al*., 2018; Saleh, 2016). Nanoparticles are added to materials forming nanosized clay materials which are referred to as composites to enhance their thermal resistance and mechanical and flame retardant properties (Bratovcic, 2019).

Metal–based nanomaterials widely regarded as nanosilver and nanogold are applied in pharmaceutical and biomedical industries since they have unique physicochemical properties which avail wide biomedical applications. Silver nanoparticles have optical properties and hence are used in making sensors and other various products. They absorb and scatter light efficiently producing a colour that depends on the size and shape of the nanoparticles. Metal nanoparticles have been applied as antibiotic agents in wound dressings and medical devices and also in washing machines and refrigerators (Bratovcic, 2019).

2.4.2 Chemical Synthesis

The synthesis of nanoparticles in polymeric materials has shown promise due to the processing ease, solubility, minimal toxicity, and the potential to control the resulting nanoparticles' growth (Shameli *et al.*, 2010). Nanoparticles can be synthesized using chemical or biological methods. Chemical methods that have been employed include the use of sodium borohydride as a reducing agent. This method though it's a faster way of getting nanoparticles with the required size, involves the use of a lot of energy, pressure and involves production of poisonous by–products and high amounts of heat (Harshiny *et al*., 2015; Shahwan *et al*., 2011; Smuleac *et al*., 2011).

2.4.3 Physical Synthesis

This involves the use of physical methods such as gas condensation and vacuum deposition and vapourization. In gas condensation techniques, a metallic or inorganic substance is evaporated using thermal evaporation sources such as Joule heated intractable containers, and electron ray evaporation strategies, in an atmosphere of 1 – 50 m bar where a highly stable gas pressure causes the creation of ultrafine elements

(100 nm) through gas phase collision. The nanoparticles are formed by the impact of evaporated atoms with residual gas molecules. In vacuum deposition and vapourization, elements, alloys, or compounds are vaporized and deposited in a vacuum under a pressure of less than 0.1 Pa (1 m Torr), temperature ranges from ambient to 500°C and vacuum levels of 10 to 0.1 MPa (Yadav, 2018).

2.4.4 Green Synthesis

Green synthesized nanoparticles exhibit a wide range of uses due to their great unique physical, thermal, chemical, and catalytic properties, their large surface area to volume ratio, stability, biocompatibility and high surface energy as well as unique adsorption phenomenon (Devatha *et al*., 2016; Izadiyan *et al*., 2018; Seigneuric *et al*., 2010; Shameli *et al*., 2010; Yew *et al*., 2016). Plant extracts are the best candidates for the synthesis of metallic nanoparticles as they exhibit high chemical diversity due to genetic variations, and ecological and environmental factors meaning that plant extracts contain different concentrations of natural reducing agents which can influence the characteristics of the nanoparticles (Shaik *et al*., 2017). Synthesized iron nanoparticles from plants offer an alternative for exploitation of plants for pharmaceutical, water treatment, biomedical and catalytic applications (Groiss *et al*., 2017; Kanagasubbulakshmi and Kadirvelu, 2017; Saif *et al*., 2016; Silveira *et al*., 2017; Yuan *et al*., 2017). Recently, biosynthetic methods for synthesis of both metal oxide and metal nanoparticles have been employed by either using biological microorganisms such as bacteria, fungi or plant extract and have widely emerged as simple and viable alternatives to chemical synthetic methods and are environmentally eco-friendly and compatible for pharmaceuticals/drugs and other biomedical applications (Hasan and Hasan, 2015; Kanagasubbulakshmi and Kadirvelu, 2017). Metals such as copper, zinc, titanium, gold, iron, silver and many others have been used in the synthesis of nanoparticles with biological extracts being used as reducing and stabilizing agents as they produce inorganic materials which exist in microscale and can synthesize nanoparticles of various sizes and chemical composition (Amendola and Meneghetti, 2009; Biao *et al*., 2018; Kanagasubbulakshmi and Kadirvelu, 2017; Logeswari *et al*., 2015; Sravanthi *et al*., 2018; Vaishnav *et al*., 2017).

The extracts reduce metal ions by significantly converting them to zero valent state metallic nanoparticles through bioreduction (Madivoli *et al*., 2019; Makarov *et al.*, 2014).

B. pilosa, C. bonariensis, and *G. parviflora* have been reported to contain polyphenols, sugars, flavonoids, and terpenoids which provide electrons that reduce and stabilize metal ions forming metallic nanoparticles. According to literature, plants in the Asteraceae family have an excellent ability to synthesize nanoparticles in non-toxic ways, and these nanoparticles have a wide range of applications (Pappuswamy *et al*., 2023; Yi *et al*., 2021). Asteraceae members have successfully synthesized nanoparticles such as silver, gold, copper, iron oxide, and zinc oxide (Jalab *et al*., 2021; Madivoli *et al*., 2019; Nguyen *et al*., 2018; Suresh *et al*., 2017). The biosynthesis of nanoparticles using plant extract from Asteraceae members is simple, inexpensive, and environmentally friendly. Besides, the particles formed are stable, biocompatible, eco-friendly, economical and facile (Naveen *et al*., 2021).

In this study, plant-mediated iron nanoparticles were synthesized using extracts of local herbal plants *G. parviflora, C. bonariensis* and *B. pilosa* leaf aqueous extracts as reducing and stabilizing agents. These plants were chosen based on their availability as well as the presence of large amounts of biodegradable and water–soluble polyphenols which aid in the safe synthesis of the nanoparticles through reduction and stabilization (Devatha *et al*., 2016, 2018; Murgueitio *et al*., 2018). The synthesis of iron nanoparticles was performed in a one-step by adding the plant extracts to 0.1 M of Ferric Chloride solution as the iron precursor leading to formation of a black precipitate of GpNPs, CbNPs and BpNPs iron nanoparticles. These were analysed using UV-VIS, FTIR, XRF, XRD, and SEM to determine composition, structure and size. The iron nanoparticles were then evaluated for their antimicrobial activity against *S. aureus, B. subtilis, E. coli, P. aureginosa* and *C. albicans* and degradation effects against Rifampicin and Methylene blue. This is to showcase that the synthesized iron nanoparticles can provide a solution in eliminating microbes as well as removing water pollutants such as pharmaceuticals and dyes.

CHAPTER THREE

MATERIALS AND METHODS

3.1 Sampling and Sample Preparation

Fresh leaves of *G. parviflora, C. bonariensis,* and *B. pilosa* were collected from Bungoma East Sub-County, Bungoma County in Kenya at GPS code 0° 36' 59.99" N, 34° 45' 59.99" E, at an altitude of 1,523 meters after being authenticated by a taxonomist. The samples were then transported in plastic bags to the JKUAT GK Botany Laboratory for confirmation. Samples of the voucher specimens were deposited (in triplicates) at JKUAT Botany Herbarium and given accessory voucher numbers SIW–JKUATBH/001/2018, SIW–JKUATBH/002/2018, and SIW–JKUATBH/003/2018 (**Appendices I (A)–I (F)**) for *G. parviflora, C. bonariensis,* and *B. pilosa* respectively.

The samples were separately cut into small parts and washed thoroughly with running laboratory tap water and further with distilled water and air–dried at room temperature (20–25°C) for 14 days to remove moisture (Igwe and Nwamezie, 2018). The dry plant materials were then ground finely using a milling machine (no model number, assembled locally).

3.2 General Experimental Requirements

3.2.1 Reagents

Ferric Chloride ($FeCl_3$) (Anhydrous), Hydrogen peroxide (H_2O_2) (30%) and 98% Methanol AR grade were purchased at Sigma Aldrich, and Rifampicin, Methylene blue, 1 N Folin–Ciocalteau reagent, 5% Rutin, 99.8% Garlic acid (GA), Aluminium Chloride ($AlCl_3$), and Acetone were obtained from Vision Scientific Ltd, Kenya.

3.2.2 General Preparation

The glassware used in the experiments was cleaned thoroughly with hot water and detergent, rinsed with distilled water, and acetone, and then oven dried at 100 ˚C. 1 N

Folin-Ciocalteau reagent was prepared by diluting 25 mL of 2 N Folin-Ciocalteau reagent with an equal volume of water. 200 µg/mL of Rutin was prepared by weighing 50 mg and dissolving it in 1 mL methanol and diluting it to 50 mL. 5 mL of the solution was then diluted to 50 mL with distilled water. 50 µg/mL of Garlic acid was prepared by dissolving 50 mg of garlic acid in 1 mL Methanol and diluting 50 mL with distilled water to 50 mL. 0.1 M Ferric Chloride was prepared by dissolving 13.14 g in 100 mL of distilled water and topping to half a litre with distilled water. 5% of Aluminium Chloride was prepared by dissolving 5 g in 100 mL of distilled water.

3.2.3 Apparatus

The apparatus used included UV–Vis spectrophotometer (UV 1800, Shimadzu), FTIR spectrophotometer (Shimadzu, FTS–8000, Japan), X–Ray Diffraction STOE STADIP P X-ray Powder Diffraction System (STOE and Cie GmbH, Darmstadt, Germany), Extech PH110 Waterproof ExStik pH Meter, X-ray Powder Diffraction, Tescan Mira3 LM FE Scanning Electron Microscope, and Milling machine (assembled locally).

3.2.4 Extraction

3.2.4.1 Methanol Extraction

Dry and ground plant material (0.1 g) was extracted using 5 mL 80% methanol and filtered through a Whatman filter paper NO.1 to make the stock crude extract for polyphenol and flavonoid quantification.

3.2.4.2 Aqueous Extraction of Phytochemicals

Twenty grams of the dried and ground *G. parviflora, C. bonariensis,* and *B. pilosa* were transferred into different labeled 250 mL volumetric flasks. 200 mL of distilled water was added and the mixture boiled at 70 °C with constant stirring for 45 minutes. The extract was allowed to cool and filtered three times with cotton wool and further through Whatman NO.1 filter paper (Izadiyan *et al*., 2018; Jeyasundari *et al*., 2017; Kanagasubbulakshmi and Kadirvelu, 2017).

3.3 Quantitative Phytochemical Analysis

3.3.1 Total Phenolic Content

The total phenolic content of the crude extracts was evaluated by the Folin-Ciocalteau method with some modifications using Garlic acid as standard (Ruto *et al*., 2018). Absorbance and concentration of the standards and the samples were measured at 769 nm using a compact, double-beam UV-Vis spectrophotometer (UV 1800, Shimadzu) (Baba and Malik, 2015; Parimelazhagan, 2016). The total phenolic content was expressed in mg of garlic acid equivalents (GAE) /g of dry weight extract (DW).

3.3.2 Total Flavonoid Content

The total flavonoid content was determined using the Aluminium Chloride method with Rutin as the standard according to (Baba and Malik, 2014) and the absorption readings were done at 510 nm using a compact, double-beam UV-Vis spectrophotometer (UV 1800, Shimadzu). The calibration curve was used to determine the total flavonoid content and was expressed as mg of Rutin equivalent (RE)/g of the dry weight of the sample.

3.4 Synthesis of Iron Nanoparticles from Leaf Extract

The 0.1 M $FeCl_3 \cdot 6H_2O$ solution (working standard) was prepared by weighing 13.52 g of $FeCl_3.6H_2O$ and dissolving in 100 mL of distilled water and further topped to 500 mL with enough distilled water (Fazlzadeh *et al*., 2017). The nanoparticles were synthesized by adding the extract to Ferric Chloride dropwise as shown in the schematic diagram below **(Plate 4.1)**.

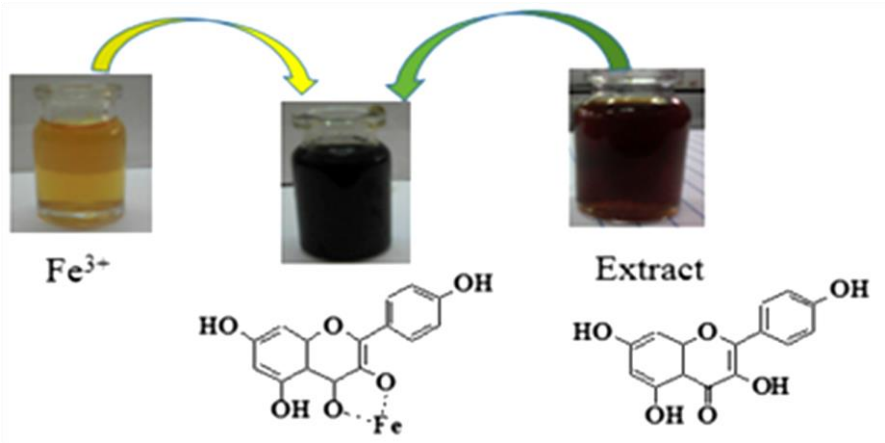

Plate 3.1: Flow diagram for synthesis of iron nanoparticles

Synthesis of Iron nanoparticles was done by adding 30 mL of aqueous plant extracts to 10 mL of 0.1 M Ferric Chloride dropwise using a burette (Balamurugan *et al*., 2014; Borja *et al*., 2015) with constant stirring at room temperature and pressure. The Fe^{3+} salt and the phyto extracts are chemically responsible for the formation of the nanoparticles. The instantaneous colour changes indicated the formation of iron nanoparticles which involved bio-reduction and stabilization of the Ferric ions by the electrons produced by chemical components in the plant extract (Izadiyan *et al*., 2018). The black precipitate was washed several times with distilled water, and centrifuged at 6000 rpm for 10 minutes (Centurion 6000). The obtained nanoparticles were dried at 60 ˚C in the oven for 3 hours (Fazlzadeh *et al*., 2017).

3.5 Characterization of Iron Nanoparticles

3.5.1 UV-Vis Spectra

UV-Vis absorption spectra were recorded using a compact, double-beam UV-Vis spectrophotometer (UV 1800, Shimadzu) in the range of 200–800 nm (Siddiqi *et al*., 2016).

3.5.2 FTIR Spectra

The Shimadzu FTIR spectrophotometer (FTS–8000, Japan) was used to analyse functional groups present on the plant extract as well as the iron nanoparticles by the

standard KBr method, with spectral resolution set at 4 cm^{-1} and the scanning range from 400 to 4000 cm^{-1} (Ponce *et al*., 2013). Briefly, the samples were ground with KBr in the ratio of 1:10 (1 mg of sample to 10 mg of KBr). The samples were then pressed using a hydraulic press to obtain the pellets which were then analysed using the FTIR Instrument.

3.5.3 X-Ray Fluorescence

The elemental composition was done using the X-ray fluorescence machine Bruker model at the Mines and Geological Department laboratories, in Kenya. The nanoparticles' elemental content was analyzed according to the American Society of Testing Materials standard D 4326 for mineral content. One gram of the powdered sample nanoparticles was weighed and mixed with 4 g of anhydrous sodium carbonate (AR) before scanning for the percentage elemental contents.

3.5.4 XRD Analysis

The crystallinity phase was identified using STOE STADIP P X-ray Powder Diffraction System (STOE and Cie GmbH, Darmstadt, Germany). The X–ray generator was equipped with a copper tube operating at 40 kV and 40 mA and the sample was irradiated with a monochromatic Cu Kα radiation with a wavelength of 1.5409 nm and 2θ range of 2–90˚ at 0.05˚ intervals.

3.5.5 Scanning Electron Microscope

Morphological analysis was performed using Tescan Mira3 LM FE Scanning Electron Microscope, Germany operated at an accelerating voltage of 3 kV. The samples were gold sputtered before observation to avoid the charging effect.

3.6 Degradation of Methylene Blue and Rifampicin

3.6.1 Degradation of Methylene Blue

Methylene blue degradation was established using the previous methodology as a model for the degradation of dyes (Lassoued *et al*., 2018). The reagent was prepared

by dissolving 1 g of Methylene blue in 1000 mL of distilled water to get a 1000 ppm concentration. A working concentration of 20 ppm was prepared according to the dilution law. Two spectral scans were done on 3 mL of the solution in the range of 800–300 nm in 5 minutes intervals using a double-beam UV–Vis spectrophotometer. 1 mL hydrogen peroxide was added and two more scans were allowed, after which 50 mgs of the iron nanoparticles were sprinkled on the solution and allowed to run for 10.5 hours in 5 minutes intervals. A spectral scan for the degradation of Methylene blue solution using hydrogen peroxide without the nanoparticles and the nanoparticles alone as a control was done under the same conditions for 1 hour.

The photocatalytic activity of the nanoparticles was studied by taking 30 mL of 20 ppm concentration of Methylene blue in a 100 mL conical flask and 30 mg of the nanoparticles and 1 mL of hydrogen peroxide were sprinkled on the solution and kept under direct sunlight irradiation on a sunny day in March 2019 between 11 am and 2 pm for 3 hours on a laboratory stool. The progress of degradation of Methylene blue was monitored in various time intervals and the absorbance at a wavelength of 665 nm was recorded (Bishnoi *et al.*, 2018; Nathan *et al.*, 2018). FTIR analysis of the nanoparticles after degradation was carried out to evaluate any shifts, dissappearances as well as additional fuctional groups.

3.6.2 Degradation of Rifampicin

To study the degradation of pharmaceuticals by green iron nanoparticles, Rifampicin was used as a model drug using previously modified methods (Kansal *et al.*, 2014). Rifampicin (2.5 mg) was dissolved in 1 mL of methanol and diluted with distilled water to 250 mL in a volumetric flask to make 10 mg/L (12.15 µM) and sealed in an aluminium foil. The degradation experiments were carried out by scanning Rifampicin solution in the range 600–350 nm using a Shimadzu 1800 UV–Vis spectrophotometer (Shimadzu Corporation, Kyoto, Japan), at JKUAT. Thereafter, 50 mg iron nanoparticles were added and the solution and scanned repeatedly till a contant absorbance was obtained. 250 µL of 30% H_2O_2 solution was then added and the mixture was scanned in 2 minute interval using a Shimadzu 1800 UV–Vis spectrophotometer (Shimadzu Corporation, Kyoto, Japan) and more scans taken upto

a contant absorbance. Separate scans of hydrogen peroxide and the nanoparticles as controls were taken under the same condition (Bhamare and Kulkarni, 2019). To determine how different reaction parameters affected the rate of degradation of Rifampicin, the reactions were carried out by varying the dosage of the nanoparticles, temperature, and pH of the reaction media. The degradation was studied at pH 3, 7 and 12 which were adjusted using 0.1 M NaOH and 0.1 M HCl. The photocatalytic activity of the nanoparticles under sunlight was studied by taking 30 mL of Rifampicin and Methylene blue at pH 7 in a 100 mL conical flask. 30 mg of the nanoparticles and 1 mL of hydrogen peroxide were sprinkled on the solution and kept under direct sunlight irradiation on a sunny day in between 11 am and 2 pm on laboratory stool. The degradation progress was monitored in various time intervals and the absorbance at 476 nm was recorded (Bishnoi *et al*., 2018; Nathan *et al*., 2018). FTIR was done for the nanoparticles after degradation to evaluate any shifts, dissappearances as well as any new fuctional groups introduced during the degradation process.

3.6.3 Degradation Efficiency

Since absorbance is directly proportional to concentration at the ultra violet region, the percentage degradation efficiency for Methylene blue dye and Rifampicin were calculated using **Equation 1** (Xu *et al*., 2020).

$$Degradation\ efficiency\ (\%) = \frac{A_0 - A_t}{A_0}\ x\ 100 \ldots\ldots\ldots\ldots\ldots \mathbf{1}$$

where A_0 is the initial Absorbance and A_t is the final absorbance of Methylene blue or Rifampicin at time *t* in minutes

3.6.4 Reaction Kinetics

The order of the reaction was determined experimentally by plotting the data assuming a first-order reaction **(Equation 2)** and a second-order reaction **(equation 3)**. The reaction order was determined from the best line of fit obtained from the graphs (Aksu Demirezen *et al.*, 2019; Atkins and Paula, 2009; Ebbing and Gammon, 2009).

$$ln[A]_t = -kt + \ln[A]_0 \ldots\ldots\ldots \mathbf{2}$$

$$\frac{1}{[A]_t} = -kt + \frac{1}{[A]_0} \ldots\ldots\ldots \mathbf{3}$$

where *t* is the time taken, A_0 and A_t are the initial and final absorbances of Methylene blue or Rifampicin while *k* is the equilibrium constant.

3.6.5 Thermodynamic Properties

The thermodynamic parameters associated with Rifampicin degradation were determined based on the linear form of Van't Hoff equation:

$$\ln K_{eq} = \frac{\Delta H}{RT} + \frac{\Delta S}{R} \ldots\ldots\ldots\ldots\ldots \mathbf{4}$$

where **ΔH**, and **ΔS** denote the enthalpy, and entropy of the degradation reaction while R is the universal gas constant; 8.31 $Jmol^{-1}K^{-1}$ and T refers to temperature (Kelvin) (Atkins and Paula, 2009; Ebbing and Gammon, 2009).

3.7 Disc Diffusion Assay for Antimicrobial Potency

The standard disc diffusion method (Kirby Bauer method) was used to evaluate the antimicrobial activity of the synthesized iron nanoparticles against *E. coli*, *B. subtilis*, *S. aureus, P. aeruginosa* and *C. albicans.*

3.7.1 Culture of the Test Organisms

The Agar diffusion assay was done in triplicates. 20 mL of 38 g/L solution of Mueller Hinton Agar was autoclaved at 121℃ for 15 mis, cooled to 45℃. Using a sterile pipette, 100 µL of overnight bacterial broth culture of the test organism was inoculated in 10 mL aliquots of nutrient broth, spread evenly with a sterile spreader onto sterile Petri dishes to get bacterial lawn and incubated at 37°C to solidify for 24 hours.

3.7.2 Preparation of the Standards

The samples (nanoparticles) and the conventional drugs were prepared by dissolving the 10 mg of the solid in 10 mL of Dimethyl sulphoxide (DMSO). From the concentrations prepared, 15%, 7%, 4%, 2%, and 1% concentrations of the nanoparticles were prepared by serial dilution. The extracts of *G. parviflora, C. bonariensis,* and *B. pilosa* were used as prepared.

3.7.3 Incubation of the Bacteria Treated Culture

Two circular wells were made, whichserved as a negative reference with DMSO and 0.1 M Ferric chloride. The positive controls used were ampicillin and ciprofloxacin. The nutrient Agar surface was spread on with inoculum suspension using a sterile swab and 6 mm disc sterilized at 120°C for 20 minutes and loaded with ampicillin and ciprofloxacin as positive controls. Paper discs were prepared by dipping in Whatman filter paper in the plant extracts and the nanoparticles and placed on the surface of the inoculated plates using sterilized forceps. The plates were thereafter incubated at 37°C for 24 hours. The zones of inhibition were measured in millimeters using a ruler. The zones of inhibition with 1–6, 7–10 and 11–15 mm were considered to be low activity, moderate activity, and very high activity respectively (Da'na *et al*., 2018; Groiss *et al*., 2017).

CHAPTER FOUR

RESULTS AND DISCUSSION

4.1 Total Flavonoid and Polyphenol Content

The total flavonoid content in the *G. parviflora*, *B. pilosa* and *C. bonariensis*, leaf powder was determined and the results are shown below **(Table 4.1)**.

Table 4.1: Total Flavonoid

Sample	Total Flavonoids (mg RE/g DW)
G. Parviflora	39.00 ± 0.56
B. pilosa	33.13 ± 0.81
C. bonariensis	45.50 ± 0.59

From the results, *C. bonariensis* had relatively highest total flavonoids (45.50±0.59) (mg RE/g DW) while *G. parviflora* the lowest (39.00 ± 0.56) (mg RE/g DW). The total flavonoid content in the *G. parviflora*, *B. pilosa* and *C. bonariensis* leaf powders was determined and the results are shown below **(Table 4.2)**.

Table 4.2: Total Polyphenols

Sample	Total Polyphenols (mg GAE/gDW)
G. Parviflora	57.67 ± 1.27
B. pilosa	126.27 ± 0.01
C. bonariensis	117.13 ± 0.03

The results revealed that *B. pilosa* had the highest total polyphenol content (126.27±0.01) (mg GAE/g DW) as compared to *C. bonariensis* (117.13 ± 0.03) (mg GAE/g DW) **(Table 4.2)** and *G. Parviflora* (57.67 ± 1.27). *G. Parviflora* was found to have less than half of the total polyphenol content in *B. pilosa* and *C. bonariensis*. The results indicated a relatively higher concentration of the total flavonoids as compared to the total polyphenol content. The phytochemicals present in the extract offer a complementary role in the mechanism of nanoparticle formation through bio-reduction

as well as stabilization of the iron nanoparticles. The postulate underlying the green synthesis perspective is that the phytochemicals present in the plant naturally reduce as well as stabilize the nanoparticles formed (Iravani, 2016; Kaushik and Joshi, 2015; Makarov *et al.*, 2014; Velusamy *et al*., 2016; Yadi *et al*., 2018).

4.2 Characterization of Iron Nanoparticles

4.2.1 UV-Vis Spectra

The UV–Vis absorption spectra of an aqueous solution of *C. bonariensis* leaf extracts, synthesized CbNPs and Iron III Chloride were obtained and the results are presented below **(Figure 4.1)**.

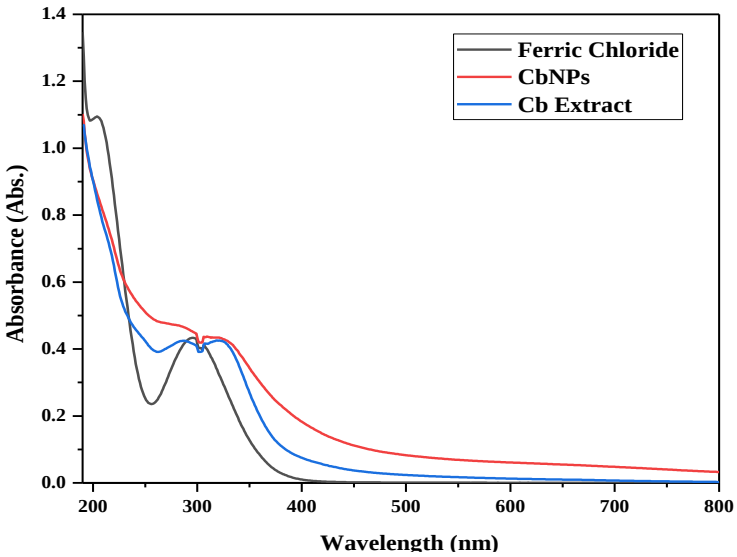

Figure 4.1: UV-visible absorption spectrum of Fe^{3+}, *C. bonariensis* extracts and CbNPs

From **Figure 4.1**, the spectra revealed that the *C. bonariensis*, aqueous extract and Ferric Chloride displayed two peaks while the CbNPs had no peaks. *G. parviflora* extract had a peak at 288 nm and 322 nm. UV–Vis absorption spectra of an aqueous solution of *B. pilosa* leaf extracts, synthesized iron BpNPs and iron III Chloride was collected and the results are shown below **(Figure 4.2)**.

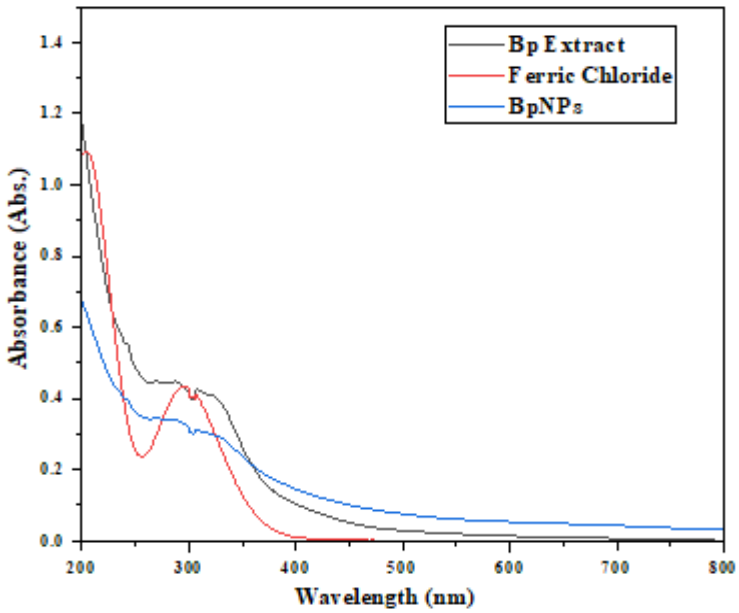

Figure 4.2: UV-visible absorption spectrum of Fe^{3+}, *B. pilosa* extracts and BpNPs

From **Figure 4.2**, the spectra revealed that the *B. pilosa* extract and Ferric Chloride displayed two peaks while the BpNPs had no peaks. *B. pilosa* extract had a peak at 286 nm and 322 nm. UV–Vis absorption spectra of an aqueous solution of *G. parviflora* leaf extracts, synthesized iron GpNPs and iron III Chloride **(Figure 4.3)** as shown below.

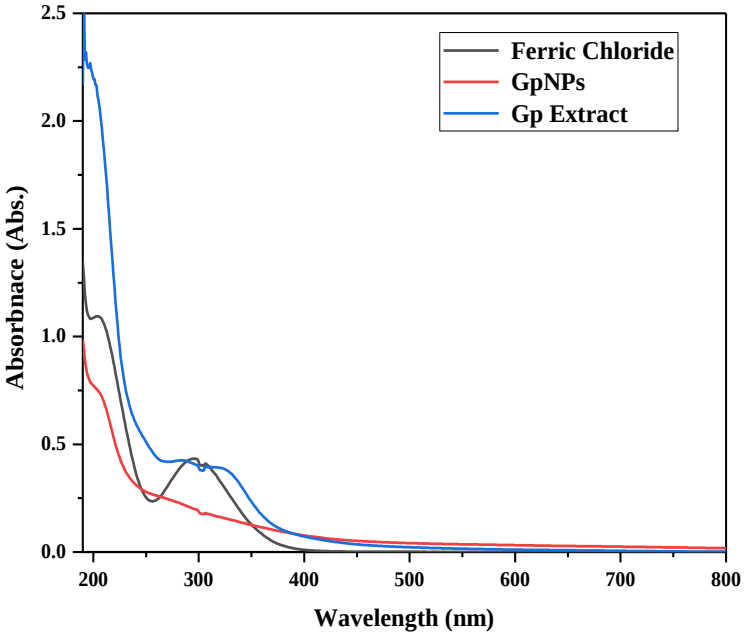

Figure 4.3: UV-visible absorption spectrum of Fe^{3+}, *G. parviflora* extract and GpNps

From **Figure 4.3**, the spectra revealed that the *G. parviflora* extract and Ferric Chloride displayed two peaks while the GpNPs had no peaks. *G. parviflora* extract had a peak at 267 nm and 322 nm.

From the spectra obtained, the aqueous leaf extracts of *G. parviflora*, *C. bonariensis*, and *B. pilosa* were brown in colour and had higher absorption peaks at 267 nm, 288 nm and 286 nm respectively. These suggested that the leaf extracts contain electron–rich polyphenols, amino acids as well as sugars which are responsible for the reduction of Ferric ion (Fe^{3+}) (Huang *et al*., 2014; Sravanthi *et al*., 2018). Fe^{3+} spectra displayed peaks at absorption peaks of 203 nm and 295 nm. Upon the addition of the extract into the 0.1 M Ferric Chloride solution, black–colored colloidal solutions developed gradually. The strong absorption peaks of the extract, and the Fe^{3+} in the range of 200 to 350 nm disappeared, and a broad absorption peak was observed, which demonstrated the formation of polydispersed iron nanoparticles through electron transfer and Surface Plasmon Resonance (Alam *et al*., 2013). The color change is associated with the excitation of electrons as the Fe^{3+} ions are reduced to Fe^{0} and the

changes in the original peaks in the extract and Ferric solution illustrates their interactions (Katata-Seru *et al*., 2018; Mirza *et al*., 2018; Sravanthi *et al*., 2018).

4.2.2 FTIR Spectra of the Extracts and the Nanoparticles

The functional groups present in the aqueous leaf extracts and the nanoparticles were determined using FTIR. The functional groups present in *G. parviflora*, *C. bonariensis*, and *B. pilosa* leaf extracts are illustrated in the spectra below **(Figure 4.4)**.

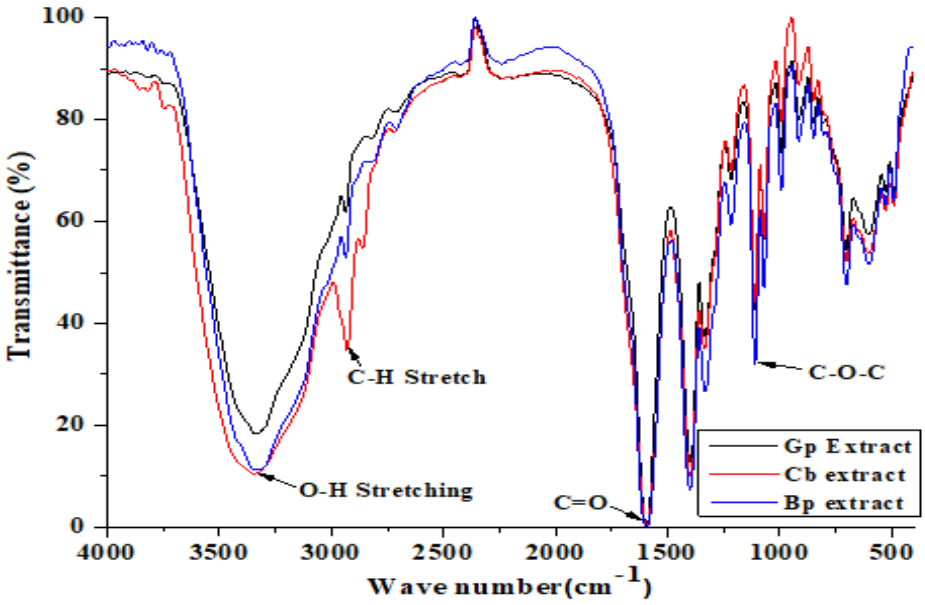

Figure 4.4: FTIR spectra of *C. bonariensis*, *G. parviflora* and *B. pilosa* extract

Based on the spectra obtained **(Figure 4.4)**, the *G. parviflora*, *C. bonariensis*, and *B. pilosa* extracts depicted O-H stretching of phenolic groups at 3309 cm^{-1}, 3329.7 cm^{-1} and 3336 cm^{-1} respectively, which suggests responsibility for bioreduction of the Ferric Chloride (Da'na *et al*., 2018). To compare the influence of the extracts on the nanoparticles, spectra of the GpNPs, CbNPs, and BpNPs were obtained **(Figure 4.5)** as illustrated below.

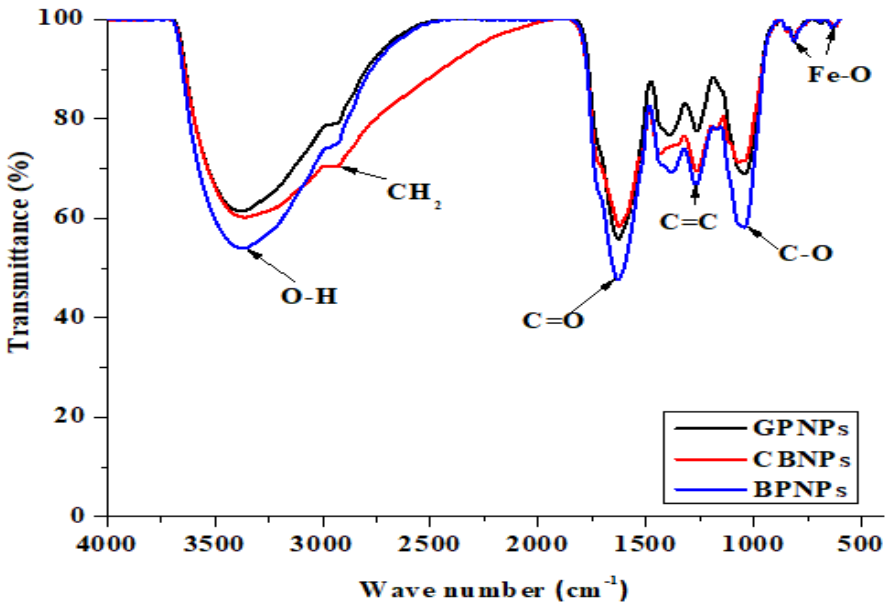

Figure 4.5: FTIR spectra of CbNPs, GpNPs and BpNPs

Based on the spectra obtained **(Figure 4.5)**, the nanoparticles displayed considerable peaks which were related to the extracts. The O–H stretching vibration in the extracts *C. bonariensis*, *G. parviflora*, and *B. pilosa* shifted to 3406 cm^{-1}, 3438.3 cm^{-1} and 3402.6 cm^{-1} **(Figure 4.5)** in CbNPs, GpNPs and BpNPs. The O–H stretch in the nanoparticles is due to the secondary metabolites such as polyphenols, sugars, and amino acids that were involved in the chelation and bioreduction of Fe^{3+} and Fe^{2+} to Fe^{0} (Azam *et al*., 2012; Fazlzadeh *et al*., 2017; Groiss *et al*., 2017; L. Huang *et al*., 2014; Izadiyan *et al*., 2018). These also explain their roles as capping agents as they are also observed in the spectra of the iron nanoparticles, though there was a slight shift in the vibrational frequencies observed. The peaks at 1027 cm^{-1}, 1037 cm^{-1} and 1031 cm^{-1} in CbNPs, GpNPs and BpNPs and at 1000 cm^{-1} for the extracts respectively are due to C–O–C vibrational frequencies of glycosidic linkage in the extracts (Mashjoor *et al*., 2018). Those in 1400 cm^{-1} for the nanoparticles are assigned to the C–C and C=C for aromatic stretching (Izadiyan *et al*., 2018). The bands at 1631, 1630 and 1627 cm^{-1} in BpNPS, CbNPs and GpNPs respectively indicate the presence of C=C vibrational mode for unsaturated metabolites such as terpenoids. The iron–oxygen bond observed at 671, 621 and 636 cm^{-1} **(Figure 4.5)** (Betancur *et al*., 2012; Fazlzadeh *et al*., 2017; Hwang *et al*., 2014; Jagathesan and Rajiv, 2018; Jeyasundari

et al., 2017; Kanagasubbulakshmi and Kadirvelu, 2017; Wang *et al*., 2014). The FTIR bands for the synthesized iron nanoparticles matched well with those for their respective plant extracts, which demonstrates that the components present in the extracts capped the synthesized nanoparticles. However, shifts in the bands between the nanoparticles and the extracts, weakening in the transmittance as well as disappearance designate that water–soluble biomolecules such as reducing sugars and polyphenols are responsible for bio-reduction of Fe^{3+} to Fe^{0} (Jeyasundari *et al*., 2017; Xiao *et al*., 2016).

To understand the influence of Methylene blue/hydrogen peroxide on the functional groups present on the nanoparticles, FTIR spectra after degradation was done and the results are shown in **Figure 4.6** below.

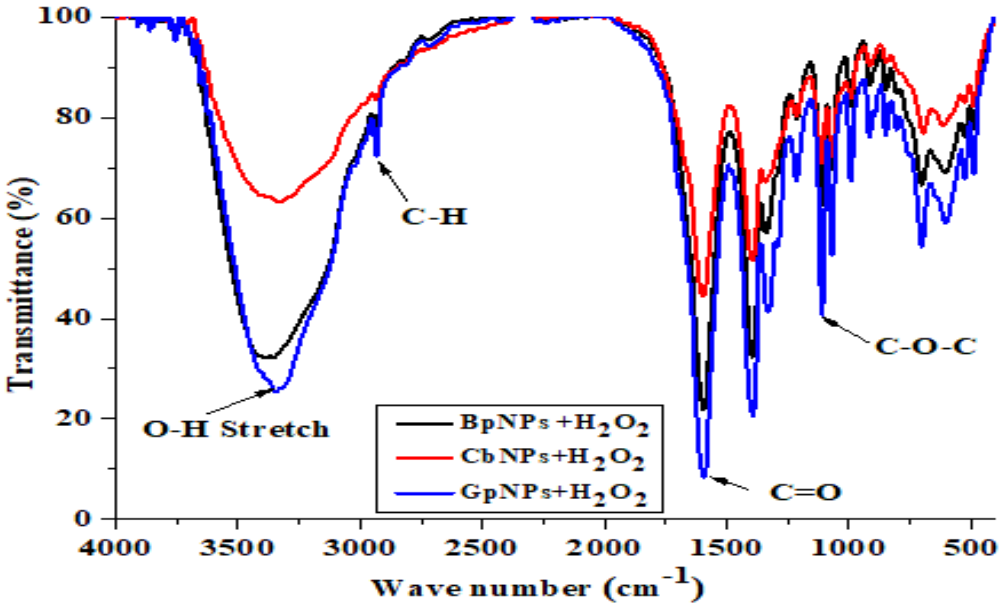

Figure 4.6: FTIR spectra of BpNPs, CbNPs and GpNPs after degradation of Methylene blue in H_2O_2

It was observed that the O-H stretch peaks for the used CbNPs, GpNPs and BpNPs nanoparticles shifted from 3406 cm^{-1}, 3438 cm^{-1} and 3402 cm^{-1} to 3337 cm^{-1}, 3320 cm^{-1} and 3308 cm^{-1}, respectively. The shifts in peak intensity of the nanoparticles after degradation is due to photoexcitation of the catalyst, which is brought about by the

exothermic reaction between the dye, and the hydroxyl groups attached to the surface of the nanoparticles (Chauhan *et al*., 2013a; Kushwaha *et al*., 2018). The infrared spectra of iron nanoparticles before and after degradation of Rifampicin under different reaction conditions are depicted in **Figure 4.7** below.

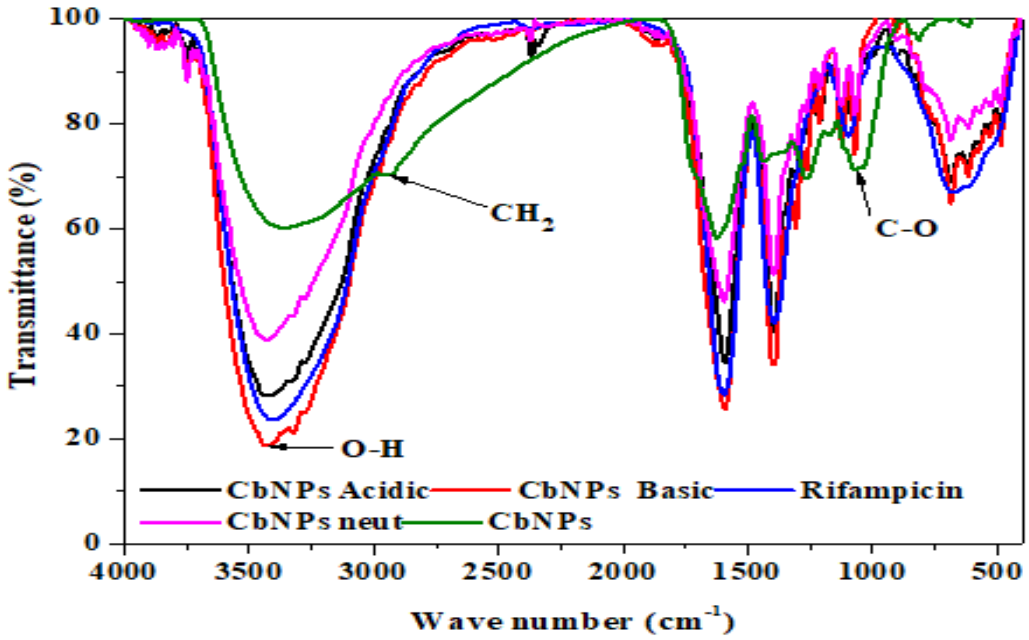

Figure 4.7: FTIR of Rifampicin, CbNPs/ Rifampicin and CbNPs before and after degradation at different pH

From the spectra, there was a change in spectra in terms of the intensity of the peaks in the nanoparticles due to the Rifampicin compound attached to the surface. The wave number of the O-H functional group shifted towards 4000 cm^{-1}. Besides, the peaks at around 1500 cm^{-1} got sharper as the pH changed. To observe the influence of Rifampicin on the structure of the nanoparticles, infrared spectra of nanoparticles before and after degradation of Rifampicin under different reaction conditions were obtained and the spectra are depicted in **Figure 4.8**.

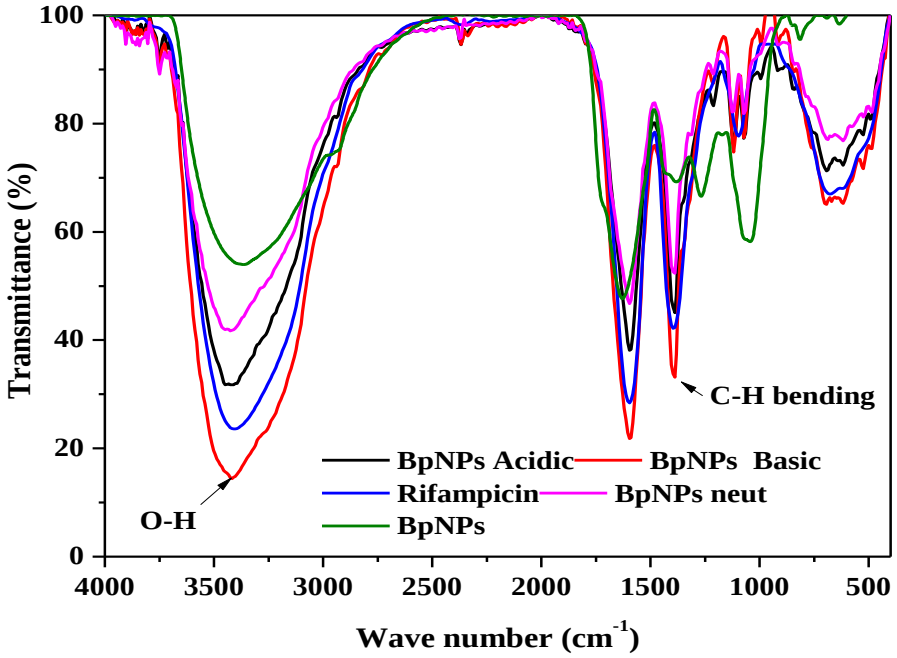

Figure 4.8: FTIR of Rifampicin, BpNPs, and BpNPs/ Rifampicin before and after degradation at pH 3, 7 and 12

From the spectra **(Figure 4.8)**, there was a change in spectra in terms of the intensity of the peaks in the nanoparticles. The wave number of the O-H functional group shifted towards and several peaks at around 1500 cm^{-1} got sharper as the pH changed. The infrared spectra of nanoparticles before and after degradation of Rifampicin under different pH are depicted in **Figure 4.9** below.

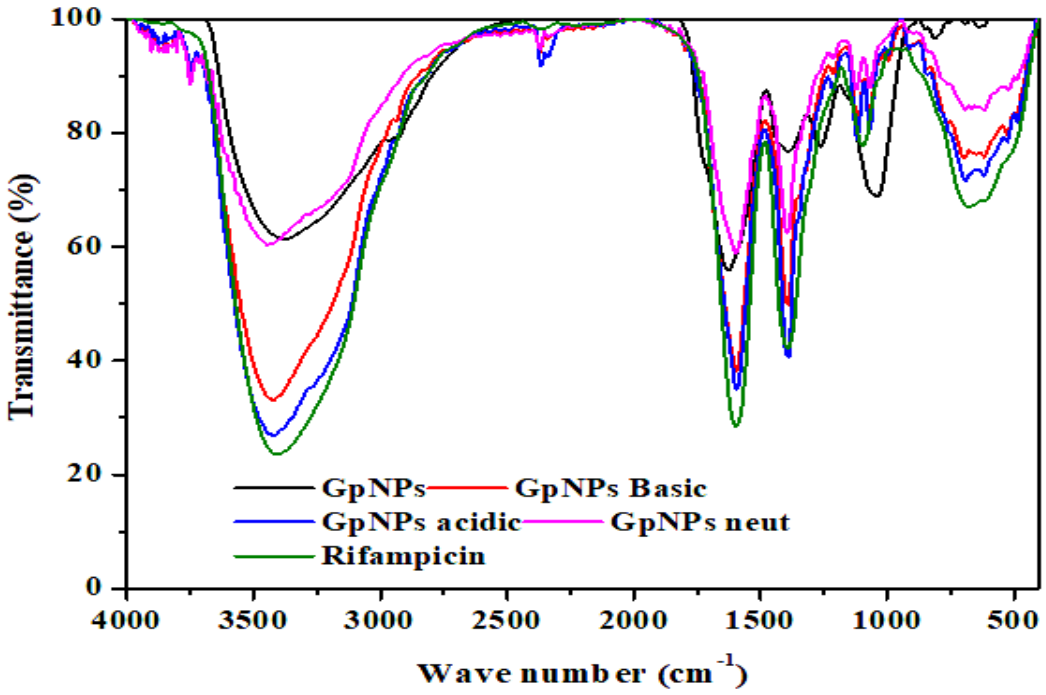

Figure 4.9: FTIR Spectra of Rifampicin and GpNPs/ Rifampicin before and after degradation at pH 3, 7 and 12

From the spectra **(Figure 4.9)**, there was a change in spectra in terms of the intensity of the peaks in the GpNPs. The wave number of the O-H functional group shifted towards 4000 cm^{-1} and the peaks at around 1500 cm^{-1} got sharper as the pH changed while the peak at around 1000 cm^{-1} reduced in intensity.

The FTIR spectra of the synthesized nanoparticles had the O–H stretching vibration for CbNPs, BpNPs and GpNPs at 3406 cm^{-1}, 3402.6 cm^{-1} and 3438.3 cm^{-1} while the C–O–C glycosidic linkages at 1027.0 cm^{-1}, 1031.0 cm^{-1} and 1037.7 cm^{-1} and the C = C was reported as a vibrational mode for the unsaturated metabolites which were depicted by the vibrational bands at 1630 cm^{-1}, 1631 cm^{-1} and 1627.4 cm^{-1} in, CbNPs, BpNPS and GpNPs respectively. From the spectra obtained, Rifampicin shows the organic nature by the numerous peaks of carbon, nitrogen, and oxygen in the range of 800-1200 cm^{-1} with a broad O–H bending vibration at 3419 cm^{-1} (Cai *et al.*, 2019). The FTIR spectra of the nanoparticles before and after exposure to Rifampicin showed relatively several changes in various peaks indicating that the nanoparticles were

relatively stable but had acquired the characteristic properties of Rifampicin through adsorption (Xu *et al*., 2020). There was an addition of the number of peaks of the nanoparticles after degradation at 1121 cm^{-1} with slight shifts of the peaks. The peak at 1630 cm^{-1} in the nanoparticles shifted to 1602 cm^{-1} while those at 1255 cm^{-1} shifted to 1393 cm^{-1}. In addition, the sizes of the peaks of the nanoparticles after degradation had increased in intensity indicating the adsorption of the Rifampicin onto the surface of the iron nanoparticles which increases the number of functional groups (Cai *et al*., 2019; Xu *et al*., 2020).

4.2.3 X-ray Fluorescence Analysis

The percentage elemental composition of GpNps, BpNPs and CbNPs iron nanoparticles were evaluated using XRF and the results are depicted in **Figure 4.10** below.

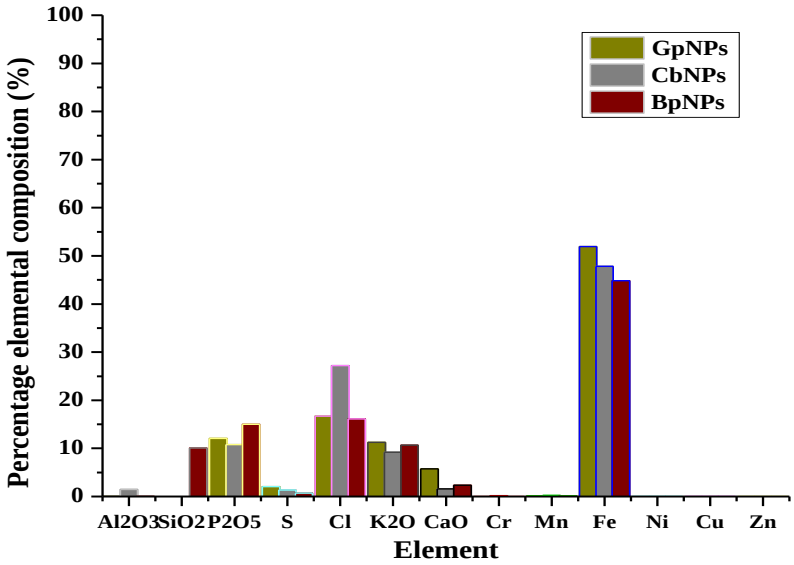

Figure 4.10: Elemental composition of the synthesized particles

From the bar graph, it was clear that the plant–mediated iron nanoparticles of *G. parviflora*, *C. bonariensis*, and *B. pilosa* had 52%, 47.8% and 45% of iron respectively. The synthesized nanoparticles revealed highest percentage of iron than other elements

in the total weight of the nanoparticles (Kanagasubbulakshmi and Kadirvelu, 2017). The higher percentage of chlorine must have originated from $FeCl_3$ precursors used in the synthesis protocol while oxygen is from the extracts used as a component of the various compounds such as polyphenols, flavonoids, saponins, and tannins (Balamurugan *et al*., 2014). Therefore, the elemental analysis of the nanoparticles confirmed the synthesis of the nanoparticles using aqueous extracts of the selected plants with impurity peaks of various oxides and hydroxides of phosphorous, potassium and calcium (P_2O_5, K_2O and CaO) which may coat the surface of the nanoparticles contributing to their agglomeration nature.

4.2.4 SEM Micrographs

The surface morphology of the nanoparticles was determined and below **(Figure 4.11)** are the SEM micrographs of the nanoparticles synthesized from *G. parviflora, C. bonariensis,* and *B. pilosa* aqueous extracts.

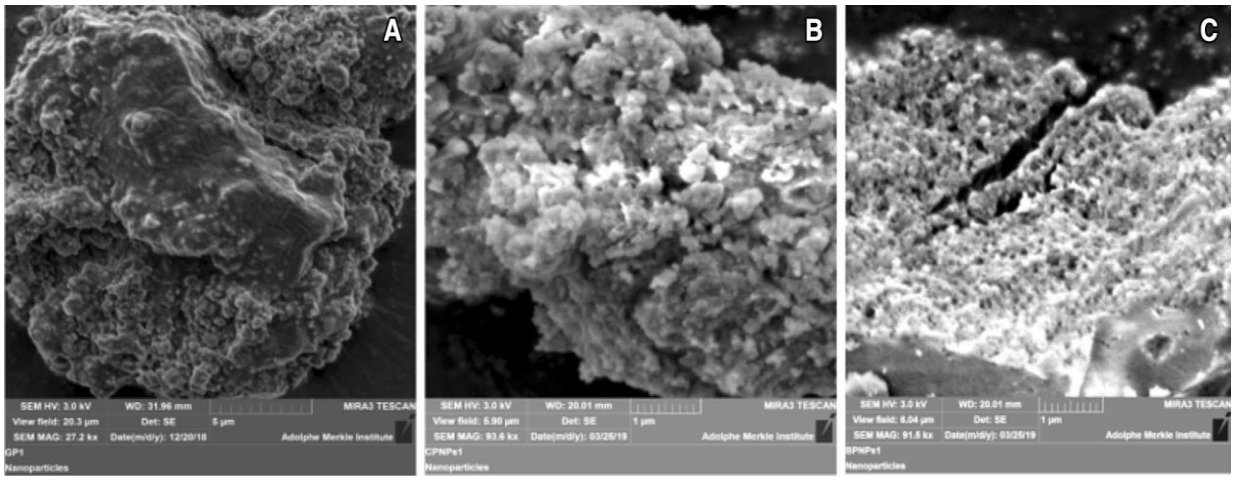

Figure 4.11: SEM images of synthesized CbNPs (A), BpNPs (B), and GpNPs (C) iron particles

From the SEM micrographs obtained **(Figure 4.11)**, CbNPs and BpNPs appeared agglomerated into spherical nanoparticles while the GpNPs are irregularly spherical. The aggregation is due to presence of various biomolecules, chloride, and potassium compounds present in the leaf extracts which influence the morphology of the

nanoparticles (Groiss *et al*., 2017). Polyphenols present in the aqueous extracts of *G. parviflora*, *C. bonariensis*, and *B. pilosa* play a vital role as reducing agents and control the agglomeration of the nanoparticles through Van der Waals interaction (Sulaiman *et al*., 2018; T. Wang *et al*., 2014). The sizes of the synthesized nanoparticles were analyzed on the SEM Images using Image J software. Specific images of the nanoparticles were selected using a scale of 20 nm and their average sizes were determined using histograms. **Figure 4.12** displays the histogram obtained from the BpNPs SEM micrograph.

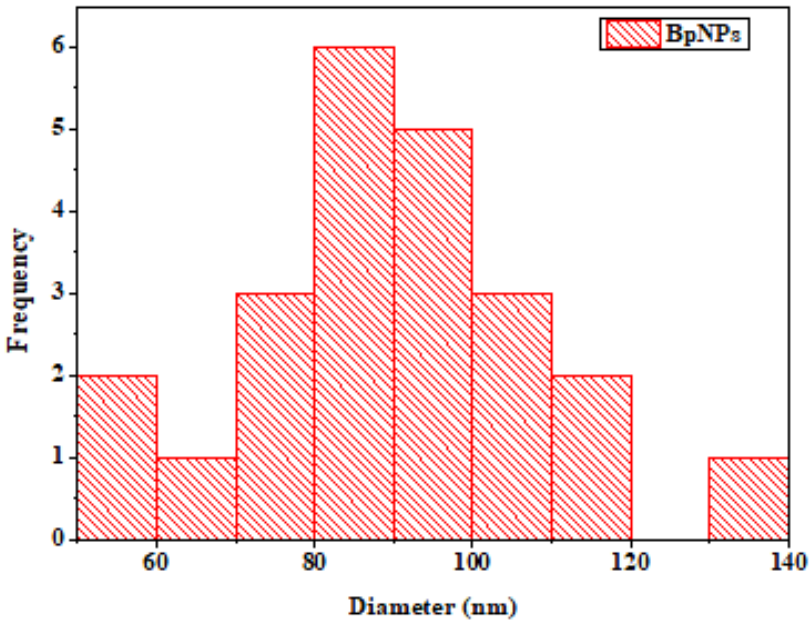

Figure 4.12: Histogram for the diameter of BpNPs

From the histogram, the nanoparticles had an average diameter ranging between 80-90 nm at a mean of 84 nm. For the GpNPs SEM micrograph, a histogram was drawn as shown below **(Figure 4.13).**

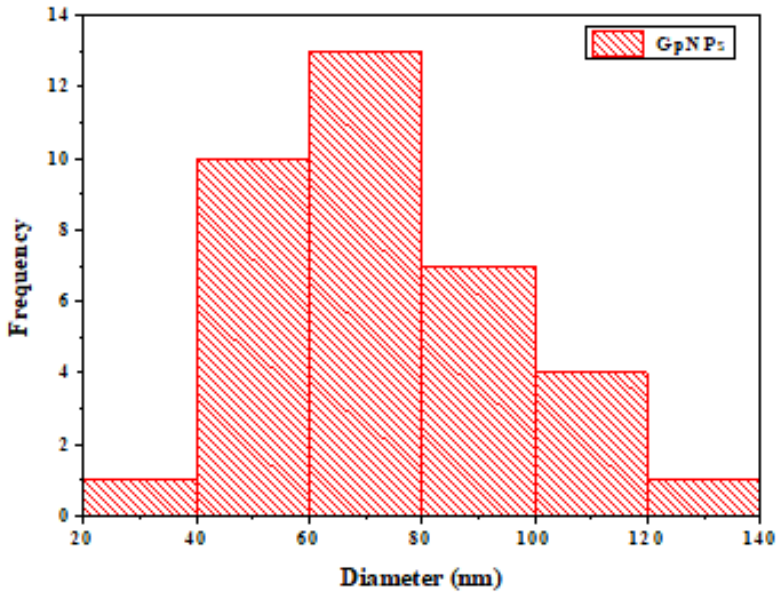

Figure 4.13: Histogram for the diameter of GpNPs

From the histogram, the nanoparticles had an average diameter ranging between 50-80 nm at a mean of 84 nm. **Figure 4.14** displays the histogram of CbNPs obtained from the CbNPs SEM micrograph.

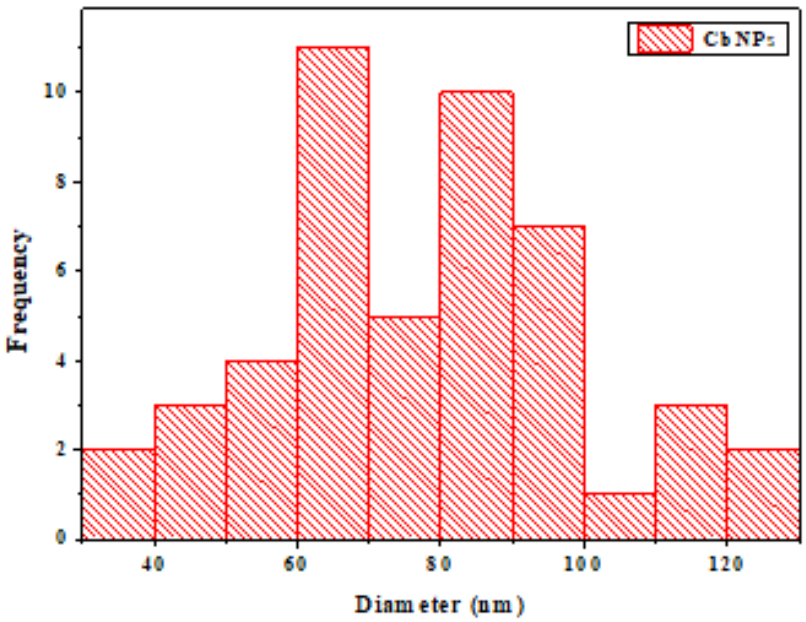

Figure 4.14: Histogram for the diameter of CbNPs

The histograms for CbNPs displayed an average size of 78 nm. In general, from the histograms, the diameters of BpNPs, GpNPs, and CbNPs NPs ranged from 60–90 nm and the mean sizes were 84, 51, and 78 nm, respectively which clearly showed that synthesized iron nanoparticles were nanoscale since the sizes ranged from 1 to 100 nm.

4.2.5 X-ray Diffractograms

The crystallinity of the nanoparticles was determined using XRD and the X-ray diffraction patterns obtained for the iron nanoparticles synthesized using *B. pilosa* leaf extracts is shown in **Figure 4.15** below.

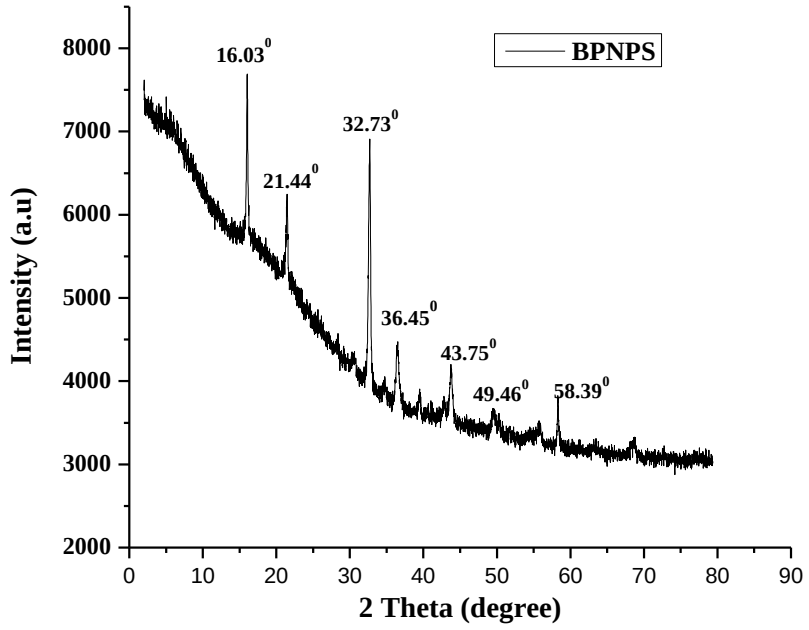

Figure 4.15: XRD diffractogram of BpNPs

From **Figure 4.15**, BpNPs displayed several diffraction peaks at 2θ values ranging between 16 and 60º. The values were of 16.03º, 21.44º, 32.73º, 36.45º, 43.75º, 49.46º, and 58.39º. The crystallinity of GpNPs was determined using XRD and the X-ray diffraction pattern is shown in **Figure 4.16** below.

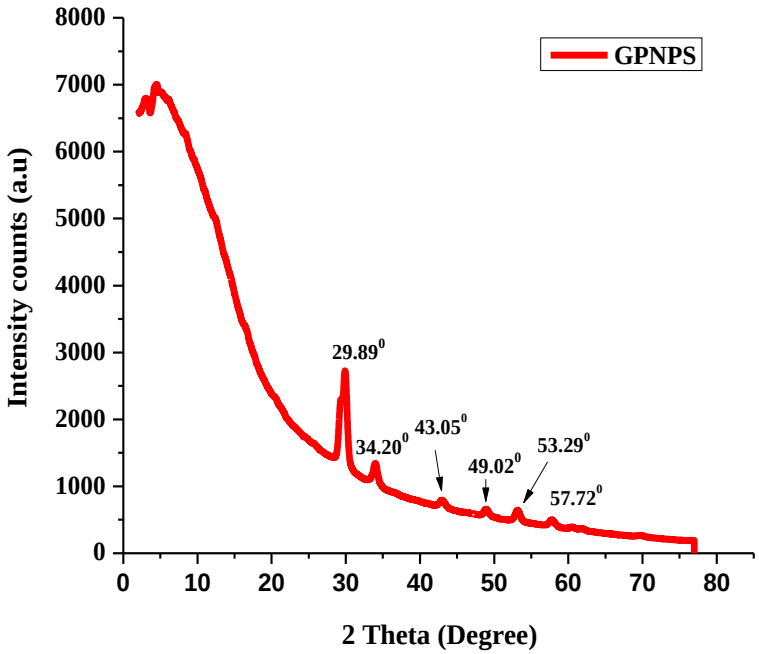

Figure 4.16: XRD diffractogram of GpNPs

From **Figure 4.16**, GpNPs had diffraction peaks that ranged between 29 to 60º. 2θ values were 29.89º, 34.20º, 43.05º, 49.02º, 53.29º and 57.72º. 2θ values between 20 and 60º displayed a mixture of iron oxides such as magnetite and maghemite (Mishra *et al*., 2014). Shoulders depicted at the range of 2 theta = 10˚ - 20˚ at around 20˚ relate to the presence of polyphenols from leaf extracts as capping and stabilizing agents caused by organic matter (Ebrahiminezhad *et al*., 2017; Soliemanzadeh *et al*., 2016; Z. Wang *et al*., 2014). A typical peak at 36.45º in BpNPs shows magnetite (Fe_3O_4) (Al-Kalifawi, 2015; Groiss *et al*., 2017; L. Huang *et al*., 2014; Mishra *et al*., 2014; Wang *et al*., 2014). CbNPs did not display any peaks but an interference pattern. This showed that CbNPs had an amorphous nature while GpNPs with poor crystallinity due to the amorphous nature hence the diffraction patterns do not depict any distinctive diffraction peaks suggesting that the green synthesis approach resulted in the production of amorphous iron nanoparticles (Ebrahiminezhad *et al*., 2017; Veeramanikandan *et al*., 2017; Z. Wang *et al*., 2014).

4.3 Degradation of Methylene Blue

4.3.1 Influence of Solution pH on Degradation of Methylene blue

The iron nanoparticles were investigated for their catalytic properties in the degradation of Methylene blue dye at pH of 3, 7 and pH 12 for 3 hours. **Figure 4.17** displays the spectral analysis of the degradation process of Methylene blue in the presence of CbNPs and H_2O_2, for a time of 12 hours.

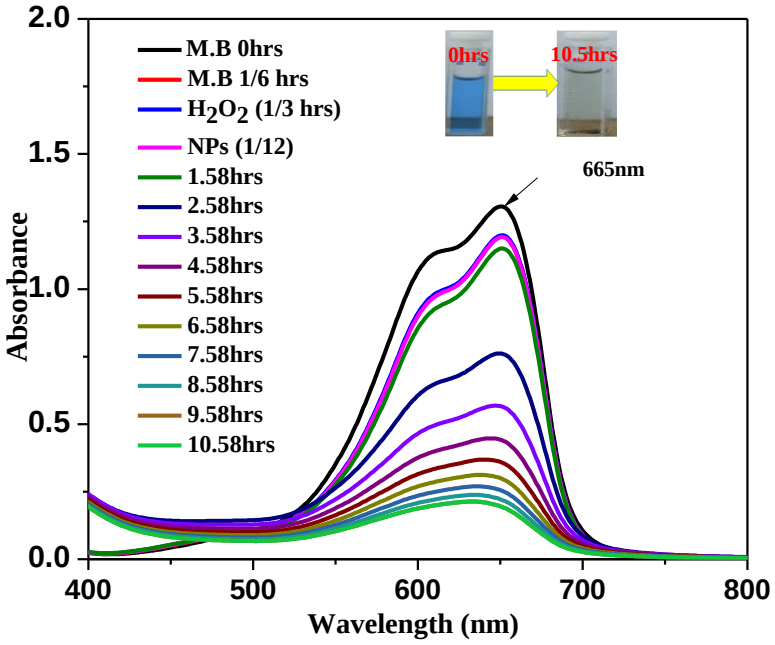

Figure 4.17: Degradation of Methylene blue using CbNPs in the presence of H_2O_2 at pH 7

From the graph, it was observed that the blue color of Methylene blue disappeared with time as the absorbance also reduced revealing degradation of Methylene blue after 10 and half hours (Chauhan *et al.*, 2013a). The degradation process of Methylene blue in the presence of CbNPs and H_2O_2 at pH 3 was performed and the spectra are presented below **(Figure 4.18)**.

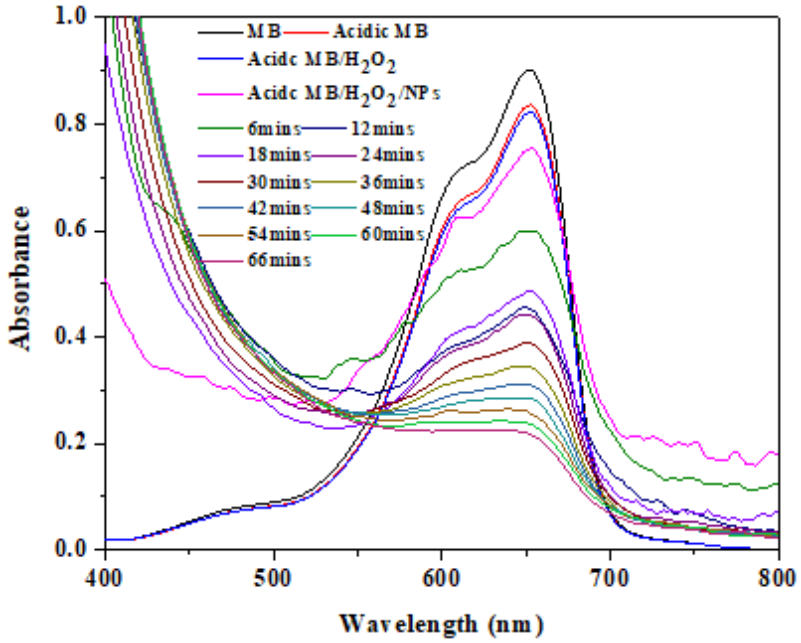

Figure 4.18: Degradation of Methylene blue using CbNPs at pH 3 in the presence of H_2O_2

From the graph **(Figure 4.18)** it was observed that the blue color of Methylene blue at pH 3 disappeared with time as the absorbance also reduced revealing degradation of Methylene blue after about 1 hour. **Figure 4.19** displays the spectral analysis of the degradation process of Methylene blue in the presence of CbNPs and H_2O_2 at pH 12.

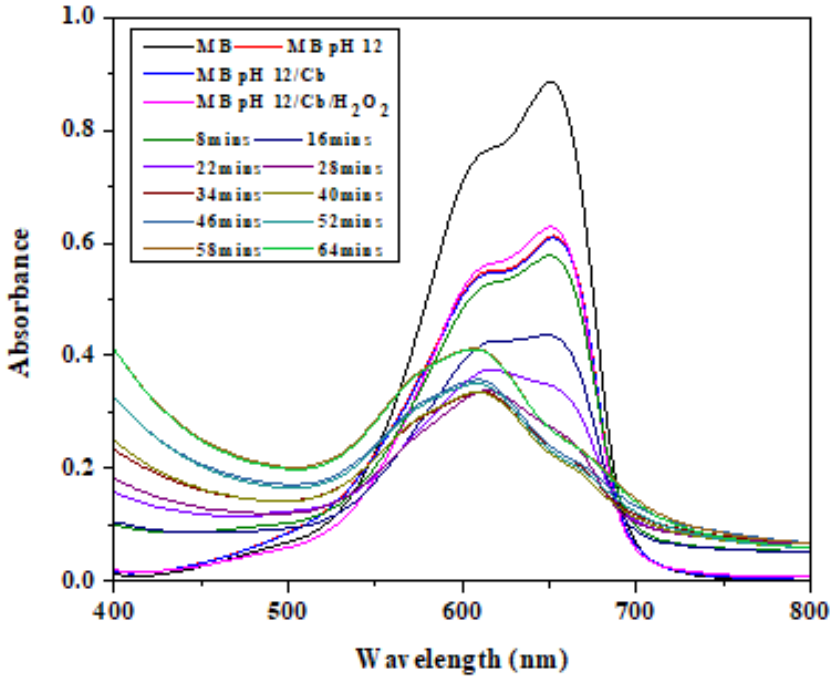

Figure 4.19: Degradation of Methylene blue using CbNPs at pH 12 in the presence of H_2O_2

From the graph **(Figure 4.19)** it was observed that the blue color of Methylene blue at pH 12 disappeared with time as the absorbance also reduced revealing degradation of Methylene blue after about 1 hour. From the spectra obtained **(Figures 4.17–4.19** and **Appendix III (A)–III (D))**, it was clear that CbNPs can degrade Methylene blue and the process is determined by the pH of the solution. **Table 4.3** illustrates the percentage degradation of Methylene blue at pH 3, 7 and 12 using GpNP, BpNP and CbNP in the presence of 0.5 microlitres of hydrogen peroxide.

Table 4.3: Percentage Degradation of Methylene blue at Neural pH, pH 3 and 12 Using Iron Nanoparticles

Nanoparticles	pH	Time taken (mins)	Percentage Degradation (%)
GpNPs/ H_2O_2	3	84	91
CbNPs/ H_2O_2		66	74
BpNPs/ H_2O_2		90	91
GpNPs/ H_2O_2	12	88	65
CbNPs/ H_2O_2		64	64
BpNPs/ H_2O_2		64	67
GpNPs/ H_2O_2	7	256	93
CbNPs/ H_2O_2		635	86
BpNPs/ H_2O_2		330	84

As observed from **Figures 4.17–4.19** above and **Table 4.3**, hydrogen peroxide alone degraded the dye by 6.85% while the GpNPs, BpNPs and CbNPs alone degraded it by 0.47%, 0.55% and 2.13% respectively taking a longer time. The absorbance of Methylene blue at a wavelength range of 400–800 nm remained the same for about 20 minutes but upon the addition of hydrogen peroxide, there was a small drop in absorption spectra due degradation of the dye by hydrogen peroxide. The addition of the nanoparticles (GpNP, BpNP and CbNP) provoked further degradation of the dye up to 93, 84 and 86% within contact times of 256, 330 and 635 minutes respectively. The nanoparticles, as well as hydrogen peroxide alone had no appreciable effect on the degradation of the dye but the introduction of the nanoparticles in the hydrogen peroxide–treated dye caused degradation to happen. It reported that the main active species responsible for the degradation of the dye is the hydroxyl radical and the catalytic degradation activity of the iron nanoparticles is a result of electronic transitions between iron and oxygen in the nanoparticles which leads to an exciton emission (electron) in the valence band, consisting of Fe (3d) and O (2p) being excited to the conduction band that consists of Fe (4s and 3d) and O (2p). This creates a positively charged hole in the valence band and negatively charged conduction band, which reacts with hydrogen peroxide and water producing reactive hydroxyl radicals

that cleave on the chromophore of the dye reacting with it and converting it into harmless chemicals such as carbon IV oxide and water through Fenton and Fenton like reactions (Chauhan *et al*., 2013b; Gui *et al*., 2012; Lassoued *et al*., 2018; Luo *et al*., 2010; Shah *et al*., 2019; Shahwan *et al*., 2011). Since the Fenton reagent (Fe^{2+}/H_2O_2) is active in the easy formation of active intermediates, it is widely applied in forming highly reactive $OH^{\bullet}$ radicals and high valent iron oxo species. The mechanism of production of the active free radicals involves the reduction and oxidation of Ferric and ferrous cations through reaction with hydrogen peroxide as shown in **Equations 5** and **6** below (Wang *et al.*, 2014).

$$Fe^{2+} + H_2O_2 \rightarrow Fe^{3+} + {\cdot}OH + OH^- \ldots\ldots\ldots\ldots\ldots\ldots\ldots\ldots \mathbf{5}$$

$$Fe^{3+} + H_2O_2 \rightarrow Fe^{2+} + {\cdot}OOH + H^+ \ldots\ldots\ldots\ldots\ldots\ldots\ldots\ldots \mathbf{6}$$

When the pH of the dye was adjusted to 3 using 0.1 M HCl and to 12 using 0.1 M NaOH by adding the drop of the solution by drop and monitoring using a pH meter. It was observed that degradation was fast as it took 66 minutes for CbNPs and 90 minutes for GpNPs and BpNPs, respectively to degrade the dye. While at a basic pH of 12, degradation was slow with much of a shift in the peak at 665 nm to a lower wavelength and a gradual drop in the absorbance, however, the process was faster than at pH 7. The pH of the solution plays a big role in the degradation of any pollutant as it modifies the surface charge of the catalyst and the chemical structure of the pollutant, hence influencing the photocatalytic activity of the nanoparticles. Before the reaction, the zero valent nanoparticles are dominant and when treated with the acid the basic Fe_3O_4 is dissolved and the content of Fe^{3+} and Fe^{2+} increases. However, in the basic environment, the nature of degradation is attributed to the adsorptive behavior of the dye onto the nanoparticles as a result of basic media (Freyria *et al.*, 2017).

4.3.2 Influence of Dosage on Degradation of Methylene blue

The degradation of Methylene blue was evaluated using dosages of 1 mg, 5 mg, 10 mg and 20 mg of CbNPs, BpNp and GpNP nanoparticles at pH 7. Degradation of

Methylene blue at a dosage of 1 mg of CbNPs in the presence of H_2O_2 was performed and the spectra were recorded as shown below **(Figure 4.20)**.

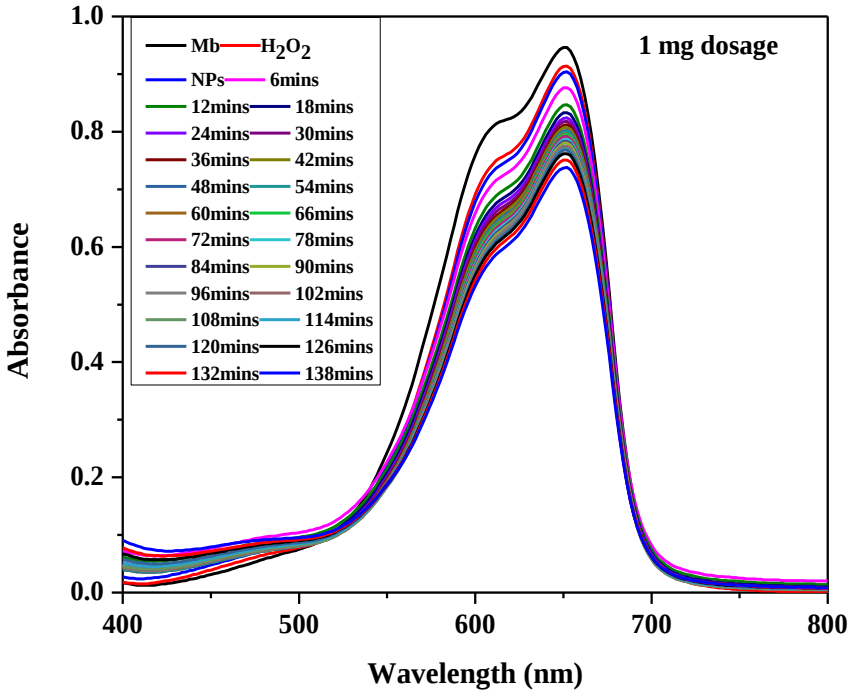

Figure 4.20: Degradation of Methylene blue using 1 mg of CbNPs in the presence of H_2O_2

From the spectra **(Figure 4.20)**, degradation of Methylene blue at a dosage of 1 mg took 138 minutes though degradation did not come to completion. This is observed with the peak not yet flattened. In comparison to a dosage of 1 mg, degradation of Methylene blue at a dosage of 10 mg of CbNPs in the presence of H_2O_2 was also performed and the spectra were drawn as below **(Figure 4.20)**.

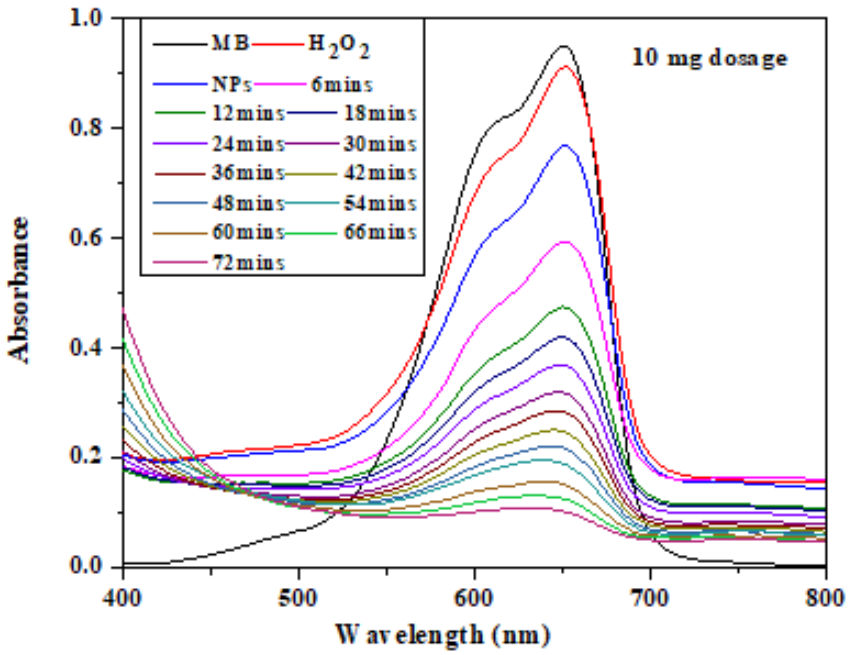

Figure 4.21: Degradation of Methylene blue using 10 mg of CbNPs in the presence of H_2O_2

From the spectra **(Figure 4.21)**, degradation of Methylene blue at a dosage of 10 mg took 72 minutes and degradation was complete. This is observed with the flattened peak. From the spectra obtained **(Figure 4.20** and **4.21)**, the degradation of Methylene blue depends on the dose of the nanoparticles used. When the dose is increased, degradation increases due to an increase in the surface area of the nanoparticles. The percentage removal of Methylene blue using the nanoparticles at various dosages was performed and percentage removal efficiency was obtained **(Table 4.4)** as shown below.

Table 4.4: Percentage Removal Efficiency of Methylene Blue using Particle Dosage

Nanoparticles	Dosage	Time (mins)	Removal efficiency (%)
CbNP	1 mg	Over 222	17.27
	5 mg	222	98.24
	10 mg	72	98.84
	20 mg	42	92.33
BpNP	1 mg	Over 200	20.15
	5 mg	164	93.20
	10 mg	78	90.13
	20 mg	66	89.38
GpNP	1 mg	Over 200	19.16
	5 mg	122	97.78
	10 mg	78	92.93
	20 mg	68	93.72

From **Table 4.4**, it is clear that the percentage degradation increases with an increase in the dosage of the nanoparticles and the time taken reduces. It was observed that the rate of degradation of Methylene blue increased with an increase in the particle dose at room temperature. It was observed that when the amount of nanoparticles dose used was 10 and 20 mg, the percentage degradation achieved, and the time required to degrade the antibiotic were higher and faster, respectively. The high nanoparticles dosage increases the total surface area to volume ratio of the catalyst thereby increasing the high pore–filling effect and active sites needed for producing the radicals needed to degrade Methylene blue and the high chances of colliding with the dye (Cai *et al*., 2019; Chauhan *et al*., 2018; Nasuhoglu *et al*., 2012; Rezaei and Vione, 2018; Teixeira *et al*., 2016; Weng *et al*., 2016).

4.3.3 Influence of Reaction Temperature on Degradatin of Methylene blue

The effect of reaction temperature was studied on the degradation of Methylene blue at temperatures of 25ºC (298 K), 30ºC (303 K), 40ºC (313 K), 50ºC (323 K) and 60ºC

(333 K). Degradation of Methylene blue using CbNPs in presence of H_2O_2 at 25℃ was determined and the spectral results are shown below **(Figure 4.22)**.

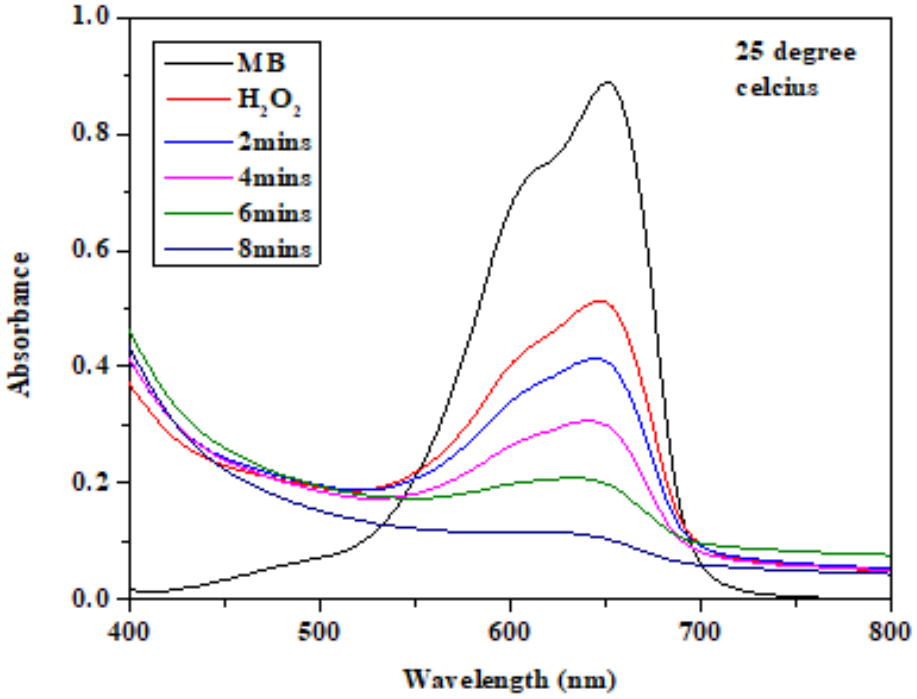

Figure 4.22: Degradation of Methylene blue using CbNPs in presence of H_2O_2 at 25 ℃

From the graph **(Figure 4.22)**, at room temperature, the degradation of Methylene blue took 8 minutes. Degradation of Methylene blue using CbNPs in the presence of H_2O_2 was performed at a temperature of 60 ℃ and results are as shown below **(Figure 4.23)**.

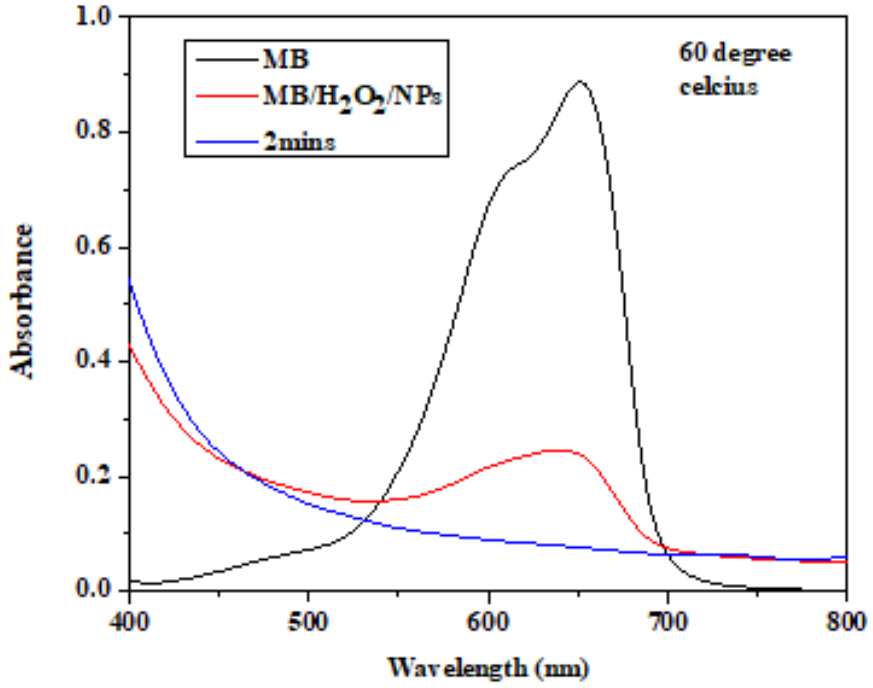

Figure 4.23: Degradation of Methylene blue using CbNPs in the presence of H_2O_2 at 60℃

The degradation rate increased at a temperature of 60 ℃ **(Figure 4.23)**. From **Figure 4.22–4.23** and **Appendix IV (A) – IV (C)**, degradation of Methylene blue is temperature dependent as an increase in temperature for degradation of the dye using the nanoparticles in the presence of H_2O_2 showed a higher percentage removal in a shorter time. It was observed that degrading Methylene blue at 60℃ (333 K) took a shorter time than at 25℃ (298 K). **Table 4.5** below shows a summary of the percentage degradation of Methylene blue using CbNPs in the presence of H_2O_2 at various temperatures.

Table 4.5: Percentage Degradation of Methylene blue at Various Temperatures

Nanoparticles	Temperature (K)	Time (in minutes)	Percentage degradation (%)
CbNPs	298	8	88
	303	6	89
	313	4	86
	323	3	90
	333	2	92
GpNPs	298	12	88
	303	10	88
	313	8	87
	323	8	85
	333	6	91
BpNPs	298	10	95
	303	8	96
	313	6	96
	323	4	95
	333	3	96

This process is temperature dependent as it took a shorter time for oxidation, decolorization and degradation of Methylene blue to occur and the effect of solution temperature on the removal efficiency illustrates that as the temperature increased, the removal efficiency was high and high percentages were obtained in 2 and 3 minutes for CbNPs and BpNPs, respectively and 6 minutes for GpNPs **(Table 4.5)**. Increase in temperature enhances the degradation of Methylene blue by the nanoparticles as it activates the surface and promotes charge repulsions favouring adsorption and catalytic reactions (Das *et al*., 2018; Nan *et al*., 2010). To determine the heat change and entropy of the processes, Van't Hoff's equation was employed and the results were obtained for the degradation of Methylene blue using CbNPs at various temperatures as illustrated in the below graphical summary **(Figure 4.24)**.

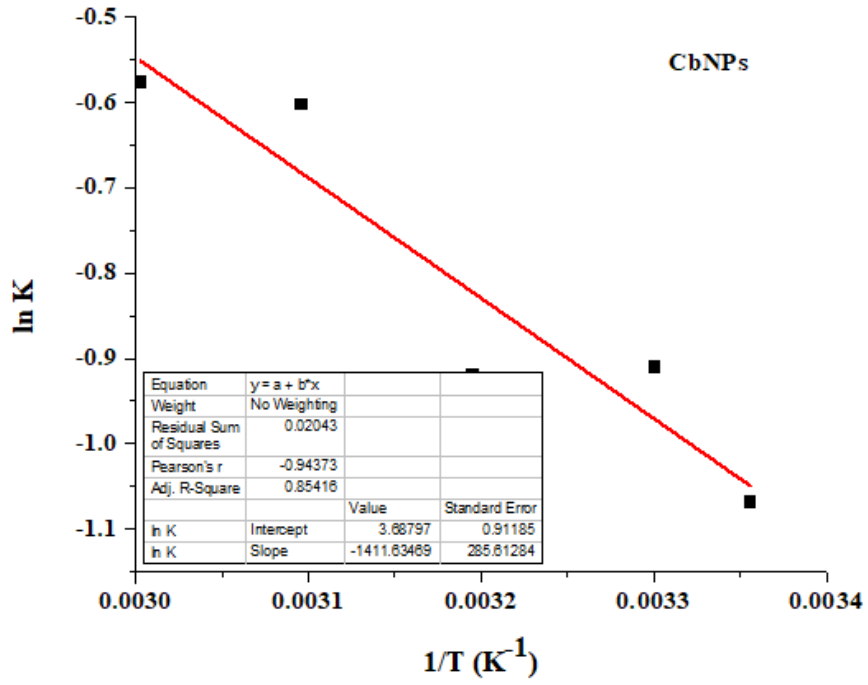

Figure 4.24: Van't Hoff's Plot of Methylene blue degradation by CbNPs at various temperatures

From the study **(Figure 4.24)**, it was observed that the degradation of Methylene blue was temperature dependent as at higher temperatures it took less time for the pollutant to be oxidized, decolorized and degraded unlike at lower temperatures. This shows that the degradation of Methylene blue was an endothermic reaction implying that at higher temperatures the rate of degradation was higher. For an endothermic reaction, the entropy of the reaction increases and is reduced when the temperature of the reaction system is raised propelling the reaction towards the formation of the products, in this case degradation of Methylene blue. According to Le Chatelier's principle, for an endothermic reaction, when the temperature increases, the system shifts to the right to alleviate the stress of additional heat hence an increase in the products and a decrease in the reactants. A shift to the left leads to a decrease in products and an increase in reactants, which decreases the equilibrium constant as predicted by the Van't Hoff equation (Atkins and Paula, 2009). Since degradation of the dye was temperature depend, this provided an experimental way of determining the heat change **(ΔH)** and change in entropy **(ΔS)** using the equilibrium

constant and was found to be 28.81 kJ mol^{-1} and 69.39 J mol^{-1}, respectively (Atkins and Paula, 2009).

4.3.4 Influence of Exposure to Sunlight on Degradation of Methylene blue

The photocatalytic efficiency of the catalysts (using CbNPs, BpNPs and GpNPs) nanoparticles was evaluated by photocatalytic degradation of Methylene blue in aqueous solution through natural sunlight irradiation and monitoring the intensity of the characteristic Methylene blue absorption peak at 665 nm and the results are shown below **(Figure 4.25)**.

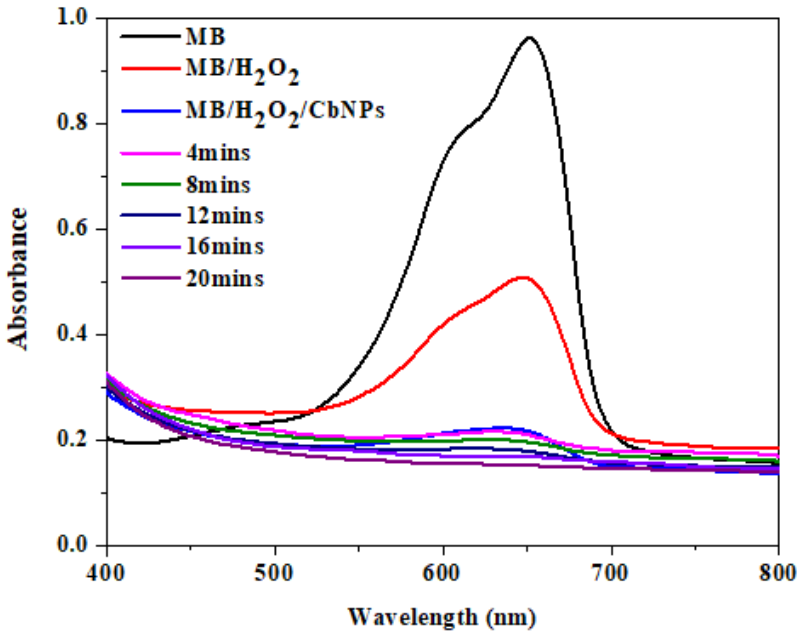

Figure 4.25: Sunlight assisted degradation of Methylene blue by CbNPs/H_2O_2 catalyst

From the spectra obtained, it took 20 minutes to degrade Methylene blue with CbNp as a catalyst in the presence of sunlight. To check on the possibility of the effect of sunlight on the degradation of Methylene blue using the nanoparticles, spectral scanning was performed and the results are summarized below **(Table 4.6)**.

Table 4.6: Sunlight Assisted CbNps, BpNps and GpNps for Methylene blue Removal Efficiency

Nanoparticles	Time (mins)	Percentage Removal (%)
CbNP	20	95
GpNP	18	92
BpNP	18	93

From **Figure 4.25** and **Table 4.6** above, the photolytic degradation of Methylene blue was slow without the photocatalysts under sunlight irradiation, suggesting its high stability under visible sunlight illumination. Oxidation, decoloration and degradation of the dye without the catalyst and sunlight were found negligible indicating that the availability of the catalyst and sunlight is effective in the photodegradation of Methylene blue (Akram *et al*., 2020; Das *et al*., 2018; Hou *et al*., 2012; Salama *et al*., 2018; Sukanya *et al*., 2020). In the presence of sunlight, iron nanoparticles absorb enough photons and electrons in the valence band are excited to the conduction band thereby producing valence band holes. The photogenerated holes on the surface of the nanoparticle and electrons react with water and hydrogen peroxide producing $OH^{\cdot}$ radicals that oxidize the dye (Parhizkar and Habibi, 2017). The photogenerated electrons are also available for reaction with O_2 and H_2O_2 producing superoxide ions and OH radicals as shown in **Equations 7–10** below. These numerous amounts of radicals produced then engage in reacting with the dye thereby oxidizing and degrading it.

$$Fe_3O_{4(VB)} \rightarrow Fe_3O_{4(CB)} + e^- \ldots\ldots\ldots\ldots \mathbf{7}$$

$$h^+ + OH^- \rightarrow OH^{\cdot} \ldots\ldots\ldots\ldots\ldots\ldots\ldots\ldots\ldots \mathbf{8}$$

$$e^- + O_2 \rightarrow O_2^{\cdot} - \ldots\ldots\ldots\ldots\ldots\ldots\ldots\ldots\ldots\ldots \mathbf{9}$$

$$H_2O_2 + O_2^{\cdot} - \rightarrow OH^{\cdot} + OH^- + O_2 \ldots\ldots\ldots\ldots\ldots\ldots \mathbf{10}$$

4.3.5 Degradation Kinetics of Methylene blue at Different pH

The kinetics of the degradation of Methylene blue was studied by employing the first and second–order models at pH 7, pH 3 and pH 12. The results for degradation of Methylene blue at first–order and pH 3 are illustrated in **Figure 4.26**.

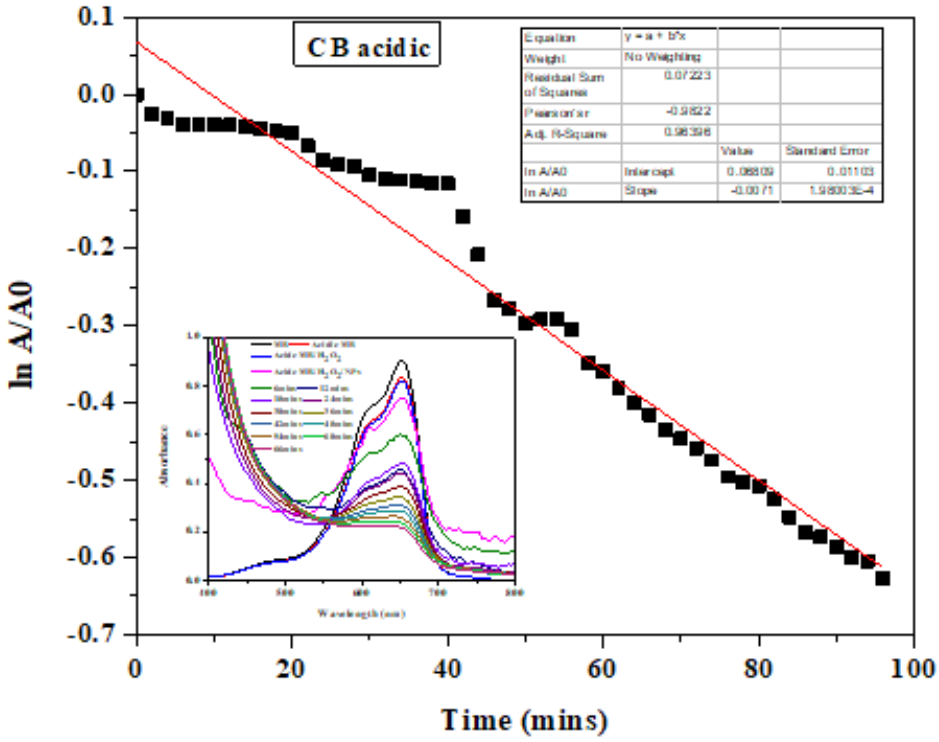

Figure 4.26: Second–order kinetics for Methylene blue degradation by *C. bonariensis* at pH 3

From **Figure 4.26**, the reaction clearly followed a first–order reaction and the process was pH dependent. Degradation of Methylene blue was also performed at pH 7 and the results are illustrated in the graph below **(Figure 4.27)**.

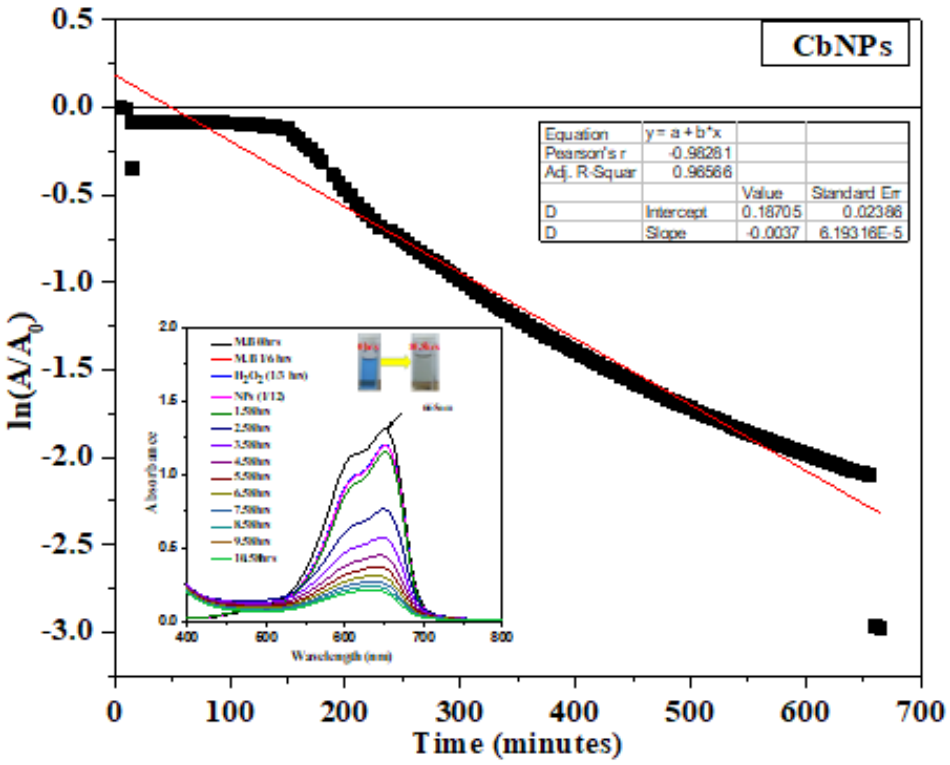

Figure 4.27: Kinetics of Methylene blue degradation using CbNPs at pH 7

From the results **(Figure 4.27)**, the degradation of Methylene blue followed a first–order process in a basic environment. Methylene blue was degraded within 20 minutes depecting that the process depends on the pH of the solution. To determine the kinetic behavior of degradation of Methylene blue at pH 3, pH 7, and pH 12 using the nanoparticles, the R^2, k and rate constants **(Table 4.7)** were determined and listed as shown below.

Table 4.7: Rate Constant (k) for Degradation of Methylene blue at pH 3, pH 7 and 12

Sample ID	pH	1st Order		2nd Order		Rate (µmol/L min)
		R^2	k	R^2	k	
BpNPs	3	0.9765	-0.0011	0.8920	0.2312	-2.8×10^{-4}
CbNPs		0.9640	-0.0071	0.9172	0.0424	-1.8×10^{-3}
GpNPs		0.9749	-0.0011	0.8999	0.3548	-2.8×10^{-4}
BpNPs	12	0.9239	-0.0031	0.8764	0.1267	-7.8×10^{-4}
CbNPs		0.9310	-0.0067	0.9330	0.2277	-1.8×10^{-4}
GpNPs		0.9709	-0.0021	0.8602	0.2178	-1.1×10^{-4}
BpNPs	7	0.9516	-0.0064	0.9334	0.1024	-3.2×10^{-4}
CbNPs		0.9657	-0.0037	0.9784	0.2105	-9.3×10^{-4}
GpNPs		0.9837	-0.0041	0.9685	0.1130	-5.1×10^{-4}

From **Table 4.7**, CbNPs, BpNPs and GpNPs degradation of Methylene blue and studies on the first–order and second–order performed. The rate constants were –3.37 x 10^{-3}, –8.35 x 10^{-3}, and –1.456 x 10^{-3} per minute respectively as the R^2 value was closer to 1 than in the second–order (Shah *et al*., 2019). As observed in **Figures 4.27–4.28** and **Table 4.7**, degradation seemed to follow first–order as pH alters the state of the catalyst and the solution and accounts for the ease of formation of the hydroxyl groups which activates the active sites of the nanoparticles thus initiating the reaction. For example, in acidic media, the removal efficiency was higher as the particles were more positively charged leading to a collision with hydrogen peroxide producing numerous hydroxyl radicals (Rezaei and Vione, 2018; Cai *et al*., 2019; Weng *et al.*, 2016).

4.4 Degradation of Rifampicin

The iron nanoparticles were investigated for their catalytic properties in the degradation of Rifampicin at various pH, temperature and nanoparticle dosages.

4.4.1 Influence of Solution pH on Degradation

The effect of the pH on the catalytic degradation of Rifampicin by iron nanoparticles was studied and the results for H_2O_2 alone are depicted in **Figure 4.28**.

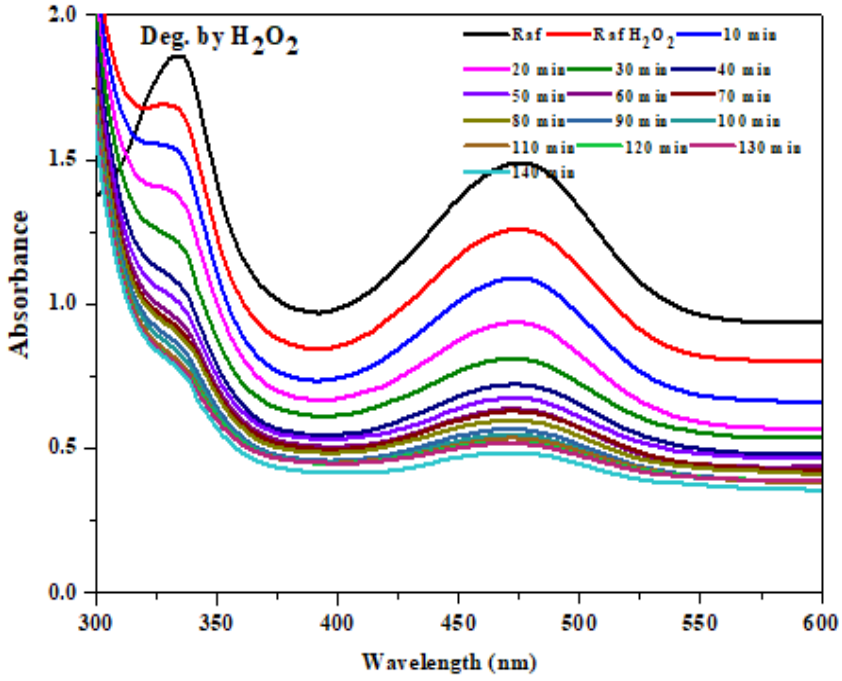

Figure 4.28: Degradation of Rifampicin using H_2O_2 at pH 7

The degradation of Rifampicin depends on the environment of the solution. The use of H_2O_2 alone showed that the process took longer to degrade the antibiotic. The effect of pH on the catalytic degradation of Rifampicin by iron nanoparticles was studied and the results for H_2O_2 and CbNps are depicted in **Figure 4.29**.

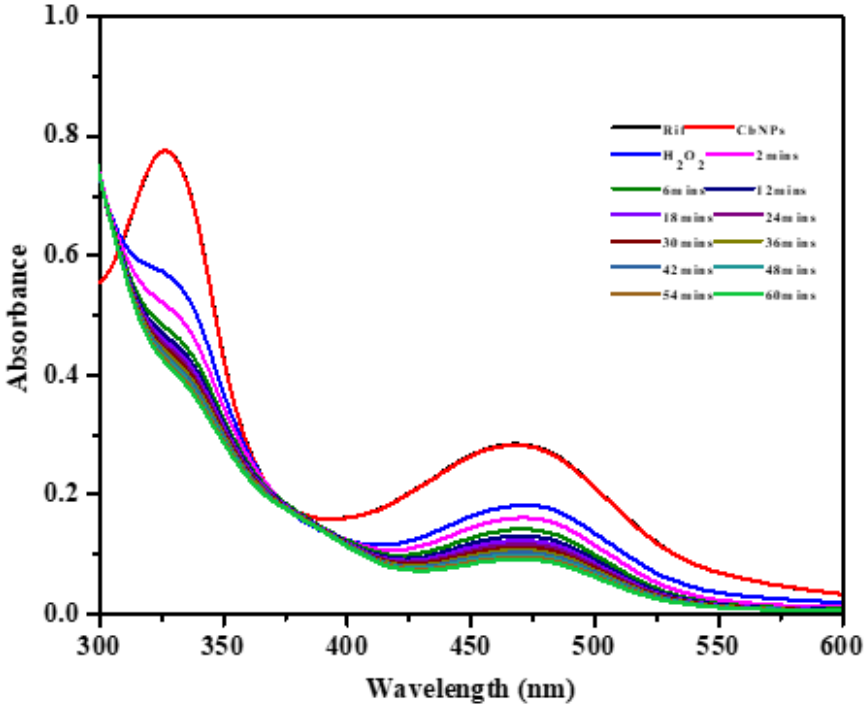

Figure 4.29: Degradation of Rifampicin by CbNPs/H_2O_2 at pH 7

The additon of the nanoparticles in the solution revealed a shorter time of degradation of Rifampicin H_2O_2 alone took 140 minutes to degrade Rifampicin. However, the addition of nanoparticles to H_2O_2 containing Rifampicin solution took 60 minutes. The addition of nanoparticles initiates further effect on the compounds thereby degrading them. Besides, a change in the pH of the solution initiates a faster reaction due to the development of radicals. The presence of the nanoparticles and H_2O_2 in the solution helps in development of radicals that initiate degradation (Aksu Demirezen *et al*., 2019; Rezaei and Vione, 2018). Degradation of Rifampicin by iron nanoparticles was studied at a pH of 3 and the results are depicted in **Figure 4.30**.

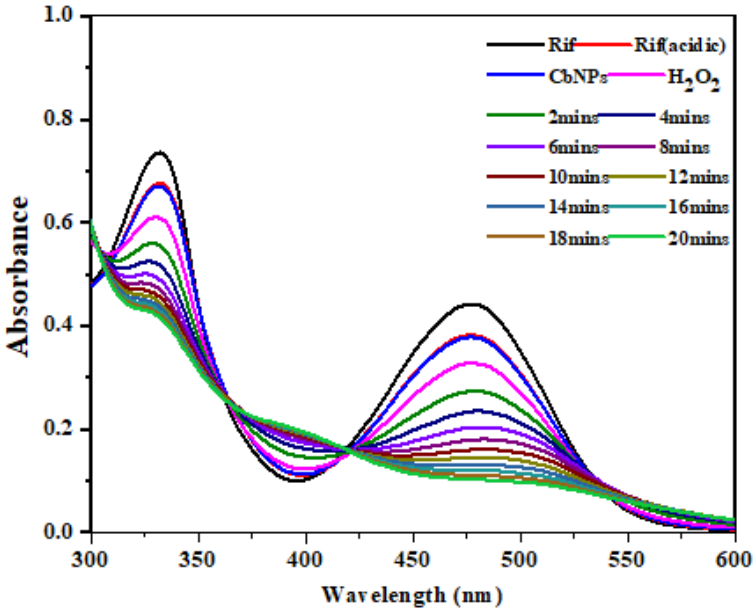

Figure 4.30: Degradation of Rifampicin by CbNPs in presence of H_2O_2 at pH 3

From **Figure 4.30**, Rifampicin was degraded in 20 minutes at a pH of 3. The effect of the pH on the catalytic degradation of Rifampicin by iron nanoparticles was studied and the results are depicted in **Figure 4.31**.

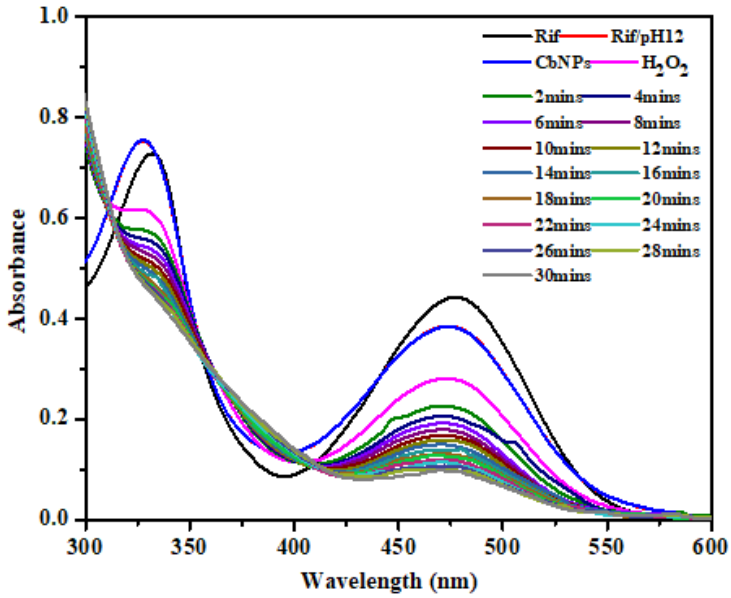

Figure 4.31: Degradation of Rifampicin by CbNPs in presence of H_2O_2 at pH 12

From **Figure 4.31**, Rifampicin was degraded in 30 minutes at a pH of 12. A summary of the degradation of Rifampicin by the nanoparticles at pH 3, 7 and 12 **(Table 4.8)** as shown below.

Table 4.8: Degradation Efficiency of Rifampicin by CbNP, BpNP and GpNP at Various pH

Reaction Parameters	pH	Percentage degradation (%)	Time (min)
H_2O_2	7	58	180
CbNPs/ H_2O_2	7	68	68
GpNPs/ H_2O_2		78	52
BpNPs/ H_2O_2		80	64
CbNPs/ H_2O_2	3	87	20
GpNPs/H_2O_2		87	16
BpNPs/ H_2O_2		89	12
CbNPs/ H_2O_2	12	88	30
GpNPs/H_2O_2		86	24
BpNPs/ H_2O_2		82	24

From the results obtained in **Figures 4.28–4.31**, the oxidation of Rifampicin was influenced greatly by pH which resulted in spectral changes in the degradation process. It was observed that when degradation of the antibiotic using hydrogen peroxide alone was done, it took 180 minutes for the drug to be oxidized with a removal efficiency of 58% as compared to when it was done in the presence of the nanoparticles. In acidic and basic pH, degradation happened in a short time and with higher efficiencies. However, degradation was faster in acidic than in basic media which is influenced by the kind of ions present in the two solutions. The use of hydrogen peroxide and the nanoparticles in the degradation of Rifampicin was higher compared to when nanoparticles and hydrogen peroxide were used alone. This is attributed to the generation of additional hydroxyl radicals when the electrons in the conduction band

of the iron nanoparticles interacted with hydrogen peroxide according to **Equations 11** and **12** below (Chauhan *et al.*, 2018; Liu *et al*., 2016; Pantelidou *et al*., 2015).

$$2H^+ + 2H_2O_2 + e^- \rightarrow OH^{\cdot} + OH^- + 2H_2O \ldots\ldots\ldots\ldots\ldots\ldots\ldots\ldots\ldots\ldots \mathbf{11}$$

$$H_2O_2 + O_2- \rightarrow OH^{\cdot} + OH^- + O_2 \ldots\ldots\ldots\ldots\ldots\ldots\ldots\ldots\ldots\ldots\ldots\ldots\ldots \mathbf{12}$$

The oxidation of Rifampicin in the presence of iron nanoparticles and hydrogen peroxide was faster when the pH of the solution was acidic or basic than at pH 7. As observed in **Figures 4.28–4.31**, varying the pH of the Rifampicin solution resulted in a remarkable decrease in the absorption intensity of Rifampicin solution as alteration of the pH to either acid or basic media resulted in a hypsochromic shift in the absorption intensities of Rifampicin. The degradation of Rifampicin at a pH of 3 and 12 was higher as it took approximately between 10 and 30 minutes for the drug to be degraded as confirmed by the rapid decrease in the absorption intensities centered at 480 nm respectively. The synthesized nanoparticles had a remarkable degradation behaviour in acidic and basic media. BpNPs, CbNPs and GpNPs nanoparticles in the presence of H_2O_2 at pH 3 degraded Rifampicin within 12, 20 and 16 minutes and at pH 12 in 24, 24 and 30 minutes with removal efficiencies of over 80%). The increase in degradation in the basic media is attributed to the increase in the hydroxyl groups which activates the active sites of the nanoparticles thus initiating the reaction while in acidic media, the removal efficiency was higher as the nanoparticles were more positively charged leading to collision with hydrogen peroxide producing numerous hydroxyl radicals (Rezaei and Vione, 2018; Cai *et al*., 2019; Weng *et al*., 2016). The basic environment was not favored as compared to the acidic due to the formation of an oxide layer on the surface of the nanoparticles which decreased the diffusion of Rifampicin into the nanoparticles, thereby reducing the production of hydroxyl radicals thus deactivating the active site (Aksu Demirezen *et al*., 2019; Rezaei and Vione, 2018).

4.4.2 Influence of Dosage on Degradation of Rifampicin

The effect of the number of iron nanoparticles on the rate of degradation was studied and the results for the impact of nanoparticles dosage on the percent removal of Rifampicin are illustrated in **Figure 4.32–4.33** and **Appendix III (G) – (I). Figure 4.32** illustrates degradation of Rifampicin by 1 mg of CbNPs in the presence of H_2O_2.

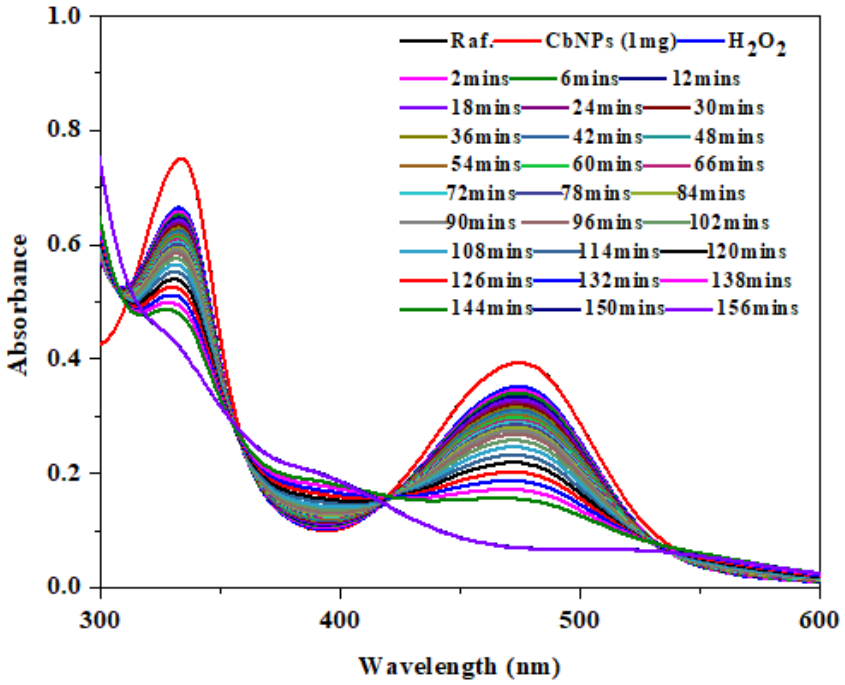

Figure 4.32: Degradation of Rifampicin by 1 mg of CbNPs in the presence of H_2O_2

From **Figure 4.32**, it was clear that a dose of 1 mg of CbNPs took 156 minutes to degrade Rifampicin. To check the effect of increasing the dosage of nanoparticles in degrading Rifampicin, degradation as performed at a dosage of 20 mg of CbNPs in the presence of H_2O_2 **(Figure 4.32)**.

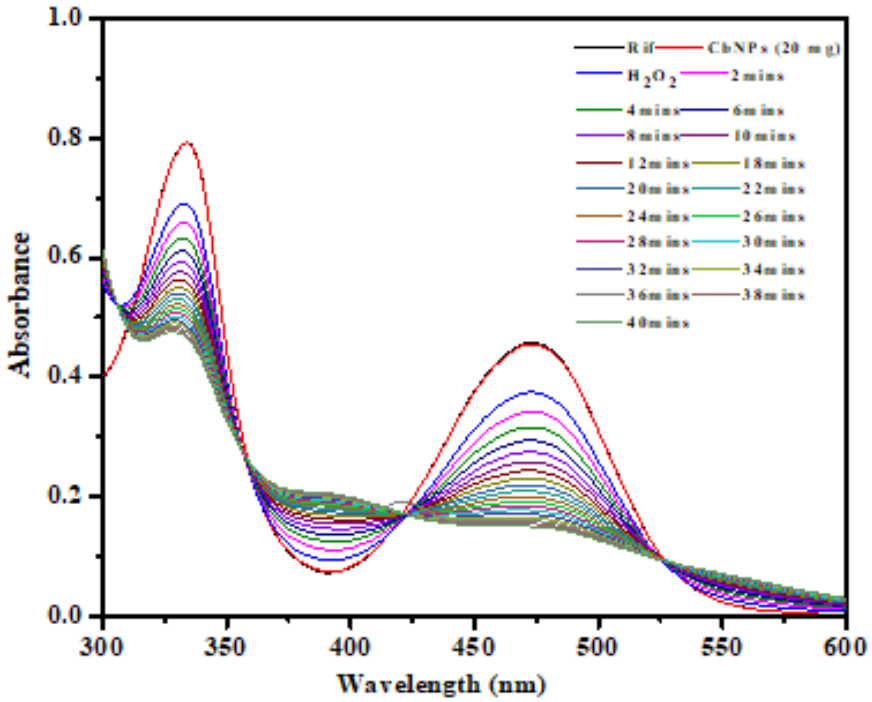

Figure 4.33: Degradation of Rifampicin by 20 mg of CbNPs in presence of H_2O_2

From **Figure 4.32**, it was clear that a dose of 20 mg of CbNPs took 40 minutes to degrade Rifampicin. To determine the percentage removal as a result of increasing dosage **(Table 4.9)** illustrates the percentage removal of Rifampicin at different nanoparticle dosages at room temperature.

Table 4.9: Percentage Removal Efficiency of Rifampicin at Different Nanoparticle Dosage

Dosage	CbNPs		GpNPs		BpNPs	
	Time (mins)	Percentage removal	Time (mins)	Percentage removal	Time (mins)	Percentage removal
1 mg	156	69	138	54	144	48
5 mg	102	70	92	62	80	58
10 mg	84	74	68	64	60	62
20 mg	40	86	44	78	40	66

From **Table 4.9**, as the dosage increased, the time taken to degrade reduced and the percentage degradation increased. From **Figures 4.32–4.33** and **Table 4.8** above, it was inspected that an increase in the catalyst dosage increases the percentage removal within a short time, as a dosage of 20 mg increased the rate at which Rifampicin was degraded as compared to when the amount of catalyst used was 1 mg. It was observed that when the amount of iron nanoparticles used was 20 mg, the percent degradation achieved, and the time required to degrade the antibiotic were 86%, 78%, and 66% for CbNPs, GpNPs and BpNPs, within 40, 44, and 40 minutes, respectively. It was observed that as the dose increased, the rate of removal also increased due to the increase in the total surface area to volume ratio of the nanoparticles, which increased the high pore–filling effect and active sites needed for collision with the Rifampicin and H_2O_2–producing the radicals needed to degrade the antibiotic (Chauhan *et al*., 2018; Nasuhoglu *et al*., 2012; Rezaei and Vione, 2018; Teixeira *et al.*, 2016; Cai *et al.*, 2019; Weng *et al*., 2016).

4.4.3 Influence of Reaction Temperature on Degradation

The effect of the reaction temperature on the rate of degradation of Rifampicin was studied at temperatures ranging from 25, 30, 40, 50 and 60℃ and the results are illustrated in **Figures 4.34–4.35**. **Figure 4.34** depicts the degradation of Rifampicin using iron nanoparticles at 25℃

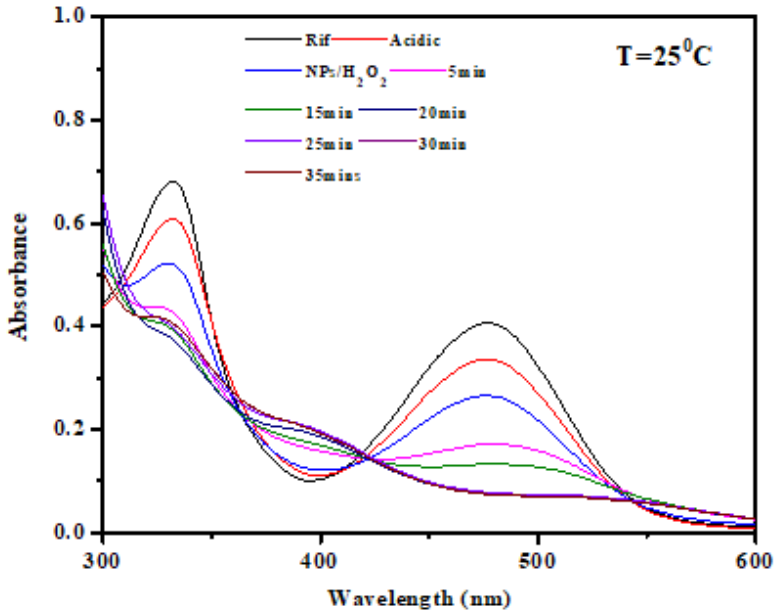

Figure 4.34: Degradation of Rifampicin using iron nanoparticles at 25℃

From **Figure 4.34**, the spectra displayed a degradation time of 35 minutes at a temperature of 25℃. Degradation of Rifampicin using iron nanoparticles at 60 ℃ **(Figure 4.35)** as depicted below.

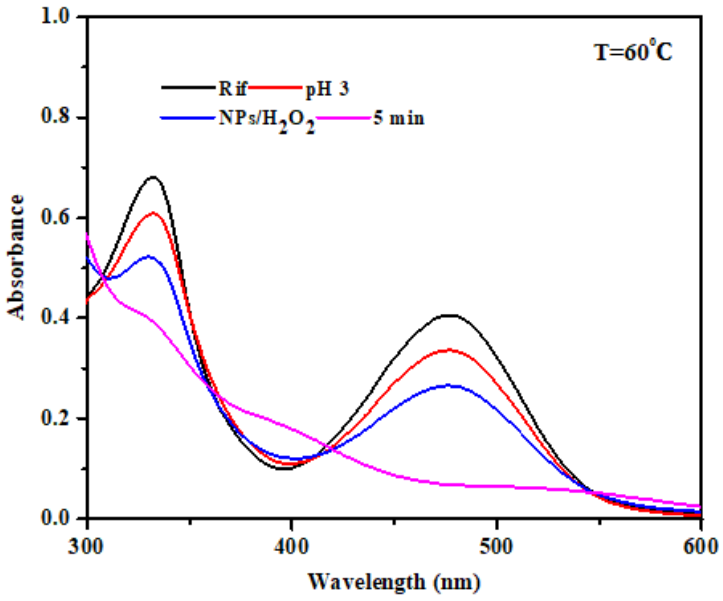

Figure 4.35: Degradation of Rifampicin using iron nanoparticles at 60℃

Figure 4.35 depicts the time taken to degrade Rifampicin at 60°C. From the results, the antibiotic was degraded within 5 minutes. Usually, the rate of any chemical reaction is sensitive and influenced by temperature changes and is important in providing insight into the reaction mechanism (Elkady *et al*., 2014). To determine the entropy and enthalpy of the for the degradation process, the Van't Hoff plot for the degradation of Rifampicin at various temperatures was determined **(Figure 4.36)**.

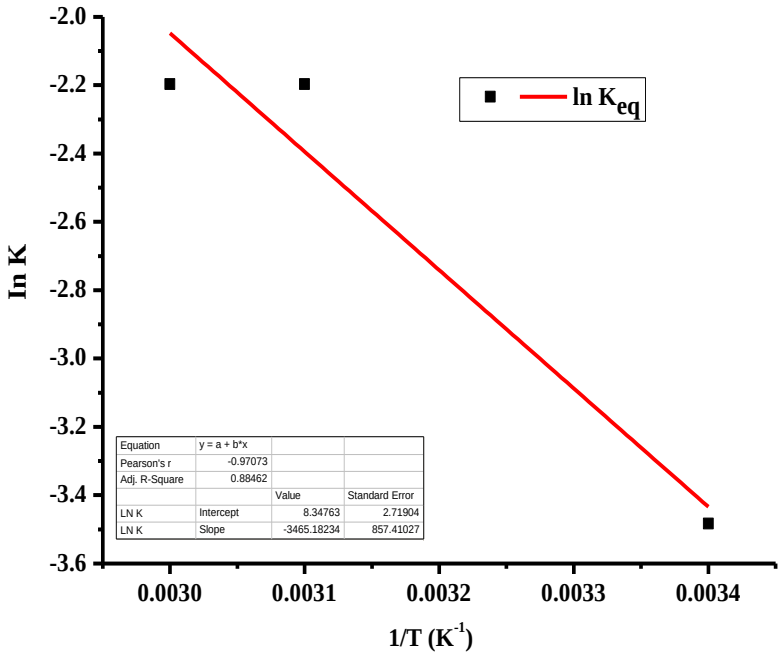

Figure 4.36: Van't Hoff plot for Degradation of Rifampicin by CbNPs

From **Figures 4.34**–**4.35**, it was observed that the degradation of Rifampicin was temperature dependent as raising the temperature had a positive influence on the degradation of Rifampicin. It was observed that Rifampicin could be degraded in 5 minutes at 60 °C. For such a reaction, Le Chatelier's principle predicts that if the temperature increases, the system will therefore shift to the left to alleviate the stress of additional heat. A shift to the left leads to a decrease in products and an increase in reactants, which decreases the equilibrium constant as predicted by the Van't Hoff equation (Atkins and Paula, 2009). The degradation of Rifampicin **(Figure 4.36)** was

an endothermic reaction which implies that at higher temperatures, the reaction shifted to the right and the rate of degradation was higher. For an endothermic reaction, there is a decrease in entropy of the reaction which is increased when the temperature of the reaction system is raised and the reaction moves towards the formation of the products, hence degradation of Rifampicin. The temperature dependence of the equilibrium constant provided a basis in which the Heat Change ($\Delta\mathbf{H}$) and change in Entropy ($\Delta\mathbf{S}$) were experimentally determined from the slope and intercept of the curve **(Figure 4.36)** in this case 28.81 kJ $mol^{-1}$and 69.39 J mol^{-1} respectively (Atkins and Paula, 2009).

4.4.4 Influence of Exposure to Sunlight on Degradation

The photocatalytic efficiency of the catalysts (using CbNPs, BpNPs and GpNPs) nanoparticles was evaluated by photocatalytic degradation of Rifampicin in an aqueous solution through natural sunlight irradiation and monitoring the intensity of the characteristic Rifampicin absorption peak at 476 nm and the results are shown in **Figure 4.37** below.

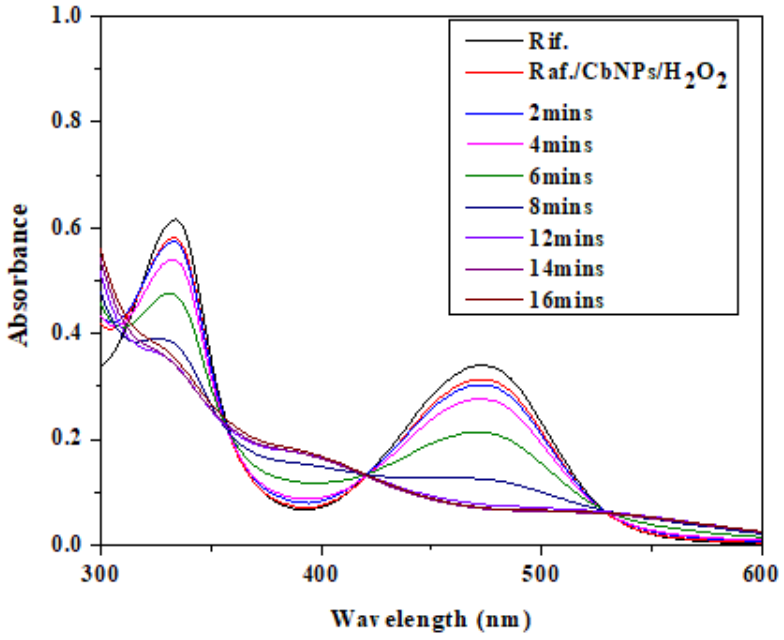

Figure 4.37: Sunlight assisted degradation of Rifampicin using CbNPs

From **Figure 4.37**, Rifampicin was degraded by CbNPs in the presence of sunlight within 16 minutes. **Table 4.10** below illustrates sunlight–assisted degradation of Rifampicin by the nanoparticles at a 10 mg dosage.

Table 4.10: Sunlight Assisted Degradation Efficiency of Rifampicin

Nanoparticles	Time (mins)	Percentage Removal (%)
CbNP	16	92
GpNP	12	94
BpNP	12	93

From **Table 4.10**, it was illustrated that the photolytic degradation of Rifampicin was slow without the photocatalysts suggesting that it is highly stable under visible sunlight illumination. Oxidation, decoloration and degradation of Rifampicin without the catalyst and sunlight were found negligible indicating that the availability of the catalyst and sunlight is effective in the photodegradation of the drug just as for Methylene blue (Akram *et al.*, 2020; Das *et al*., 2018; Hou *et al*., 2012; Salama *et al.*, 2018; Sukanya *et al*., 2020)

4.4.5 Degradation Kinetics of Rifampicin

The pseudo–first–order and second–order were used to analyze the kinetics of the catalytic removal of Rifampicin at various conditions by iron nanoparticles and the results are depicted in **Figures 4.38–4.41, Appendices III (A)** to **III (I)** and **Table 4.11**.

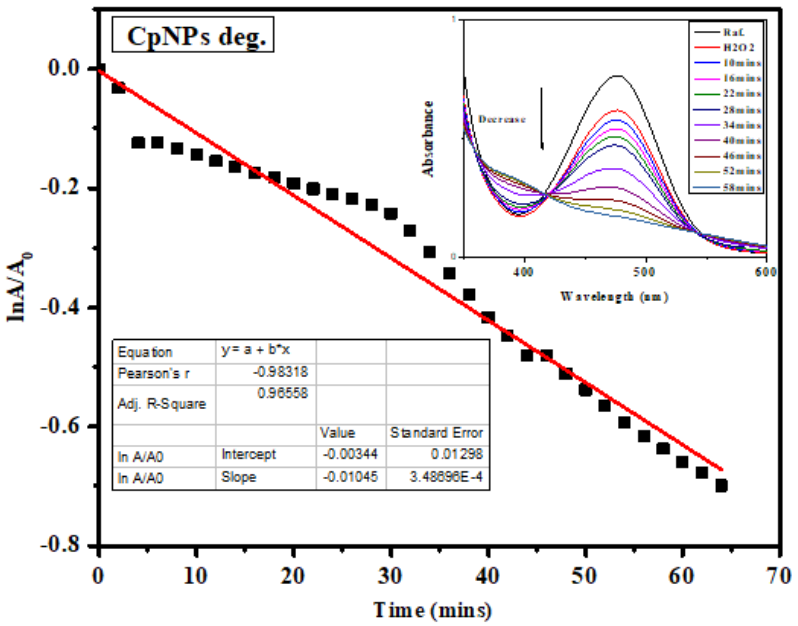

Figure 4.38: First–order plot of Rifampicin degradation using CbNPs/H_2O_2

From the graph **(Figure 4.38)**, the degradation of Rifampicin using CbNPs/H_2O_2 showed that the process took 58 minutes.

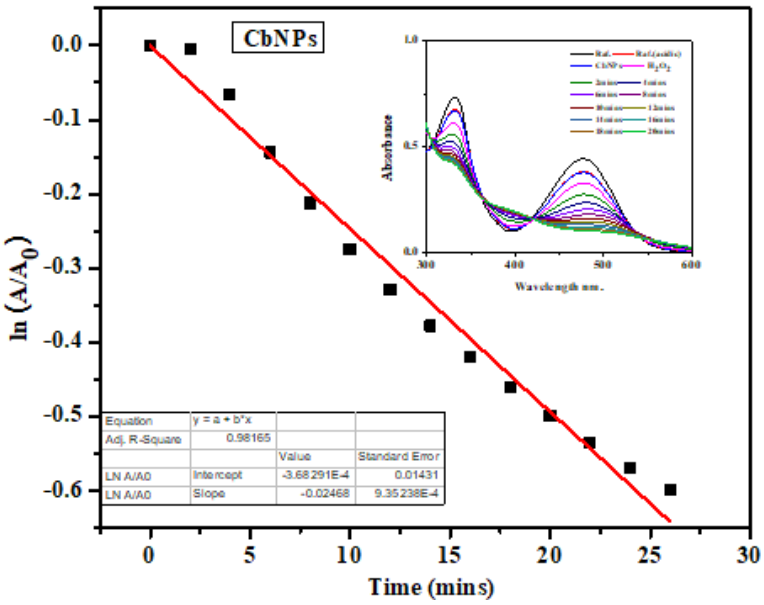

Figure 4.39: First–order plot of Rifampicin degradation using CbNPs/H_2O_2 at pH 3

From **Figure 4.39**, it was observed that the degradation process of Rifampicin using CbNPs/H_2O_2 at pH 3 took 26 minutes and followed a first–order route.

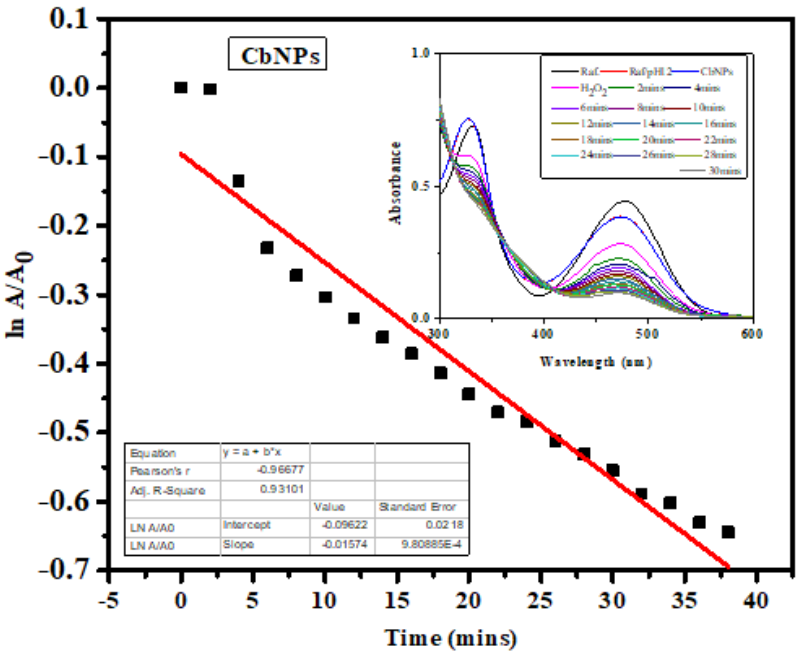

Figure 4.40: First–order plot of Rifampicin degradation using CbNPs/H_2O_2 at pH 12

From **Figure 4.40**, it was observed that the degradation process of Rifampicin was first order.

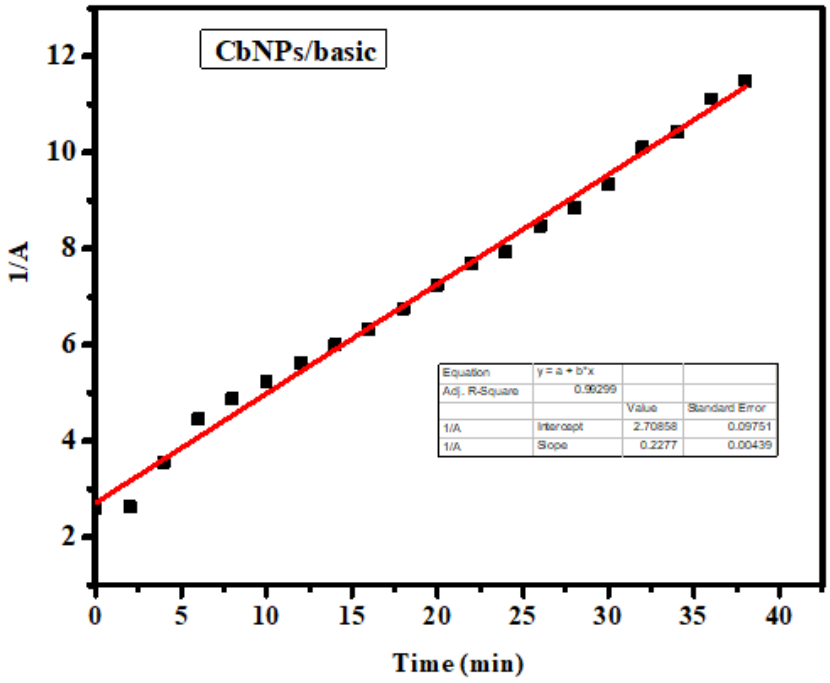

Figure 4.41: Second–order kinetics for degradation of Rifampicin by CbNPs/H_2O_2 at pH 12

From the graphs, it was clear that the degradation of Rifampicin followed a first–order and second–order kinetics. These were complied using the root square rate constants values of the models. To determine the order of reaction, the rate constants for the degradation of Rifampicin at various pH were calculated and are listed in **Table 4.11** below.

Table 4.11: Rate Constant (k) for Degradation of Rifampicin at Different pH

Sample ID	pH	1st Order		2nd Order		Rate (µmol/L min)
		R^2	k	R^2	k	
BpNPs	3	0.9408	-0.0420	0.9004	0.5390	-2.1×10^{-2}
CbNPs		0.9817	-0.0247	0.8022	0.1547	-3.0×10^{-3}
GpNPs		0.9917	-0.0029	0.9829	0.3548	-1.4×10^{-2}
BpNPs	12	0.9339	-0.0131	0.9764	0.1267	-7.8×10^{-3}
CbNPs		0.9310	-0.0167	0.9930	0.2277	-6.6×10^{-3}
GpNPs		0.9709	-0.0200	0.9902	0.2178	-1.1×10^{-2}
BpNPs	7	0.8211	-0.0127	0.9334	0.1024	-3.2×10^{-3}
CbNPs		0.7914	-0.0084	0.9122	0.1409	-2.9×10^{-3}
GpNPs		0.9167	-0.0117	0.9685	0.1130	-7.2×10^{-3}

Depending on pH the kinetic data revealed that the degradation of Rifampicin followed a pseudo second–order model rather than a first–order model because most of the R^2 values in second–order were higher, which showed that the degradation process is pH dependent as the protons/H^+ play an important role in the generation of the hydroxyl groups (Cai *et al*., 2019). In addition, the acidic pH alters the superficial charge of the nanoparticles improving their degree of ionization and electrostatic interactions with the organic molecule thereby destroying it (Malakootian *et al*., 2020). The faster rate of degradation is also attributed to the ability of the protons to destroy the iron complexes and precipitants which helps the recovery of fresh and active sites (Velichkova *et al*., 2013).

4.4.6 Kinetics of the Variation of nanoparticles Dosage

To determine the order of reaction and kinetics of the reaction at various dosages, first ad second–order reaction equations were employed. **Figure 4.42** below illustrates the first–order kinetics for the degradation of Rifampicin at a 20 mg dosage of CbNPs.

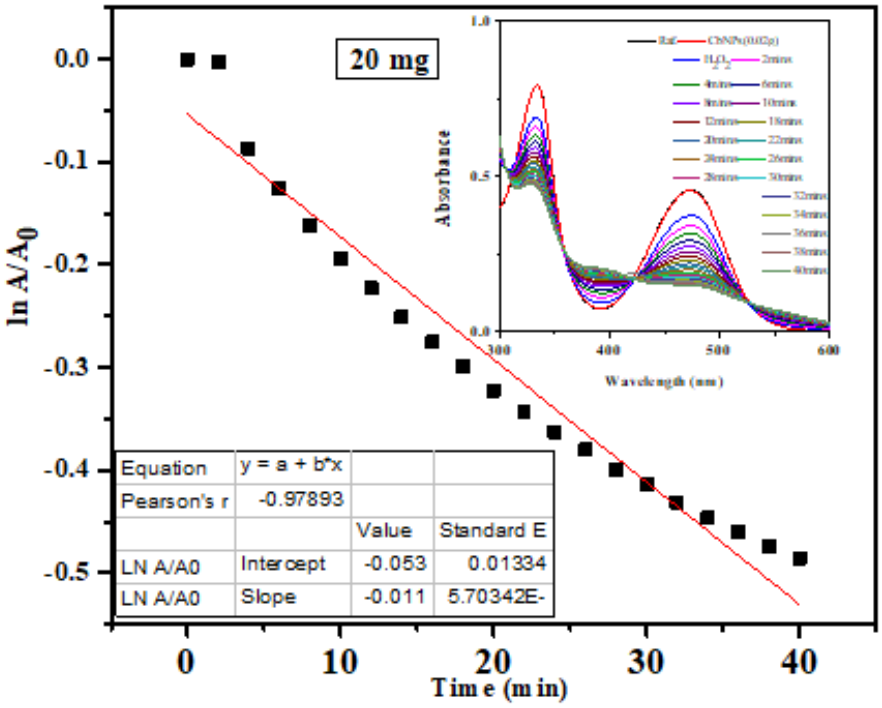

Figure 4.42: First–order plot of Rifampicin degradation using 20 mg of CbNPs

From the graph, the degradation of Rifampicin using 20 mg of the sample revealed that the process took less time due to the increase in the surface area of the nanoparticles. As the dosage increases, the surface area for degradation activity increases due to an increase in surface area. **Table 4.12** below illustrates the rate constants for the degradation of Rifampicin using various dosages of CbNPs, BpNPs and GpNPs at room temperature.

Table 4.12: Rate constant for Rifampicin degradation at different dosage at pH 7

Sample ID	Dosage (mg)	1st Order		2nd Order		Rate (µmol/L min)
		R^2	k	R^2	k	
CbNPs	20	0.9688	-0.0200	0.9969	0.1150	-7.1×10^{-3}
	10	0.9561	-0.0119	0.9008	0.0310	-3.5×10^{-3}
	5	0.9389	-0.0045	0.8593	0.0196	-3.3×10^{-3}
	1	0.8894	-0.0027	0.4333	0.0579	-2.1×10^{-3}
GpNPs	20	0.9656	-0.0212	0.9983	0.1154	-5.3×10^{-3}
	10	0.9554	-0.0129	0.9021	0.0334	-2.2×10^{-3}
	5	0.9276	-0.0038	0.8901	0.0194	-4.8×10^{-3}
	1	0.8974	-0.0019	0.5331	0.0579	-1.6×10^{-3}
CbNPs	20	0.9778	-0.0230	0.9996	0.1251	-5.8×10^{-3}
	10	0.9465	-0.0211	0.9165	0.0312	-3.5×10^{-3}
	5	0.9432	-0.0056	0.8775	0.0195	-7.0×10^{-4}
	1	0.8886	-0.0032	0.5422	0.0634	-2.7×10^{-4}

Depending on the dosage, the kinetic data revealed that the degradation of Rifampicin followed a pseudo first–order model rather than a second–order model because most of the R^2 values in the first–order were closer to 1, which showed that the degradation process is dependent on the pH of the solution for the production of the radicals and the higher dosage which results to increase in the surface area for the reaction (Cai *et al*., 2019).

4.5 Antimicrobial Activity

Evaluation of the antibacterial activity of synthesized iron nanoparticles was done using the disc diffusion method (Jeyasundari *et al*., 2017). **Figure 4.43** below shows

the antimicrobial activity of the GpNPs against *S. aureus*, *B. subtilis*, *P. auriginosa*, *E. coli*, and *C. albicans*.

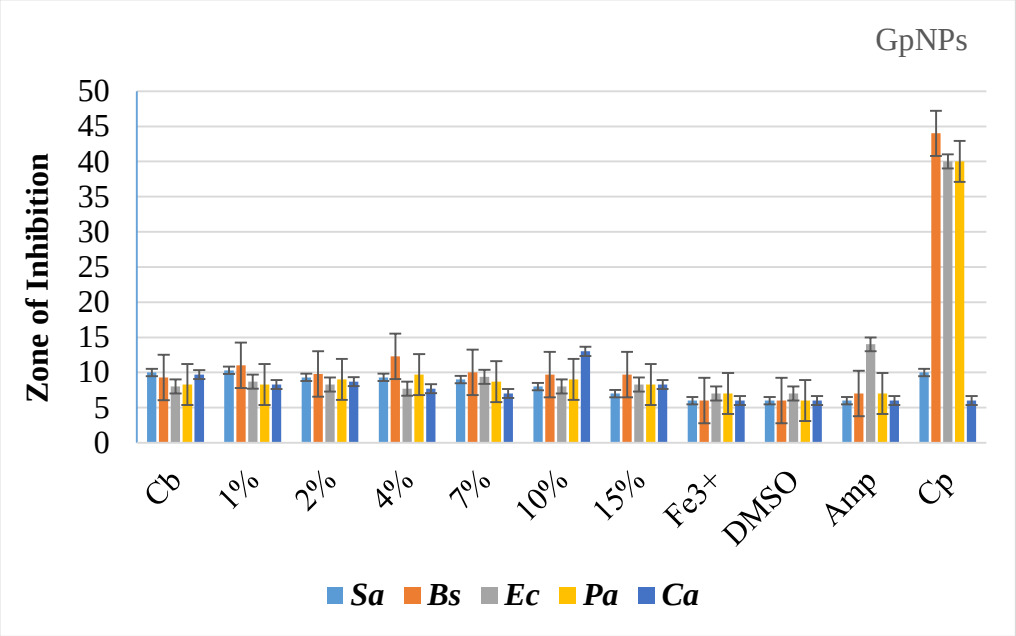

Figure 4.43: Antimicrobial activity of GpNPs, *G. parviflora* extract, Ampicillin and Ciprofloxacin

From the results in **Figure 4.43** above, it was clear that there was antimicrobial activity observed in a number of the nanoparticles. DMSO which was used for dissolving the nanoparticles depicted no inhibition as indicated by the sizes of the discs used. Antimicrobial activity was observed against *B. subtilis* than other microbes. However, the activity against other microbes was equal for all the concentrations. From the results, it was observed that the nanoparticles had higher activity against *S. aureus (Sa), B. subtilis (Bs), P. auriginosa (Pa),* and *C. albicans (Ca)* than ampicillin.

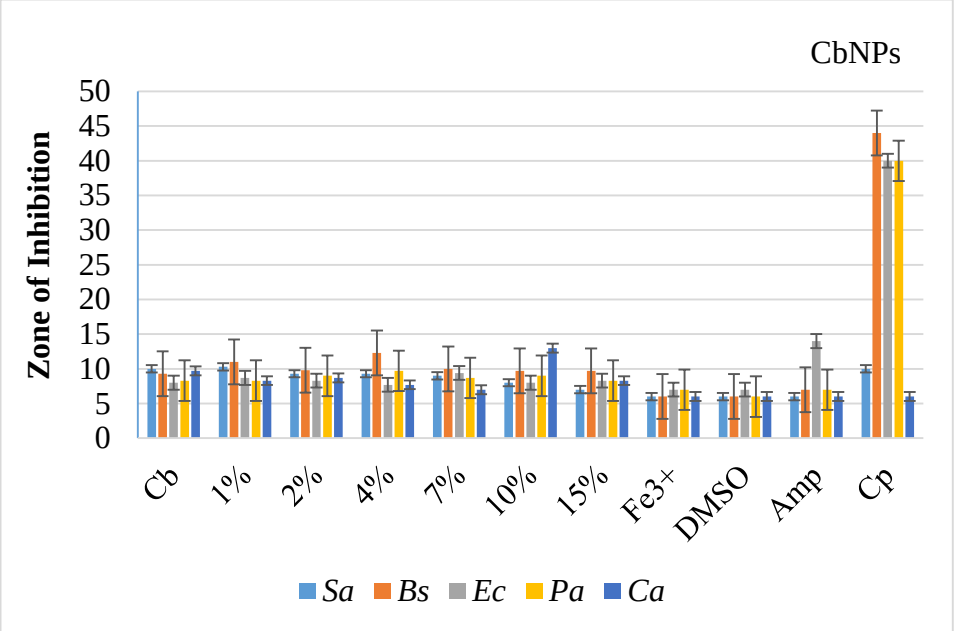

Figure 4.44: Antimicrobial activity of CbNPs, *C. bonariensis* extract, Ampicillin and Ciprofloxacin

From the results in **Figure 4.44** above, it was clear that there was antimicrobial activity observed in a number of the nanoparticles. DMSO which was used for dissolving the nanoparticles depicted no inhibition as indicated by the sizes of the discs used. From the results, it was observed that the nanoparticles had higher activity against *S. aureus*, *B. subtilis*, *P. aureginosa*, and *C. albicans* than ampicillin. Antimicrobial activity was observed against *B. subtilis* than other microbes. However, the activity against other microbes was equal for all the concentrations.

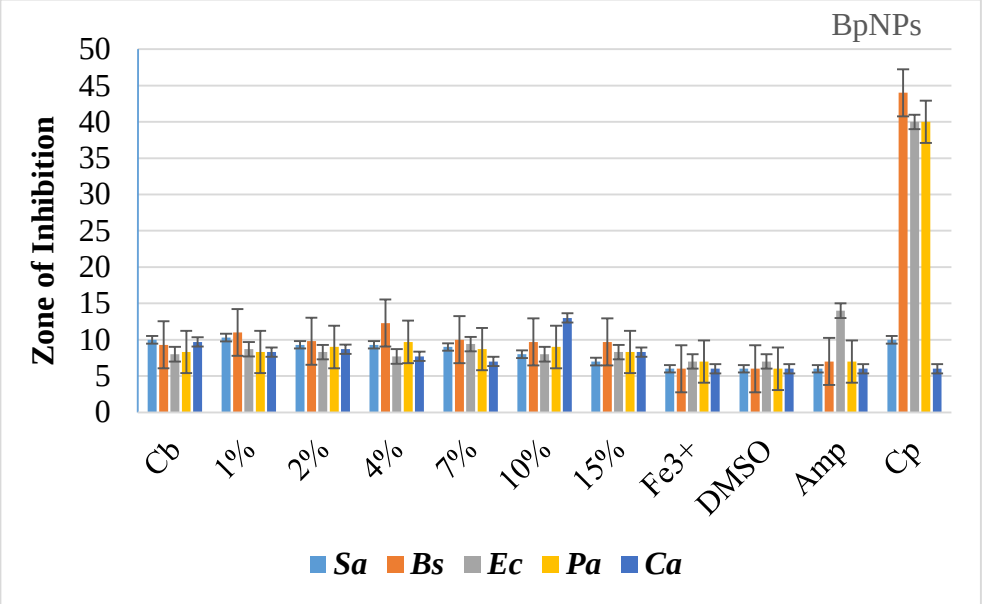

Figure 4.45: Antimicrobial activity of BpNPs, *B. pilosa* extract, Ampicillin and Ciprofloxacin

From the results obtained, it was observed that the highest inhibition was observed against *B. subtilis* in all the samples. Besides, it was observed that the nanoparticles had higher activity against *S. aureus*, *B. subtilis*, *P. auriginosa*, and *C. albican* than ampicillin.

All the synthesized iron nanoparticles showed considerably equal antimicrobial activity against all the bacteria and fungi. This is due to the presence of functional groups with herbal properties covering the surface of nanoparticles (Kanagasubbulakshmi and Kadirvelu, 2017). Fungus recorded the highest activity at 10% concentration in the iron nanoparticles. In addition, the antimicrobial activity of the synthesized iron nanoparticles was moderately higher than the ampicillin standard against *S. aureus*, *B. subtilis*, *P. aeruginosa* and *C. albicans.* Bacterial destruction occurs through the physical interaction of the cell wall and the NPs, which disrupts the membrane by producing Reactive Oxygen Species leading to cell death (Al-Kalifawi, 2015; Jagathesan and Rajiv, 2018; Saranya, 2017; Veeramanikandan *et al*., 2017). More so, the nanoparticles with a small size enter through the membrane into the cell which consequently loses the cell contents outside through the hole leading to cell

death (Ameer *et al*., 2017). However, the activity of these nanoparticles was affected by the nanoparticle aggregation which raises the size and thus its interaction with the cell membrane (Mashjoor *et al*., 2018; Moore *et al*., 2015). Statistical analysis of the data for the antimicrobial activity revealed that there was a significant difference ($p = 0.05$) in the concentration of the nanoparticles with different microbes **(Appendix VII).** However, BpNPs reported no significant difference and this is due to the high amount of flavonoids that were reported in **Table 4.1**. The plants used in this study have been found to have the ability to solve health challenges. *G. parviflora* has been reported to treat malaria, flu, cold, colorectal cancer, liver problems and inflammation and important pharmacological activities such as antibacterial antifungal, antioxidant and antidiabetic (Ripanda et al., 2023). *B. pilosa* has the ability to diseases and infections such as diarrhea, rheumatism, eyes and ear and toothache problems and antimicrobial activity against *S. aureus*, *P. aeruginosa*, *M. luteus* and *E. coli* and yeast *C. albicans* (Garima et al., 2017). A study carried out by (Girma and Jiru, 2021) revealed that *C. bonariensis* has antimicrobial activity against fungal pathogens – *C. albicans*, *Malassezia globosa*, and *Malassezia furfur*. The presence of secondary metabolites such as flavonoids, saponins, terpenoids, and tannins contributes to the medicinal properties of plant extracts (Ripanda et al., 2023). Although the nanoparticles showed relatively low antimicrobial levels, they revealed that the plant extracts can be nanoformulated unto the nanoparticles and provide health solutions against human pathogens.

CHAPTER FIVE

CONCLUSION AND RECOMMENDATIONS

5.1 Conclusion

i. Iron nanoparticles were synthesized using phytochemicals from *G. Parviflora, B. pilosa* and *C. bonariensis* leaves and characterized using UV-Vis, FTIR, XRF, XRD, and SEM. The average sizes of *B. pilosa* nanoparticles, *G. parviflora* nanoparticles, and *C. bonariensis* nanoparticles were 84, 51, and 78 nm revealing that the nanoparticles were in nano scale level. Hence, *G. parviflora*, *C. bonariensis* and *B. pilosa* leafs have phytochemicals that can reduce, stabilize and synthesize metallic nanoparticles.

ii. Synthesized iron nanoparticles show relatively high antimicrobial effects against *S. aureus, E. coli, P. aureginosa, B. subtillis,* and *C. albicans.* The results demonstrated that iron nanoparticles had antimicrobial properties that can be exploited in the field of medicine.

iii. The synthesized iron nanoparticles showed degradation efficiencies of over 80% against Rifampicin and Methylene blue. Degradation of Methylene blue and Rifampicin increased with an increase in temperature, dosage and pH with efficiencies over 90%. These demonstrated that green iron nanoparticles can be exploited in the field of environmental remediation of dyes and antibiotics in water.

5.2 Recommendations for Further Work

i. Synthesis of iron nanoparticles should be done using other plants.

ii. Evaluate the degradation effect of the iron nanoparticles against other dyes, antibiotics and antifungals.

iii. Investigate the effect caused by the iron nanoparticles against *Mycobacterium tuberculosis* (tuberculosis–causing organism).

iv. The antimicrobial activity of other metals such as silver, zinc, copper, and nickel nanoparticles synthesized from the three plants should be done and compared with iron nanoparticles of the three plants.

REFERENCES

Aftab, S., Tarik, M. M., Siddique, M. A., and Yusuf, M. A. (2015). Clinical and Microbiological Aspect of Wound Infection: A Review Update. *Bangladesh Journal of Infectious Diseases*, *1*(2), 32–37.

Ajay Handa, Sahajal Dhooria, Inderpaul Singh Sehgal, and Ritesh Agarwal. (2018). Primary cavitary sarcoidosis: A case report, systematic review, and proposal of new diagnostic criteria. *Lung India*, *35*(1), 41–46.

Akram, N., Guo, J., Ma, W., Guo, Y., Hassan, A., and Wang, J. (2020). Synergistic Catalysis of Co (OH) 2 / CuO for the Degradation of Organic Pollutant Under Visible Light Irradiation. *Scientific Reports*, 1–12.

Aksu Demirezen, D., Yıldız, Y. Ş., and Demirezen Yılmaz, D. (2019). Amoxicillin degradation using green synthesized iron oxide nanoparticles: Kinetics and mechanism analysis. *Environmental Nanotechnology, Monitoring and Management*, *11*(March). https://doi.org/10.1016/j.enmm.2019.100219

Al-Kalifawi, E. J. (2015). Green synthesis Of Magnetite Iron Oxide Nanoparticles by Using Al-Abbas's (A.S.) Hund Fruit (Citrus medica) var. Sarcodactylis Swingle Extract and Used in Al-'alqami River Water Treatment. *Journal of Natural Sciences Research Www*, *5*(20), 2225–2921.

Alam, M. N., Bristi, N. J., and Rafiquzzaman, M. (2013). Review on in vivo and in vitro methods evaluation of antioxidant activity. *Saudi Pharmaceutical Journal*, *21*(2), 143–152. https://doi.org/10.1016/j.jsps.2012.05.002

Ameer, K., Shahbaz, H. M., and Kwon, J. H. (2017). Green Extraction Methods for Polyphenols from Plant Matrices and Their Byproducts: A Review. *Comprehensive Reviews in Food Science and Food Safety*, *16*(2), 295–315. https://doi.org/10.1111/1541-4337.12253

Amendola, V., and Meneghetti, M. (2009). Size evaluation of gold nanoparticles by

UV-vis spectroscopy. *Journal of Physical Chemistry C*, *113*(11), 4277–4285. https://doi.org/10.1021/jp8082425

Anjum, M., Miandad, R., Waqas, M., Gehany, F., and Barakat, M. A. (2016). Remediation of wastewater using various nano-materials. *Arabian Journal of Chemistry*. https://doi.org/10.1016/j.arabjc.2016.10.004

Atkins, P., and Paula, J. De. (2009). Atkins' Physical chemistry 8th edition. In *Chemistry* (pp. 430–468). https://doi.org/10.1021/ed056pA260.1

Azam, A., Ahmed, A. S., Oves, M., Khan, M. S., Habib, S. S., and Memic, A. (2012). Antimicrobial activity of metal oxide nanoparticles against Gram-positive and Gram-negative bacteria: a comparative study. *Ijnm*, *7(7)*, 6003–6009.

Baba, S. A., and Malik, S. A. (2014). Evaluation of antioxidant and antibacterial activity of methanolic extracts of Gentiana kurroo royle. *Saudi Journal of Biological Sciences*, *21*(5), 493–498. https://doi.org/10.1016/j.sjbs.2014.06.004

Baba, S. A., and Malik, S. A. (2015). Determination of total phenolic and flavonoid content, antimicrobial and antioxidant activity of a root extract of Arisaema jacquemontii Blume . *Journal of Taibah University for Science*, *9*(4), 449–454. https://doi.org/10.1016/j.jtusci.2014.11.001

Badiee, P., and Hashemizadeh, Z. (2014). *Opportunistic invasive fungal infections : diagnosis and clinical management*. *February*, 195–204.

Bagheri, H., Afkhami, A., and Noroozi, A. (2016). Removal of pharmaceutical compounds from hospital wastewaters using nanomaterials: A review. *Analytical and Bioanalytical Chemistry Research*, *3*(1), 1–18.

Bairwa, K., Kumar, R., Sharma, R. J., and Roy, R. K. (2010). An updated review on Bidens Pilosa L. *Der Pharma Chemica*, *2*(3), 325–337.

Balamurugan, M., Saravanan, S., and Soga, T. (2014). Synthesis of Iron Oxide Nanoparticles by Using Eucalyptus Globulus Plant Extract. *E-Journal of Surface*

Science and Nanotechnology, *12*(0), 363–367.

Bartolome, A. P., Villaseñor, I. M., and Yang, W. (2013). *Bidens pilosa L . (Asteraceae): Botanical Properties , Traditional Uses , Phytochemistry , and Pharmacology*. *2013*.

Benelli, G. (2016). Plant-mediated biosynthesis of nanoparticles as an emerging tool against mosquitoes of medical and veterinary importance: a review. *Parasitology Research*, *115*(1), 23–34. https://doi.org/10.1007/s00436-015-4800-9

Betancur, A. F., Pérez, F. R., Correa, M. del M., and Barrero, C. A. (2012). Quantitative approach in iron oxides and oxihydroxides by vibrational analysis. *Optica Pura y Aplicada*, *45*(3), 269–275. https://doi.org/10.7149/OPA.45.3.269

Bhamare, V. S., and Kulkarni, R. M. (2019). Photocatalytic degradation of pharmaceutical drug zidovudine by undoped and 5 % barium doped zinc oxide nanoparticles during water treatment: Synthesis and characterisation. *International Journal of Applied Pharmaceutics*, *11*(1), 227–236.

Biao, L., Tan, S., Meng, Q., Gao, J., Zhang, X., Liu, Z., and Fu, Y. (2018). Green Synthesis, Characterization and Application of Proanthocyanidins-Functionalized Gold Nanoparticles. *Nanomaterials*, *8*(1), 53.

Bishnoi, S., Kumar, A., and Selvaraj, R. (2018). Facile synthesis of magnetic iron oxide nanoparticles using inedible Cynometra ramiflora fruit extract waste and their photocatalytic degradation of methylene blue dye. *Materials Research Bulletin*, *97*, 121–127. https://doi.org/10.1016/j.materresbull.2017.08.040

Borja, J. Q., Ngo, M. A. S., Saranglao, C. C., Tiongco, R. P. M., Roque, E. C., and Dugos, N. P. (2015). Synthesis of green zero-valent iron using polyphenols from dried green tea extract. *Journal of Engineering Science and Technology*, *10*(Spec.issue7), 22–31.

Bratovcic, A. (2019). Different Applications of Nanomaterials and Their Impact on

the Environment. *International Journal of Material Science and Engineering*, *5*(1), 1–7. https://doi.org/10.14445/23948884/ijmse-v5i1p101

Cai, H., An, X., Cui, J., Li, J., Wen, S., Li, K., Shen, M., Zheng, L., Zhang, G., and Shi, X. (2013). Facile hydrothermal synthesis and surface functionalization of polyethyleneimine-coated iron oxide nanoparticles for biomedical applications. *ACS Applied Materials and Interfaces*, *5*(5), 1722–1731.

Cai, W., Weng, X., and Chen, Z. (2019). Highly efficient removal of antibiotic rifampicin from aqueous solution using green synthesis of recyclable nano-Fe3O4. *Environmental Pollution*, *247*, 839–846.

Catarinense, E. S., Medicinais, P., Reitz, R., and Catarinense, E. S. (2013). *Bidens pilosa L . (Asteraceae): traditional use in a community of southern Brazil*. 34–40.

Cecilia, M., Pius, K., Patrick, H., Elijah, N., James, R., Antony, G., and Tuula, T. (2020). *Mass loading, distribution, and removal of antibiotics and antiretroviral drugs in selected wastewater treatment plants in Kenya*.

Chang, D., and Jianzhong, H. (2010). Effect of antibiotics in the environment on microbial populations. *Applied Microbiology and Biotechnology*, *87*(3), 925–941. https://doi.org/10.1007/s00253-010-2649-5

Chauhan, A., Sillu, D., and Agnihotri, S. (2018). Removal of Pharmaceutical Contaminants in Wastewater Using Nanomaterials: A Comprehensive Review. *Current Drug Metabolism*, *20*(6), 483–505.

Chauhan, R., Kumar, A., and Chaudhary, R. P. (2013a). Photocatalytic degradation of methylene blue with Fe doped ZnS nanoparticles. *Spectrochimica Acta - Part A: Molecular and Biomolecular Spectroscopy*, *113*, 250–256.

Chauhan, R., Kumar, A., and Chaudhary, R. P. (2013b). Photocatalytic degradation of methylene blue with Fe doped ZnS nanoparticles. *Spectrochimica Acta - Part A:*

Molecular and Biomolecular Spectroscopy, *113*, 250–256.

Cheun, G. Y. C., Bae, J. S., and Otto, M. (2021). Pathogenicity and virulence of Staphylococcus aureus Pathogenicity and virulence of Staphylococcus aureus. *Virulence*, *12*(1), 547–569. https://doi.org/10.1080/21505594.2021.1878688

Chhetri, B. K., Ali, N. A. A., and Setzer, W. N. (2015). *A Survey of Chemical Compositions and Biological Activities of Yemeni Aromatic Medicinal Plants*. 67–92. https://doi.org/10.3390/medicines2020067

Cortés-Rojas, D. F., Chagas-Paula, D. A., Da Costa, F. B., Souza, C. R. F., and Oliveira, W. P. (2013). Bioactive compounds in Bidens pilosa L. populations: A key step in the standardization of phytopharmaceutical preparations. *Brazilian Journal of Pharmacognosy*, *23*(1), 28–35.

Da'na, E., Taha, A., and Afkar, E. (2018). Green synthesis of iron nanoparticles by Acacia nilotica pods extract and its catalytic, adsorption, and antibacterial activities. *Applied Sciences (Switzerland)*, *8*(10), 1922.

Dang, T., Tran, X., and Khanh, D. (2016). Chemistry and pharmacology of Bidens pilosa : an overview. *Journal of Pharmaceutical Investigation*, *46*(2), 91–132. https://doi.org/10.1007/s40005-016-0231-6

Dantas, A. da S., Lee, K. K., Raziunaite, I., Schaefer, K., Wagener, J., Yadav, B., and Gow, N. A. (2016). Cell biology of Candida albicans – host interactions. *Current Opinion in Microbiology*, *34*, 111–118.

Darezereshki, E., Ranjbar, M., and Bakhtiari, F. (2010). One-step synthesis of maghemite (γ-Fe2O3) nano-particles by wet chemical method. *Journal of Alloys and Compounds*, *502*(1), 257–260. https://doi.org/10.1016/j.jallcom.2010.04.163

Das, S., Ghosh, S., Misra, A. J., Tamhankar, A. J., Mishra, A., Lundborg, C. S., and Tripathy, S. K. (2018). Sunlight assisted photocatalytic degradation of ciprofloxacin in water using fe doped zno nanoparticles for potential public health

applications. *International Journal of Environmental Research and Public Health*, *15*(11), 1–11. https://doi.org/10.3390/ijerph15112440

De Andrade, J. R., Oliveira, M. F., Da Silva, M. G. C., and Vieira, M. G. A. (2018). Adsorption of Pharmaceuticals from Water and Wastewater Using Nonconventional Low-Cost Materials: A Review. *Industrial and Engineering Chemistry Research*, *57*(9), 3103–3127. https://doi.org/10.1021/acs.iecr.7b05137

de Sousa Araújo, T. A., Alencar, N. L., de Amorim, E. L. C., and de Albuquerque, U. P. (2008). A new approach to study medicinal plants with tannins and flavonoids contents from the local knowledge. *Journal of Ethnopharmacology*, *120*(1), 72–80. https://doi.org/10.1016/j.jep.2008.07.032

Devatha, C. P., Jagadeesh, K., and Patil, M. (2018). Effect of Green synthesized iron nanoparticles by Azardirachta Indica in different proportions on antibacterial activity. *Environmental Nanotechnology, Monitoring and Management*, *9*, 85–94. https://doi.org/10.1016/j.enmm.2017.11.007

Devatha, C. P., Thalla, A. K., and Katte, S. Y. (2016). Green synthesis of iron nanoparticles using different leaf extracts for treatment of domestic waste water. *Journal of Cleaner Production*, *139*. https://doi.org/10.1016/j.jclepro.2016.09.019

Dinesh, D., Murugan, K., Madhiyazhagan, P., Panneerselvam, C., Mahesh Kumar, P., Nicoletti, M., Jiang, W., Benelli, G., Chandramohan, B., and Suresh, U. (2015). Mosquitocidal and antibacterial activity of green-synthesized silver nanoparticles from Aloe vera extracts: towards an effective tool against the malaria vector Anopheles stephensi? *Parasitology Research*, *114*(4), 1519–1529. https://doi.org/10.1007/s00436-015-4336-z

do Amaral, W., Deschamps, C., Biasi, L. A., Bizzo, H. R., Machado, M. P., and da Silva, L. E. (2018). Yield and chemical composition of the essential oil of species of the Asteraceae family from Atlantic Forest, South of Brazil. *Journal of Essential Oil Research*, *30*(4), 278–284.

Donfack, A. R. N., Tala, M. F., Wabo, H. K., Jerz, G., Zeng, G. Z., Winterhalter, P., Tan, N. H., and Tane, P. (2014). Two new anthraquinone dimers from the stem bark of Pentas schimperi (Rubiaceae). *Phytochemistry Letters*, *8*(1), 55–58. https://doi.org/10.1016/j.phytol.2014.01.012

Ebbing, D. D., and Gammon, S. D. (2009). *General chemistry* (11th ed.). Houghton Mifflin Company.

Ebrahiminezhad, A., Zare-Hoseinabadi, A., Berenjian, A., and Ghasemi, Y. (2017). Green synthesis and characterization of zero-valent iron nanoparticles using stinging nettle (Urtica dioica) leaf extract. *Green Processing and Synthesis*, *6*(5), 469–475. https://doi.org/10.1515/gps-2016-0133

Ebrahiminezhad, A., Zare-hoseinabadi, A., Sarmah, A. K., Taghizadeh, S., Ghasemi, Y., and Berenjian, A. (2018). Plant-Mediated Synthesis and Applications of Iron Nanoparticles Plant - Mediated Synthesis and Applications of Iron Nanoparticles. *Molecular Biotechnology*, *December 2017*. https://doi.org/10.1007/s12033-017-0053-4

Elkady, M. F., Farag, H. A., and Zaatout, A. A. (2014). *Assessment of Novel Synthetized Nanozirconium Tungstovanadate as Cation Exchanger for Lead Ion Decontamination*. *2014*.

Fazlzadeh, M., Rahmani, K., Zarei, A., Abdoallahzadeh, H., Nasiri, F., and Khosravi, R. (2017). A novel green synthesis of zero valent iron nanoparticles (NZVI) using three plant extracts and their efficient application for removal of Cr(VI) from aqueous solutions. *Advanced Powder Technology*, *28*(1), 122–130. https://doi.org/10.1016/j.apt.2016.09.003

Fernando, S. S. N., Gunasekara, T., and Holton, J. (2018). *Antimicrobial Nanoparticles : applications and mechanisms of action*. *8*(April), 2–11.

Ferroudja, N., Nzimotoa, J., Davidsonc, A., Delphine Talbota, E. B., Vincent Dupuisa, A. B., Medjramb, M. S., and Abramson, S. (2013). *Maghemite nanoparticles and*

maghemite / silica nanocomposite microspheres as magnetic Fenton catalysts for the removal of water pollutants. *June*.

Ferum, K., Antrakuinon, I. I., and Struktur, P. (2017). *Iron (II) Complex of Anthraquinone : Synthesis , Structural Elucidation and Antimicrobial Activity*. *21*(5), 1162–1167.

Freyria, F. S., Esposito, S., Armandi, M., Deorsola, F., Garrone, E., and Bonelli, B. (2017). *Role of pH in the Aqueous Phase Reactivity of Zerovalent Iron Nanoparticles with Acid Orange 7 , a Model Molecule of Azo Dyes*. *2017*.

Garima, S., Kumar, P. A., Pratibha, S., Leo, V. V., Subbarayan, S., Kumar, B., Singh, B. P., and Kumar, N. S. (2017). *Pharmacological potential of Bidens pilosa L . and determination of bioactive compounds using UHPLC-QqQ LIT -MS/MS and GC/MS*. 1–16. https://doi.org/10.1186/s12906-017-2000-0

Girma, Y., and Jiru, T. M. (2021). *Evaluation of Antimicrobial Activity of Conyza bonariensis Leaf Extracts against Clinically Isolated Fungi Causing Superficial Infection*. *2021*.

Govindarajan, M., and Benelli, G. (2017). A Facile One-Pot Synthesis of Eco-Friendly Nanoparticles Using Carissa carandas: Ovicidal and Larvicidal Potential on Malaria, Dengue and Filariasis Mosquito Vectors. *Journal of Cluster Science*, *28*(1), 15–36. https://doi.org/10.1007/s10876-016-1035-6

Groiss, S., Selvaraj, R., Varadavenkatesan, T., and Vinayagam, R. (2017). Structural characterization, antibacterial and catalytic effect of iron oxide nanoparticles synthesised using the leaf extract of Cynometra ramiflora. *Journal of Molecular Structure*, *1128*, 572–578. https://doi.org/10.1016/j.molstruc.2016.09.031

Guguloth, H. (2015). *R a b s*. *5*(3).

Gui, M., Smuleac, V., Ormsbee, L. E., Sedlak, D. L., and Bhattacharyya, D. (2012). Iron oxide nanoparticle synthesis in aqueous and membrane systems for oxidative

degradation of trichloroethylene from water. *Journal of Nanoparticle Research*, *14*(5). https://doi.org/10.1007/s11051-012-0861-1

Gupta, V. K., Agarwal, S., and Saleh, T. A. (2011). Synthesis and characterization of alumina-coated carbon nanotubes and their application for lead removal. *Journal of Hazardous Materials*, *185*(1), 17–23.

Halm-Lemeille, M. P., and Gomez, E. (2016). Pharmaceuticals in the environment. In *Environmental Science and Pollution Research* (Vol. 23, Issue 6).

Hameed, M., Moradkhani, H., Ahmadalipour, A., and Moftakhari, H. (2019). *A Review of the 21st Century Challenges in the Food-Energy-Water Security in the Middle East*.

Harshiny, M., Iswarya, C. N., and Matheswaran, M. (2015). Biogenic synthesis of iron nanoparticles using Amaranthus dubius leaf extract as a reducing agent. *Powder Technology*, *286*, 744–749. https://doi.org/10.1016/j.powtec.2015.09.021

Hasan, S., and Hasan, S. (2015). *A Review on Nanoparticles : Their Synthesis and Types A Review on Nanoparticles : Their Synthesis and Types*. *February*, 7–10.

Hou, L., Yang, L., Li, J., Tan, J., and Yuan, C. (2012). *Efficient Sunlight-Induced Methylene Blue Removal over One-Dimensional Mesoporous Monoclinic BiVO 4 Nanorods*. *2012*. https://doi.org/10.1155/2012/345247

Huang, G., Wang, M., Hu, Y., Lv, S., and Li, C. (2017). Synthesis, characterization, and debromination reactivity of cellulosestabilized Pd/Fe nanoparticles for 2,2',4,4'-tretrabromodiphenyl ether. *PLoS ONE*, *12*(3), 1–17. https://doi.org/10.1371/journal.pone.0174589

Huang, L., Weng, X., Chen, Z., Megharaj, M., and Naidu, R. (2014). Synthesis of iron-based nanoparticles using oolong tea extract for the degradation of malachite green. *Spectrochimica Acta - Part A: Molecular and Biomolecular Spectroscopy*, *117*. https://doi.org/10.1016/j.saa.2013.09.054

Hwang, S. W., Umar, A., Dar, G. N., Kim, S. H., and Badran, R. I. (2014). Synthesis and Characterization of Iron Oxide Nanoparticles for Phenyl Hydrazine Sensor Applications. *Sensor Letters*, *12*(1), 97–101. https://doi.org/10.1166/sl.2014.3224

Ibrahem, A. K., Abdel Moghny, T., Mustafa, Y. M., Maysour, N. E., Mohamed Saad El Din El Dars, F., and Farouk Hassan, R. (2012). Degradation of Trichloroethylene Contaminated Soil by Zero-Valent Iron Nanoparticles. *ISRN Soil Science*, *2012*, 1–9. https://doi.org/10.5402/2012/270830

Idris, O. A., Kerebba, N., Horn, S., Steve, M., and Rialet, M. (2023). *Phytochemical-Based Evidence of the Health Benefits of Bidens Pilosa Extracts and Cytotoxicity*.

Igwe, O. U., and Nwamezie, F. (2018). *Green synthesis of iron nanoparticles using flower extract of Piliostigma thonningii and their antibacterial activity evaluation*. 60–66.

Iravani, S. (2016). *Green Chemistry Green synthesis of metal nanoparticles using plants*. *October 2011*. https://doi.org/10.1039/C1GC15386B

Irshad, R. (2017). Antibacterial activity of biochemically capped iron oxide nanoparticles: A view towards green chemistry. *Journal of Photochemistry and Photobiology, B: Biology*, *170*. https://doi.org/10.1016/j.jphotobiol.2017.04.020

Izadiyan, Z., Shameli, K., Miyake, M., Hara, H., Mohamad, S. E. B., Kalantari, K., Taib, S. H. M., and Rasouli, E. (2018). Cytotoxicity assay of plant-mediated synthesized iron oxide nanoparticles using Juglans regia green husk extract. *Arabian Journal of Chemistry*. https://doi.org/10.1016/j.arabjc.2018.02.019

Jagathesan, G., and Rajiv, P. (2018). Biosynthesis and characterization of iron oxide nanoparticles using Eichhornia crassipes leaf extract and assessing their antibacterial activity. *Biocatalysis and Agricultural Biotechnology*, *13*(August 2017), 90–94. https://doi.org/10.1016/j.bcab.2017.11.014

Jalab, J., Abdelwahed, W., Kitaz, A., and Al-kayali, R. (2021). Green synthesis of silver nanoparticles using aqueous extract of Acacia cyanophylla and its antibacterial activity. *Heliyon*, *7*(September), e08033.

Jeyasundari, J., Praba, P. S., Jacob, Y. B. A., Vasantha, V. S., and Shanmugaiah, V. (2017). Green Synthesis and Characterization of Zero Valent Iron Nanoparticles from the Leaf Extract of *Psidium Guajava* Plant and Their Antibacterial Activity. *Chemical Science Review and Letters*, *6*(22), 1244–1252.

Joseph, M. M., and Sreelekha, T. T. (2014). Gold nanoparticles - synthesis and applications in cancer management. *Recent Patents on Materials Science*, *7*(1), 8–25. https://doi.org/10.1055/s-2006-944219

Kairigo, P., Ngumba, E., Sundberg, L. R., Gachanja, A., and Tuhkanen, T. (2020). Occurrence of antibiotics and risk of antibiotic resistance evolution in selected Kenyan wastewaters, surface waters and sediments. *Science of the Total Environment*, *720*, 137580. https://doi.org/10.1016/j.scitotenv.2020.137580

Kanagasubbulakshmi, S., and Kadirvelu, K. (2017). Green Synthesis of Iron Oxide Nanoparticles using Lagenaria Siceraria and Evaluation of its Antimicrobial Activity. *Defence Life Science Journal*, *2*(4), 422–427.

Kansal, S. K., Kundu, P., Sood, S., Lamba, R., Umar, A., and Mehta, S. K. (2014). Photocatalytic degradation of the antibiotic levofloxacin using highly crystalline TiO2 nanoparticles. *New Journal of Chemistry*, *38*(7), 3220–3226.

Karaman, D. Ş., Manner, S., Fallarero, A., and Rosenholm, J. M. (2017). Current Approaches for Exploration of Nanoparticles as Antibacterial Agents. *Antibacterial Agents*. https://doi.org/10.5772/68138

Katata-Seru, L., Moremedi, T., Aremu, O. S., and Bahadur, I. (2018). Green synthesis of iron nanoparticles using Moringa oleifera extracts and their applications: Removal of nitrate from water and antibacterial activity against Escherichia coli. *Journal of Molecular Liquids*, *256*, 296–304.

Kaushik, U., and Joshi, S. C. (2015). Silver nanoparticles: Green synthesis, optical properties, antimicrobial activity and its mechanism using citrus sinensis. *Asian Journal of Pharmaceutical and Clinical Research*, *8*(6), 179–184.

Kigen, G. K., Ronoh, H. K., Kipkore, W. K., and Rotich, J. K. (2013). Current trends of Traditional Herbal Medicine Practice in Kenya: A review. *J. Pharmacol. Ther*, *2*(1), 32–37.

Kurbatova, E. V., Cavanaugh, J. S., Shah, N. S., Wright, A., Kim, H., Metchock, B., Van Deun, A., Barrera, L., Boulahbal, F., Richter, E., Martín-Casabona, N., Arias, F., Zemanova, I., Drobniewski, F., Santos Silva, A., Coulter, C., Lumb, R., and Cegielski, J. P. (2012). Rifampicin-resistant Mycobacterium tuberculosis: Susceptibility to isoniazid and other anti-tuberculosis drugs. *International Journal of Tuberculosis and Lung Disease*, *16*(3), 355–357.

Kushwaha, R., Garg, S., Bajpai, S., and Giri, A. S. (2018). Degradation of Nile blue sulphate dye onto iron oxide nanoparticles: Kinetic study, identification of reaction intermediates, and proposed mechanistic pathways. *Asia-Pacific Journal of Chemical Engineering*, *13*(3), 1–16. https://doi.org/10.1002/apj.2200

Lassoued, A., Lassoued, M. S., Dkhil, B., Ammar, S., and Gadri, A. (2018). Photocatalytic degradation of methylene blue dye by iron oxide (α-Fe2O3) nanoparticles under visible irradiation. *Journal of Materials Science: Materials in Electronics*, *29*(10), 8142–8152. https://doi.org/10.1007/s10854-018-8819-4

Leal, J. E., Thompson, A. N., and Brzezinski, W. A. (2010). Pharmaceuticals in drinking water: Local analysis of the problem and finding a solution through awareness. *Journal of the American Pharmacists Association*, *50*(5), 600–603. https://doi.org/10.1331/JAPhA.2010.09186

Leung, E., Weil, D. E., Raviglione, M., and Nakatani, H. (2011). The WHO policy package to combat antimicrobial resistance. *Bulletin of the World Health Organization*, *89*(5), 390–392. https://doi.org/10.2471/BLT.11.088435

Liu, W., Sutton, N. B., Rijnaarts, H. H. M., and Langenhoff, A. A. M. (2016). Pharmaceutical removal from water with iron- or manganese-based technologies: A review. *Critical Reviews in Environmental Science and Technology*, *46*(19–20), 1584–1621. https://doi.org/10.1080/10643389.2016.1251236

Logeswari, P., Silambarasan, S., and Abraham, J. (2015). Synthesis of silver nanoparticles using plants extract and analysis of their antimicrobial property. *Journal of Saudi Chemical Society*, *19*(3).

Luo, W., Zhu, L., Wang, N., Tang, H., Cao, M., and She, Y. (2010). *Efficient Removal of Organic Pollutants with Magnetic Nanoscaled BiFeO 3 as a Reusable Heterogeneous Fenton-Like Catalyst*. *44*(5), 1786–1791.

Madivoli, E S, Kareru, P. G., Gachanja, A. N., Mugo, S. M., and Sujee, D. M. (2019). Phytofabrication of iron nanoparticles and their catalytic activity. *SN Applied Sciences*, *1*(8), 1–9. https://doi.org/10.1007/s42452-019-0951-0

Madivoli, Edwin Shigwenya, Kareru, P. G., Maina, E. G., Nyabola, A. O., Wanakai, S. I., and Nyang'au, J. O. (2019). Biosynthesis of iron nanoparticles using Ageratum conyzoides extracts , their antimicrobial and photocatalytic activity. *SN Applied Sciences*, *1*(5), 1–9. https://doi.org/10.1007/s42452-019-0511-7

Mahmud, Z. H., Islam, S., Imran, K. M., Adnan, S., Hakim, I., Worth, M., Ahmed, A., Hossan, S., Haider, M., Islam, M. R., Hossain, F., Johnston, D., and Ahmed, N. (2019). Occurrence of Escherichia coli and faecal coliforms in drinking water at source and household point - of - use in Rohingya camps , Bangladesh. *Gut Pathogens*, 1–11. https://doi.org/10.1186/s13099-019-0333-6

Makarov, V. V., Love, A. J., Sinitsyna, O. V., Makarova, S. S., Yaminsky, I. V., Taliansky, M. E., and Kalinina, N. O. (2014). "Green" nanotechnologies: Synthesis of metal nanoparticles using plants. *Acta Naturae*, *6*(20), 35–44. https://doi.org/10.1039/c1gc15386b

Makarov, Valentin V., Makarova, S. S., Love, A. J., Sinitsyna, O. V., Dudnik, A. O.,

Yaminsky, I. V., Taliansky, M. E., and Kalinina, N. O. (2014). Biosynthesis of Stable Iron Oxide Nanoparticles in Aqueous Extracts of *Hordeum vulgare* and *Rumex acetosa* Plants. *Langmuir*, *30*(20), 5982–5988.

Malakootian, M., Nasiri, A., and Amiri Gharaghani, M. (2020). Photocatalytic degradation of ciprofloxacin antibiotic by TiO2 nanoparticles immobilized on a glass plate. *Chemical Engineering Communications*, *207*(1), 56–72. https://doi.org/10.1080/00986445.2019.1573168

Maobe, M. A. G., Gatebe, E., Gitu, L., and Rotich, H. (2013). Preliminary Phytochemical Screening of Eight Selected Medicinal Herbs Used for the Treatment of Diabetes, Malaria and Pneumonia in Kisii Region, Southwest Kenya. *European Journal of Applied Sciences*, *5*(1), 1–6.

Masenga, S. K., Mubila, H., and Hamooya, B. M. (2017). Rifampicin resistance in mycobacterium tuberculosis patients using GeneXpert at Livingstone Central Hospital for the year 2015: A cross sectional explorative study. *BMC Infectious Diseases*, *17*(1), 1–4. https://doi.org/10.1186/s12879-017-2750-9

Mashjoor, S., Yousefzadi, M., Zolgharnain, H., Kamrani, E., and Alishahi, M. (2018). Organic and inorganic nano-Fe3O4: Alga Ulva flexuosa-based synthesis, antimicrobial effects and acute toxicity to briny water rotifer Brachionus rotundiformis. *Environmental Pollution*, *237*, 50–64.

Masyita, A., Mustika, R., Dwi, A., Yasir, B., Rahma, N., Bin, T., Nainu, F., and Simal-gandara, J. (2022). Food Chemistry : X Terpenes and terpenoids as main bioactive compounds of essential oils , their roles in human health and potential application as natural food preservatives. *Food Chemistry: X*, *13*(October 2021), 100217. https://doi.org/10.1016/j.fochx.2022.100217

Mbiri, A., Wittstock, G., Taffa, D. H., Gatebe, E., Baya, J., and Wark, M. (2018). Photocatalytic degradation of the herbicide chloridazon on mesoporous titania/zirconia nanopowders. *Environmental Science and Pollution Research*, *25*(35), 34873–34883. https://doi.org/10.1007/s11356-017-1023-x

Mihai, M. M., Dima, M. B., Dima, B., and Holban, A. M. (2019). *Infection Control*. 1–16.

Mirza, A. U., Kareem, A., Nami, S. A. A., Khan, M. S., Rehman, S., Bhat, S. A., Mohammad, A., and Nishat, N. (2018). Biogenic synthesis of iron oxide nanoparticles using Agrewia optiva and Prunus persica phyto species: Characterization, antibacterial and antioxidant activity. *Journal of Photochemistry and Photobiology B: Biology*, *185*, 262–274.

Mirzaei, A., Chen, Z., Haghighat, F., and Yerushalmi, L. (2017). Removal of pharmaceuticals from water by homo/heterogonous Fenton-type processes – A review. *Chemosphere*, *174*, 665–688.

Mishra, D., Arora, R., Lahiri, S., Amritphale, S. S., and Chandra, N. (2014). Synthesis and characterization of iron oxide nanoparticles by solvothermal method. *Protection of Metals and Physical Chemistry of Surfaces*, *50*(5), 628–631. https://doi.org/10.1134/S2070205114050128

Moore, T. L., Rodriguez-Lorenzo, L., Hirsch, V., Balog, S., Urban, D., Jud, C., Rothen-Rutishauser, B., Lattuada, M., and Petri-Fink, A. (2015). Nanoparticle colloidal stability in cell culture media and impact on cellular interactions. *Chemical Society Reviews*, *44*(17), 6287–6305. https://doi.org/10.1039/c4cs00487f

Morawska, L. P., and Kuipers, O. P. (2022). *Antibiotic tolerance in environmentally stressed Bacillus subtilis : physical barriers and induction of a viable but nonculturable state*. *June*, 1–18. https://doi.org/10.1093/femsml/uqac010

Mostafa, I., El-aziz, E. A., Hafez, S., and El-shazly, A. (2013). *Chemical Constituents and Biological Activities of Galinsoga parvifl ora Cav . (Asteraceae) from Egypt*.

Mullerpattan, J. B., Nikam, C., Sharma, U., Rodrigues, C., and Pinto, L. M. (2017). Rifampicin-resistant tuberculosis: What is the best initial empiric regimen in

Mumbai, India? *European Respiratory Journal*, *50*(1).

Murgueitio, E., Cumbal, L., Abril, M., Izquierdo, A., Debut, A., and Tinoco, O. (2018). Green Synthesis of Iron Nanoparticles: Application on the Removal of Petroleum Oil from Contaminated Water and Soils. *Journal of Nanotechnology*, *2018*. https://doi.org/10.1155/2018/4184769

Musembei, R., and Joyce, K. J. (2017). *Chemical Composition and Antibacterial Activity of Essential Oil from Kenyan Conyza bonariensis (L .) Cronquist*. *5*(2), 180–185.

Muthukumar, H., and Matheswaran, M. (2015). Amaranthus spinosus Leaf Extract Mediated FeO Nanoparticles: Physicochemical Traits, Photocatalytic and Antioxidant Activity. *ACS Sustainable Chemistry and Engineering*, *3*(12). https://doi.org/10.1021/acssuschemeng.5b00722

Mvelase, N. R., Balakrishna, Y., Lutchminarain, K., and Mlisana, K. (2019). Evolving rifampicin and isoniazid mono-resistance in a high multidrug-resistant and extensively drug-resistant tuberculosis region: A retrospective data analysis. *BMJ Open*, *9*(11). https://doi.org/10.1136/bmjopen-2019-031663

Nadim, A. H., Al-Ghobashy, M. A., Nebsen, M., and Shehata, M. A. (2015). Optimization of photocatalytic degradation of meloxicam using titanium dioxide nanoparticles: application to pharmaceutical wastewater analysis, treatment, and cleaning validation. *Environmental Science and Pollution Research*, *22*(20), 15516–15525. https://doi.org/10.1007/s11356-015-4713-2

Nagar, N., and Devra, V. (2018). Green synthesis and characterization of copper nanoparticles using Azadirachta indica leaves. *Materials Chemistry and Physics*, *213*, 44–51. https://doi.org/10.1016/j.matchemphys.2018.04.007

Nan, M., Jin, B., Chow, C. W. K., and Saint, C. (2010). Recent developments in photocatalytic water treatment technology : A review. *Water Research*, *44*(10), 2997–3027. https://doi.org/10.1016/j.watres.2010.02.039

Nasuhoglu, D., Rodayan, A., Berk, D., and Yargeau, V. (2012). Removal of the antibiotic levofloxacin (LEVO) in water by ozonation and TiO 2 photocatalysis. *Chemical Engineering Journal*, *189–190*, 41–48.

Nathan, V. K., Parvathi, A., and Vijayan, J. (2018). *Photocatalytic Degradation of Synthetic Dyes using Iron (III) Oxide Photocatalytic degradation of synthetic dyes using iron (III) oxide nanoparticles (Fe O -Nps) synthesised using Rhizophora mucronata Lam*. *August*. https://doi.org/10.1049/iet-nbt.2018.5230

Naveen, P., Kaur, K., and Sidhu, A. K. (2021). *Green Synthesis : An Eco-friendly Route for the Synthesis of Iron Oxide Nanoparticles*. *3*(June).

Ncc, S., and A, F. J. (2010). *Biological properties of medicinal plants : a review of their antimicrobial activity*. *16*(3), 402–413.

Nguyen, T. T., Vo, T., Nguyen, B. N., Nguyen, D., and Dang, V. (2018). *Silver and gold nanoparticles biosynthesized by aqueous extract of burdock root , Arctium lappa as antimicrobial agent and catalyst for degradation of pollutants*.

Pantelidou, N. A., Theologides, C. P., Olympiou, G. G., Savva, P. G., Vasquez, M. I., and Costa, C. N. (2015). Catalytic removal of pharmaceutical compounds in water medium under an H2 stream over various metal-supported catalysts: A promising process. *Desalination and Water Treatment*, *53*(12), 3363–3370. https://doi.org/10.1080/19443994.2014.933620

Pappuswamy, M., Anand, A. V., Al-dhabi, N. A., and Arasu, M. V. (2023). *Green Synthesis of Bioinspired Nanoparticles Mediated from Plant Extracts of Asteraceae Family for Potential Biological Applications*.

Parhizkar, J., and Habibi, M. H. (2017). *Synthesis , characterization and photocatalytic properties of Iron oxide nanoparticles synthesized by sol-gel autocombustion with ultrasonic irradiation*. *2*(2), 166–171. https://doi.org/10.22036/ncr.2017.02.002

Parimelazhagan, T. (2016). *Pharmacological Assays of Plant-Based Natural Products* (Vol. 71). https://doi.org/10.1007/978-3-319-26811-8

Patel, M., Kumar, R., Kishor, K., Mlsna, T., Pittman, C. U., and Mohan, D. (2019). Pharmaceuticals of emerging concern in aquatic systems: Chemistry, occurrence, effects, and removal methods [Review-article]. *Chemical Reviews*, *119*(6), 3510–3673. https://doi.org/10.1021/acs.chemrev.8b00299

Ponce, C., Chanona, J., Garibay, V., Palacios, E., Calderon, G., and Sabo, R. (2013). Functionalization of Agave Cellulose Nanoparticles and its Characterization by Microscopy and Spectroscopy Techniques. *Microscopy and Microanalysis*, *19*(S2), 200–201. https://doi.org/10.1017/S1431927613002997

Ranjitha, S., and Suganthi, A. (2017). *Preliminary phytochemical analysis of galinsoga parviflora (Cav) leaves and flowers*. *2*(3), 18–20.

Rezaei, F., and Vione, D. (2018). Effect of pH on zero valent iron performance in heterogeneous Fenton and Fenton-like processes: A review. *Molecules*, *23*(12). https://doi.org/10.3390/molecules23123127

Ripanda, A., Luanda, A., Sule, K. S., Mtabazi, G. S., and Makangara, J. J. (2023). *Galinsoga parviflora* (Cav .): A comprehensive review on ethnomedicinal , phytochemical and pharmacological studies. *Heliyon*, *9*(2), e13517.

Rivera-Utrilla, J., Sánchez-Polo, M., Ferro-García, M. Á., Prados-Joya, G., and Ocampo-Pérez, R. (2013). Pharmaceuticals as emerging contaminants and their removal from water. A review. *Chemosphere*, *93*(7), 1268–1287. https://doi.org/10.1016/j.chemosphere.2013.07.059

Ruto, M. C., Ngugi, C. M., Kareru, P. G., Cheruiyot, K., Rechab, S. O., Madivoli, E. S., Mutembei, J. K., Kairigo, P. K., and Maina, E. G. (2018). Antioxidant activity and antimicrobial properties of *Entada leptostachya* and *Prosopis juliflora* extracts. *Journal of Medicinal Plants for Economic Development*, *2*(1), 8. https://doi.org/10.4102/jomped.v2i1.31

S, I., Korbekandi, H., Mirmohammadi, S. V, and Zolfaghari, B. (2014). *Synthesis of silver nanoparticles : chemical , physical and biological methods*. *9*(December), 385–406.

Saif, S., Tahir, A., and Chen, Y. (2016). Green Synthesis of Iron Nanoparticles and Their Environmental Applications and Implications. *Nanomaterials*, *6*(11). https://doi.org/10.3390/nano6110209

Salama, A., Mohamed, A., Aboamera, N. M., and Khattab, T. A. O. A. (2018). Photocatalytic degradation of organic dyes using composite nanofibers under UV irradiation. *Applied Nanoscience*, *8*(1), 155–161. https://doi.org/10.1007/s13204-018-0660-9

Saleh, T. A. (2016). Nanomaterials for Pharmaceuticals Determination. *Bioenergetics: Open Access*, *5*(1), 1–6. https://doi.org/10.4172/2167-7662.1000226

Saranya, S. (2017). *Green Synthesis of Iron Nanoparticles using Aqueous Extract of Musa ornata Flower Sheath against Pathogenic Bacteria*. *79*(July), 688–694.

Seigneuric, R., Markey, L., Nuyten, D. S. a, Dubernet, C., Evelo, C. T. a, Finot, E., and Garrido, C. (2010). From nanotechnology to nanomedicine: applications to cancer research. *Current Molecular Medicine*, *10*(7), 640–652. https://doi.org/10.2174/156652410792630634

Shah, A., Haq, S., Rehman, W., Waseem, M., Shoukat, S., and Rehman, M. U. (2019). Photocatalytic and antibacterial activities of paeonia emodi mediated silver oxide nanoparticles. *Materials Research Express*, *6*(4), 45045. https://doi.org/10.1088/2053-1591/aafd42

Shahryari-ghoshekandi, and Ramin, H. S. (2014). *Study in synthesis and characterization of carbon nanotubes decorated by magnetic iron oxide nanoparticles*. 129–135. https://doi.org/10.1007/s40089-014-0128-1

Shahwan, T., Abu Sirriah, S., Nairat, M., Boyaci, E., Eroğlu, A. E., Scott, T. B., and

Hallam, K. R. (2011). Green synthesis of iron nanoparticles and their application as a Fenton-like catalyst for the degradation of aqueous cationic and anionic dyes. *Chemical Engineering Journal*, *172*(1), 258–266.

Shaik, M., Ali, Z., Khan, M., Kuniyil, M., Assal, M., Alkhathlan, H., Al-Warthan, A., Siddiqui, M., Khan, M., and Adil, S. (2017). Green Synthesis and Characterization of Palladium Nanoparticles Using Origanum vulgare L. Extract and Their Catalytic Activity. *Molecules*, *22*(1), 165.

Shameli, K., Ahmad, M. Bin, Yunus, W. M. Z. W., Rustaiyan, A., Ibrahim, N. A., Zargar, M., and Abdollahi, Y. (2010). Green synthesis of silver/montmorillonite/chitosan bionanocomposites using the UV irradiation method and evaluation of antibacterial activity. *International Journal of Nanomedicine*, *5*(1), 875–887. https://doi.org/10.2147/IJN.S13632

Sharma, B. K., Bhandari, S., Maharjan, B., Shrestha, B., and Banjara, M. R. (2014). Rapid Detection of Rifampicin and Isoniazid Resistant Mycobacterium tuberculosis Using Genotype MTBDR plus Assay in Nepal . *International Scholarly Research Notices*, *2014*, 1–6. https://doi.org/10.1155/2014/648294

Siddiqi, K. S., ur Rahman, A., Tajuddin, and Husen, A. (2016). Biogenic Fabrication of Iron/Iron Oxide Nanoparticles and Their Application. In *Nanoscale Research Letters* (Vol. 11, Issue 1). https://doi.org/10.1186/s11671-016-1714-0

Silva, J. J. da, Cerdeira, C. D., Chavasco, J. M., Cintra, A. B. P., Silva, C. B. P. da, Mendonça, A. N. de, Ishikawa, T., Boriollo, M. F. G., and Chavasco, J. K. (2014). In vitro Screening Antibacterial Activity of Bidens pilosa Linné and Annona Crassiflora Mart. against Oxacillin Resistant *Staphylococcus Aureus* (Orsa) From The Aerial Environment At The Dental Clinic. *Revista Do Instituto de Medicina Tropical de São Paulo*, *56*(4), 333–340. https://doi.org/10.1590/S0036-46652014000400011

Silveira, C., Shimabuku, Q. L., Fernandes Silva, M., and Bergamasco, R. (2017). Iron-oxide Nanoparticles by Green Synthesis Method Using *Moringa oleifera* Leaf

Extract for Fluoride Removal. *Environmental Technology*, *3330*(August), 1–40. https://doi.org/10.1080/09593330.2017.1369582

Singh, I. (2017). Chemical Biology LETTERS Antimicrobials in higher plants: classification, mode of action and bioactivities. *Chemical Biology Letters Chem. Biol. Lett. Chem. Biol. Lett.Review . Received*, *4*(4), 48–62.

Slavin, Y. N., Asnis, J., Häfeli, U. O., and Bach, H. (2017). Metal nanoparticles: Understanding the mechanisms behind antibacterial activity. *Journal of Nanobiotechnology*, *15*(1), 1–20. https://doi.org/10.1186/s12951-017-0308-z

Smuleac, V., Varma, R., Sikdar, S., and Bhattacharyya, D. (2011). Green synthesis of Fe and Fe/Pd bimetallic nanoparticles in membranes for reductive degradation of chlorinated organics. *Journal of Membrane Science*, *379*(1–2), 131–137. https://doi.org/10.1016/j.memsci.2011.05.054

Smýkalová, A., Sokolová, B., Foniok, K., Matejka, V., and Praus, P. (2019). Photocatalytic degradation of selected pharmaceuticals using g-C3N4 and TiO2 nanomaterials. *Nanomaterials*, *9*(9). https://doi.org/10.3390/nano9091194

Soliemanzadeh, A., Fekri, M., Bakhtiary, S., and Mehrizi, M. H. (2016). Biosynthesis of iron nanoparticles and their application in removing phosphorus from aqueous solutions. *Chemistry and Ecology*, *32*(3), 286–300.

Sravanthi, K., Ayodhya, D., and Yadgiri Swamy, P. (2018). Green synthesis, characterization of biomaterial-supported zero-valent iron nanoparticles for contaminated water treatment. *Journal of Analytical Science and Technology*, *9*(1), 3. https://doi.org/10.1186/s40543-017-0134-9

Sudhasree, S., Shakila Banu, A., Brindha, P., and Kurian, G. A. (2014). Synthesis of nickel nanoparticles by chemical and green route and their comparison in respect to biological effect and toxicity. *Toxicological and Environmental Chemistry*, *96*(5), 743–754. https://doi.org/10.1080/02772248.2014.923148

Sukanya, Borthakur, Purashri, Basyach, Lisamoni, Kalita, Karanika, Sonowal, Amritanjali, Tiwari, Pubali, Chetia, and Saikia., L. (2020). *View Article Online Sun Light Assisted Degradation of Pollutant dye in water by WO3@g-C3N4 DOI: 10.1039/C9NJ05142B View Article Online Sun Light Assisted Degradation of Pollutant dye in water by WO3@g-C3N4 DOI: 10.1039/C9NJ05142B View Article Online Sun L*. https://doi.org/10.1039/C9NJ05142B

Sulaiman, G. M., Tawfeeq, A. T., and Naji, A. S. (2018). Biosynthesis, characterization of magnetic iron oxide nanoparticles and evaluations of the cytotoxicity and DNA damage of human breast carcinoma cell lines. *Artificial Cells, Nanomedicine and Biotechnology*, *46*(6), 1215–1229.

Suresh, J., Pradheesh, G., and Alexramani, V. (2017). Green synthesis and characterization of zinc oxide nanoparticle using insulin plant (Costus pictus D . Don) and investigation of its antimicrobial as well as anticancer activities. *Advances in Natural Sciences: Nanoscience and Nanotechnology*.

Tadesse, S., Alemayehu, H., Tenna, A., Tadesse, G., Shibeshi, T. S. T. W., and Eguale, T. (2018). *Antimicrobial resistance profile of Staphylococcus aureus isolated from patients with infection at Tikur Anbessa*. 1–8.

Teixeira, S., Gurke, R., Eckert, H., Kühn, K., Fauler, J., and Cuniberti, G. (2016). Photocatalytic degradation of pharmaceuticals present in conventional treated wastewater by nanoparticle suspensions. *Journal of Environmental Chemical Engineering*, *4*(1), 287–292. https://doi.org/10.1016/j.jece.2015.10.045

Thabit, R. A. S., Cheng, X.-R., Al-Hajj, N., Rahman, R. T., and Le, G.-W. (2014). Antioxidant and Conyza bonariensis : A Review. *European Academic Research*, *2*(6), 8454–8474.

Vaishnav, J., Subha, V., Kirubanandan, S., Arulmozhi, M., and Renganathan, S. (2017). Green Synthesis of Zinc Oxide Nanoparticles By Celosia Argentea and Its Characterization. *Journal of Optoelectronics and Biomedical Materials*, *9*(1), 59–71. http://www.chalcogen.ro/59_VaishnavJ.pdf

Vediyappan, G., Dumontet, V., Pelissier, F., and D'Enfert, C. (2013). *Gymnemic Acids Inhibit Hyphal Growth and Virulence in Candida albicans*. *8*(9). https://doi.org/10.1371/journal.pone.0074189

Veeramanikandan, V., Madhu, G. C., Pavithra, V., Jaianand, K., and Balaji, P. (2017). Green Synthesis , Characterization of Iron Oxide Nanoparticles using Leucas Aspera Leaf Extract and Evaluation of Antibacterial and Antioxidant Studies. *International Journal of Agriculture Innovations and Research*, *6*(2), 242–250.

Velichkova, F., Julcour-Lebigue, C., Koumanova, B., and Delmas, H. (2013). Heterogeneous Fenton oxidation of paracetamol using iron oxide (nano)particles. *Journal of Environmental Chemical Engineering*, *1*(4), 1214–1222. https://doi.org/10.1016/j.jece.2013.09.011

Velusamy, P., Kumar, G. V., Jeyanthi, V., Das, J., and Pachaiappan, R. (2016). Bio-inspired green nanoparticles: Synthesis, mechanism, and antibacterial application. *Toxicological Research*, *32*(2), 95–102.

W, C., X, W., and Z, C. (2019). Highly efficient removal of antibiotic rifampicin from aqueous solution using green synthesis of recyclable nano-Fe3O4. *Environmental Pollution*, *247*, 839–846. https://doi.org/10.1016/j.envpol.2019.01.108

Wang, T., Jin, X., Chen, Z., Megharaj, M., and Naidu, R. (2014). Green synthesis of Fe nanoparticles using eucalyptus leaf extracts for treatment of eutrophic wastewater. *Science of the Total Environment*, *466–467*, 210–213.

Wang, Z., Fang, C., and Megharaj, M. (2014). Characterization of iron-polyphenol nanoparticles synthesized by three plant extracts and their fenton oxidation of azo dye. *ACS Sustainable Chemistry and Engineering*, *2*(4), 1022–1025. https://doi.org/10.1021/sc500021n

Weng, X., Jin, X., Lin, J., Naidu, R., and Chen, Z. (2016). Removal of mixed contaminants Cr(VI) and Cu(II) by green synthesized iron based nanoparticles. *Ecological Engineering*, *97*, 32–39.

WHO. (2022a). *Global report on infection prevention and control*.

WHO. (2022b). *Global Tuberclosis Report 2022*.

WHO, D. of V. and I. P. and D. (2010). Prevention and Management of Wound Infection. *Guidance from WHO's Department of Violence and Injury Prevention and Disability and the Department of Essential Health Technologies*, *January*, 1–3.

Wink, M. (2015). *Modes of Action of Herbal Medicines and Plant Secondary Metabolites*. 251–286. https://doi.org/10.3390/medicines2030251

Wood, S. J., Kuzel, T. M., and Shafikhan, S. H. (2023). *Pseudomonas aeruginosa: Infections, Animal Modeling, and Therapeutics*. 1–37.

Xiao, Z., Yuan, M., Yang, B., Liu, Z., Huang, J., and Sun, D. (2016). Plant-mediated synthesis of highly active iron nanoparticles for Cr (VI) removal: Investigation of the leading biomolecules. *Chemosphere*, *150*, 357–364.

Xu, Q., Owens, G., and Chen, Z. (2020). Adsorption and catalytic reduction of rifampicin in wastewaters using hybrid rGO @ Fe / Pd nanoparticles. *Journal of Cleaner Production*, *264*, 121617. https://doi.org/10.1016/j.jclepro.2020.121617

Yadav, A. (2018). *Syntesis Of Nanomaterials By Physical and Syntesis Of Nanomaterials By Physical And Chemical Methods*. *June 2017*, 1–4.

Yadi, M., Mostafavi, E., Saleh, B., Davaran, S., Aliyeva, I., Khalilov, R., Nikzamir, M., Nikzamir, N., Akbarzadeh, A., Panahi, Y., and Milani, M. (2018). Current developments in green synthesis of metallic nanoparticles using plant extracts: a review. *Artificial Cells, Nanomedicine and Biotechnology*, *46*(sup3), S336–S343.

Yang, Y., Ok, Y. S., Kim, K. H., Kwon, E. E., and Tsang, Y. F. (2017). Occurrences and removal of pharmaceuticals and personal care products (PPCPs) in drinking water and water/sewage treatment plants: A review. *Science of the Total Environment*, *596–597*, 303–320.

Yargeau, V., and Danylo, F. (2015). Removal and transformation products of ibuprofen obtained during ozone- and ultrasound-based oxidative treatment. *Water Science and Technology*, *72*(3), 491–500.

Yew, Y. P., Shameli, K., Miyake, M., Kuwano, N., Bt Ahmad Khairudin, N. B., Bt Mohamad, S. E., and Lee, K. X. (2016). Green Synthesis of Magnetite (Fe3O4) Nanoparticles Using Seaweed (Kappaphycus alvarezii) Extract. *Nanoscale Research Letters*, *11*(1). https://doi.org/10.1186/s11671-016-1498-2

Yi, Y., Wang, C., Cheng, X., Yi, K., Huang, W., and Yu, H. (2021). *Biosynthesis of Silver Nanoparticles by Conyza canadensis and Their Antifungal Activity against Bipolaris maydis*.

Yuan, C. G., Huo, C., Gui, B., and Cao, W. P. (2017). Green synthesis of gold nanoparticles using Citrus maxima peel extract and their catalytic/antibacterial activities. *IET Nanobiotechnology*, *11*(5), 523–530. https://doi.org/10.1049/iet-nbt.2016.0183

Zachary, J. F. (2020). *Mechanisms of Microbial Infections*. *January*.

Zamin, S. N., Naveed, M., Zada, K. A., Muhammad, S., Haroon, K., Sadia, A., Uddin, G., and Rauf, A. (2013). *Phytochemical Analysis and Antioxidant Studies of Conyza bonarensis*. *6*(3), 109–112.

Zare, K., Najafi, F., Sadegh, H., and Shahryari, R. (2013). *Studies of ab initio and Monte Carlo simulation on interaction of fluorouracil anticancer drug with carbon nanotube*. 1–8.

APPENDICES

Appendix I: Voucher Specimen deposited in the JKUAT Botany Herbarium

I (A) *Conyza bonariensis* JKUAT Botany Harbarium specimen voucher number

I (B) *Bidens pilosa* JKUAT Botany Harbarium specimen voucher number

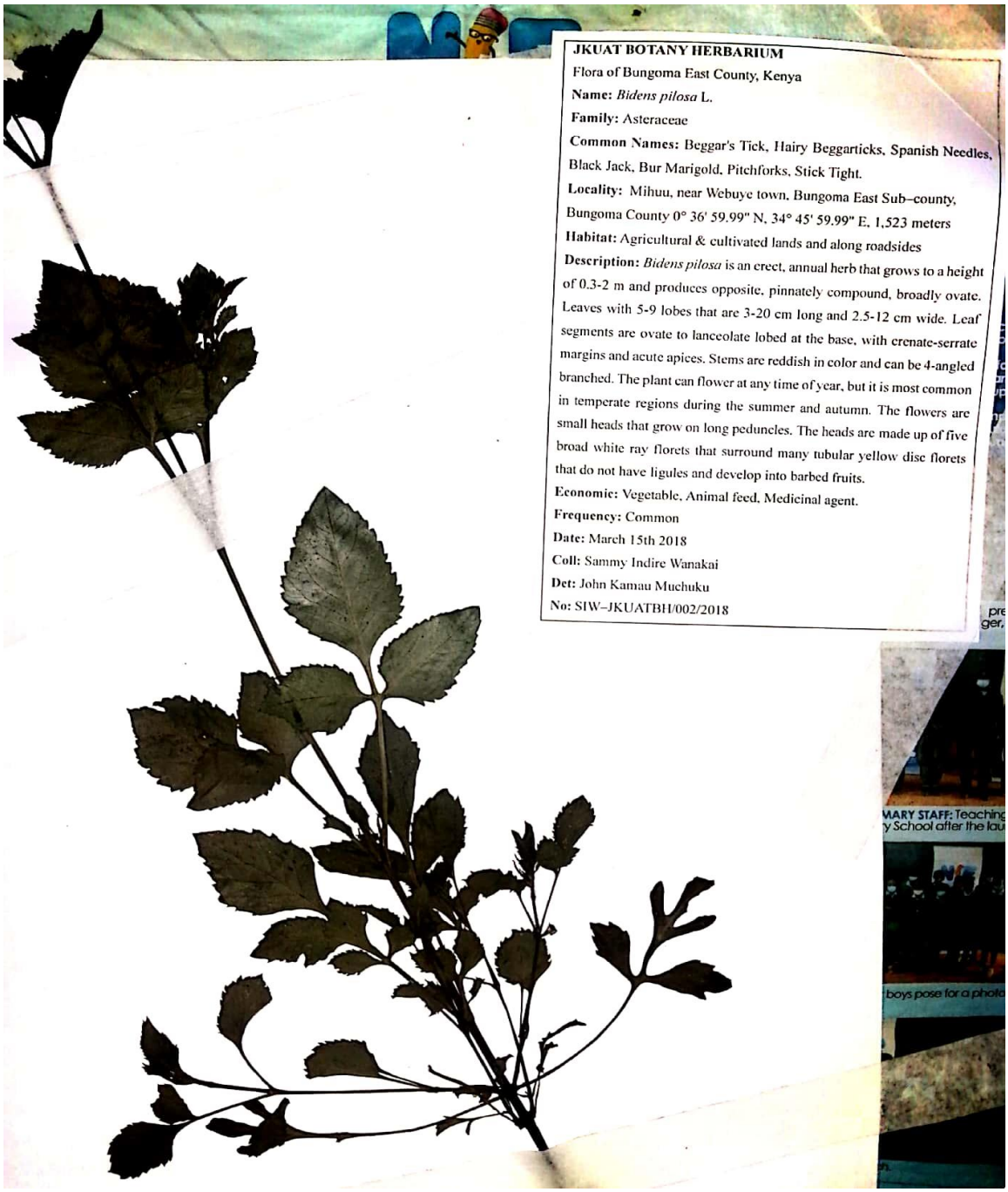

I (C) *Conyza bonariensis* JKUAT Botany Harbarium specimen voucher number

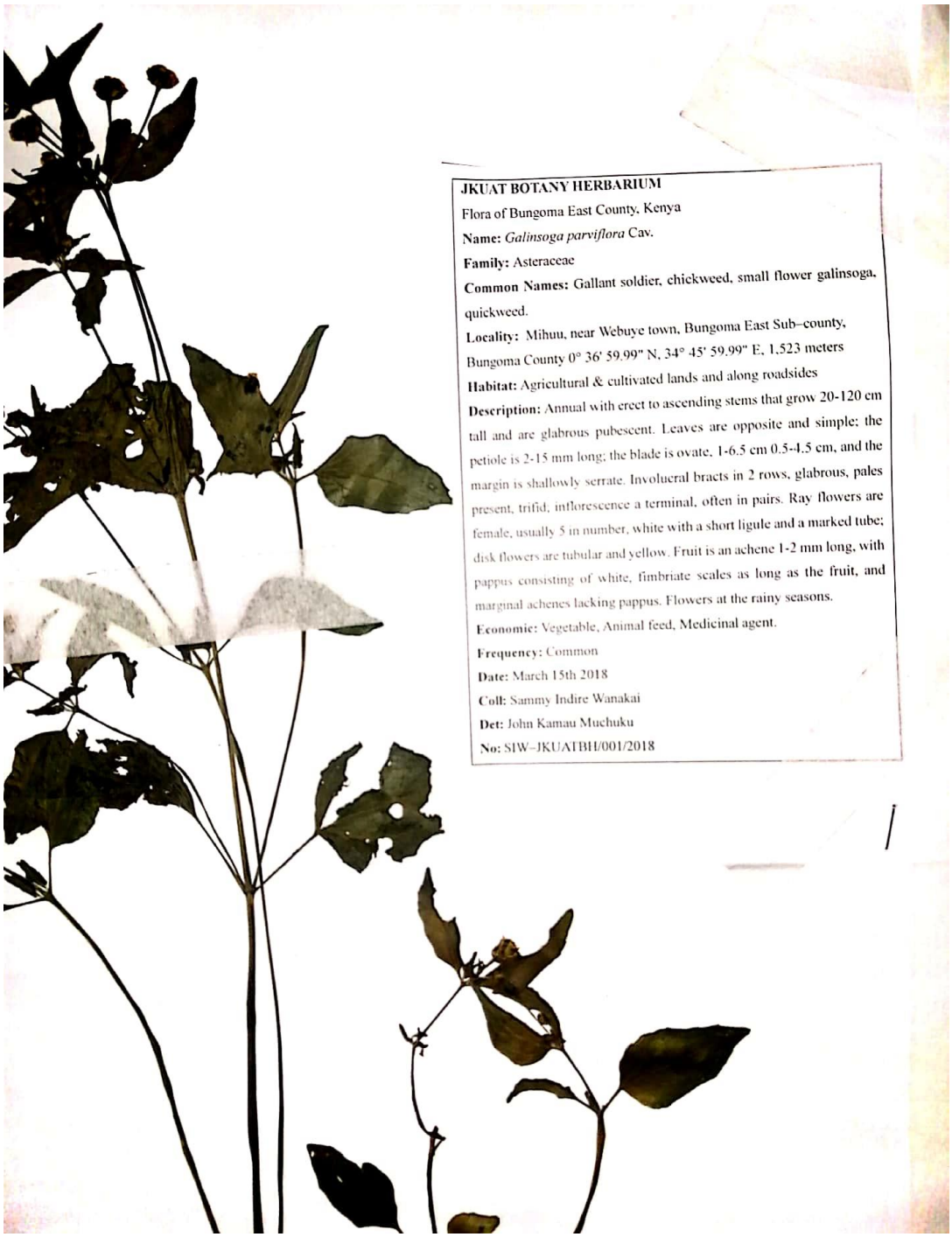

I (D) *Galinsoga parviflora*, Harbarium voucher number

JKUAT BOTANY HERBARIUM
Flora of Bungoma East County, Kenya
Name: *Galinsoga parviflora*
Family: Asteraceae
Common Names: Gallant soldier, chickweed, small flower galinsoga, quickweed.
Locality: Mihuu, near Webuye town, Bungoma East Sub–county, Bungoma County 0° 36' 59.99" N, 34° 45' 59.99" E, 1,523 meters
Habitat: Agricultural & cultivated lands and along roadsides
Description: Annual with erect to ascending stems that grow 20-120 cm tall and are glabrous pubescent. Leaves are opposite and simple; the petiole is 2-15 mm long; the blade is ovate, 1-6.5 cm 0.5-4.5 cm, and the margin is shallowly serrate. Involucral bracts in 2 rows, glabrous, pales present, trifid; inflorescence a terminal, often in pairs. Ray flowers are female, usually 5 in number, white with a short ligule and a marked tube; disk flowers are tubular and yellow. Fruit is an achene 1-2 mm long, with pappus consisting of white, fimbriate scales as long as the fruit, and marginal achenes lacking pappus. Flowers at the rainy seasons.
Economic: Vegetable, Animal feed, Medicinal agent.
Frequency: Common
Date: March 15th 2018
Coll: Sammy Indire Wanakai
Det: John Kamau Muchuku
No: SIW–JKUATBH/001/2018

I (E) *Galinsoga parviflora*, Herbarium voucher number

JKUAT BOTANY HERBARIUM
Flora of Bungoma East County, Kenya
Name: *Conyza bonariensis*
Family: Asteraceae
Common Names: Hairy Horseweed, hairy fleabane,
Locality: Mihuu, near Webuye town, Bungoma East Sub–county, Bungoma County 0° 36' 59.99" N, 34° 45' 59.99" E, 1,523 meters
Habitat: Agricultural & cultivated lands and along roadsides
Description: Annual herb up to 1 m tall with grey, stiff, bristly hairs. Below the flower-heads, the stems are densely hairy and unbranched. Leaves are toothed and narrow-oblanceolate, 4-9 cm long and 5-15 mm wide. Flower-heads in a pyramidal panicle, each 5-6 mm long and 8-12 mm diameter. The fruit is a pale, softly hairy oblong achene with a white to pale pink pappus. Flowers from late spring to late autumn.
Economic: Animal feed, Medicinal agent.
Frequency: Common
Date: March 15th 2018
Coll: Sammy Indire Wanakai
Det: John Kamau Muchuku
No: SIW–JKUATBH/002/2018

I (F) *Galinsoga parviflora*, Herbarium voucher number

JKUAT BOTANY HERBARIUM
Flora of Bungoma East County, Kenya
Name: *Bidens pilosa*
Family: Asteraceae
Common Names: Beggar's Tick, Hairy Beggarticks, Spanish Needles, Black Jack, Bur Marigold, Pitchforks, Stick Tight.
Locality: Mihuu, near Webuye town, Bungoma East Sub–county, Bungoma County 0° 36' 59.99" N, 34° 45' 59.99" E, 1,523 meters
Habitat: Agricultural & cultivated lands and along roadsides
Description: *Bidens pilosa* is an erect, annual herb that grows to a height of 0.3-2 m and produces opposite, pinnately compound, broadly ovate. Leaves with 5-9 lobes that are 3-20 cm long and 2.5-12 cm wide. Leaf segments are ovate to lanceolate lobed at the base, with crenate-serrate margins and acute apices. Stems are reddish in color and can be 4-angled branched. The plant can flower at any time of year, but it is most common in temperate regions during the summer and autumn. The flowers are small heads that grow on long peduncles. The heads are made up of five broad white ray florets that surround many tubular yellow disc florets that do not have ligules and develop into barbed fruits.
Economic: Vegetable, Animal feed, Medicinal agent.
Frequency: Common
Date: March 15th 2018
Coll: Sammy Indire Wanakai
Det: John Kamau Muchuku
No: SIW–JKUATBH/003/2018

Appendix II: Determination of the Average Crystal Lattice Constant

II (A) Average lattice constant of GpNPs

2θ **degree**	**θ** **degree**	**$Sin^2\theta$**	$\frac{Sin^2\theta}{Sin^2\theta_{min}}$	$3\left\{\frac{Sin^2\theta}{Sin^2\theta_{min}}\right\}$	$h^2+k^2+l^2$	***hkl***	**Å**
29.89	14.945	0.0665	1.0000	3.0000	3	111	5.1745
34.20	17.100	0.0865	1.2999	3.8999	4	200	5.2404
43.05	21.525	0.1346	2.0241	6.07237	6	211	5.1436
49.02	24.510	0.1721	2.5876	7.7631	8	220	5.2529
53.29	26.645	0.2011	3.0239	9.0719	9	300	5.1540
57.72	28.860	0.2330	3.5029	10.5087	11	311	5.2941
			Average				5.2099

II (B) Average lattice constant of BpNPs

2θ **degrees**	**θ** **degree**	**$Sin^2\theta$**	$\frac{Sin^2\theta}{Sin^2\theta_{min}}$	$3\left\{\frac{Sin^2\theta}{Sin^2\theta_{min}}\right\}$	$h^2+k^2+l^2$	***hkl***	**Å**
16.03	8.015	0.019441	1.000	3.00	3	111	9.5717
21.44	10.72	0.034599	1.779	5.33	5	210	9.2618
32.73	16.37	0.079386	4.083	12.25	12	222	9.4725
36.45	18.23	0.097812	5.031	15.09	15		9.5410
43.75	21.88	0.138818	7.140	21.42	21	421	9.4761
49.46	24.73	0.175011	9.002	27.01	27	511	9.5696
58.39	29.195	0.237932	12.238	36.72	36	442	9.4770
			Average				9.48

Appendix III: Degradation of Rifampicin by nanoparticles and H_2O_2

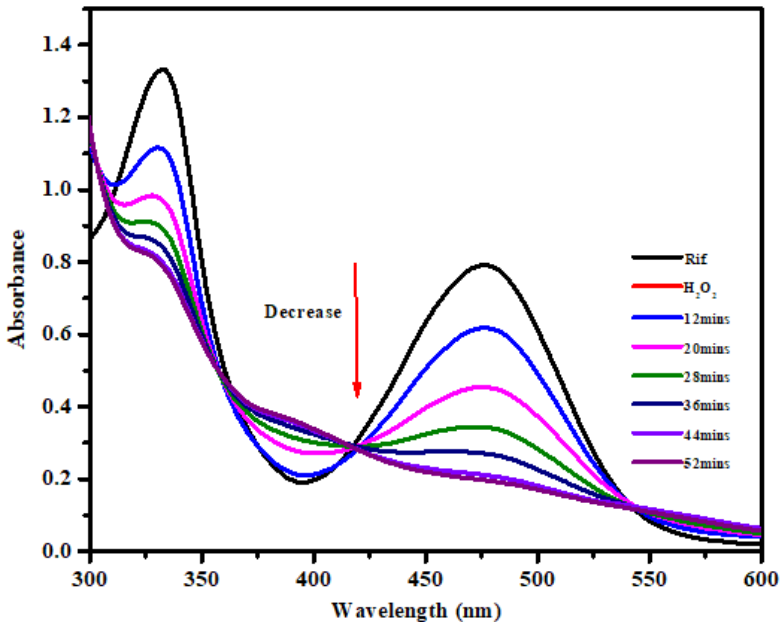

III (A) Degradation of Rifampicin by GpNPs in the presence of H_2O_2 pH 3

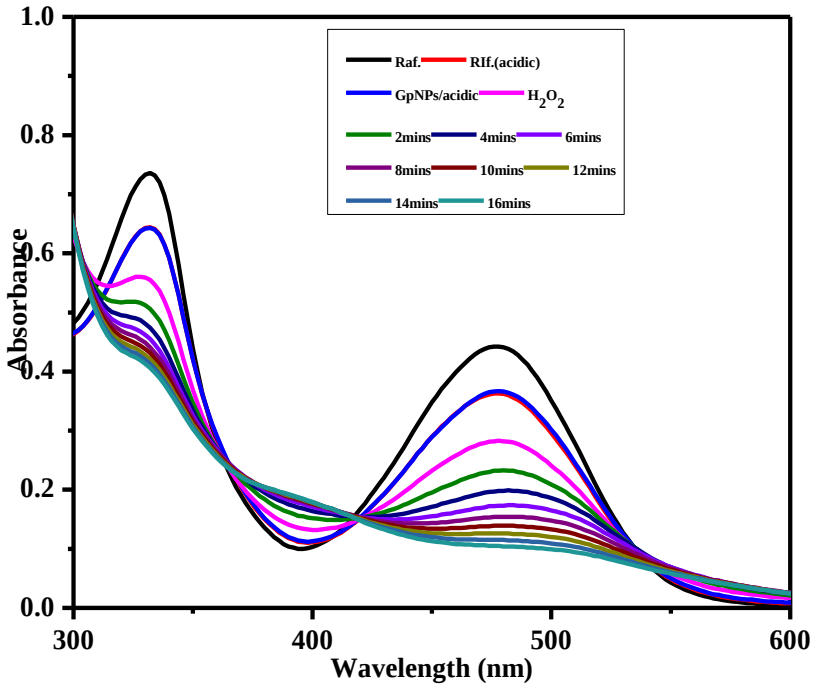

III(B) Degradation of Rifampicin by GpNPs in the presence of H_2O_2 pH 7

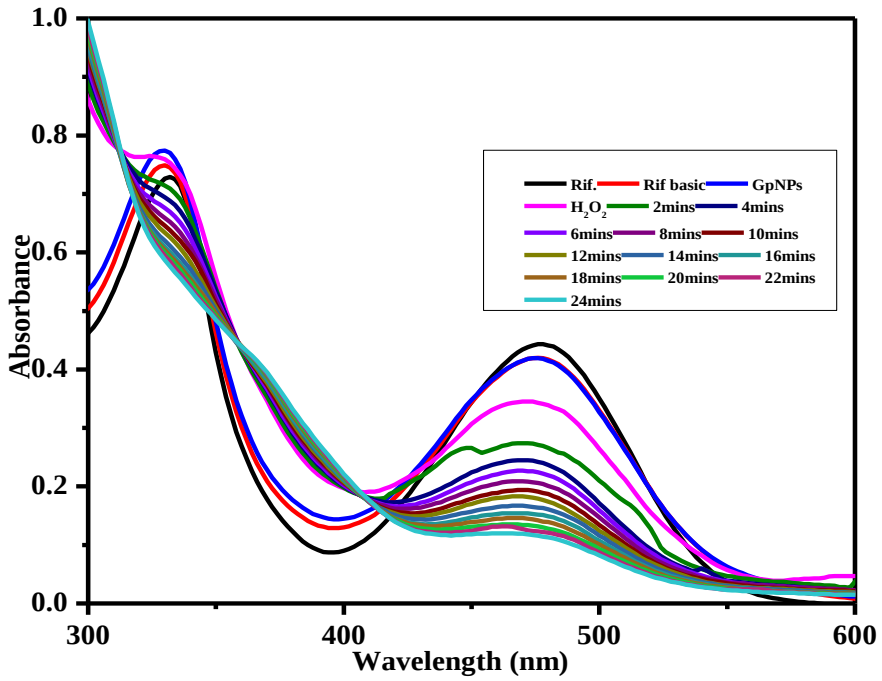

III (C) Degradation of Rifampicin by GpNPs in the presence of H2O2 pH 12

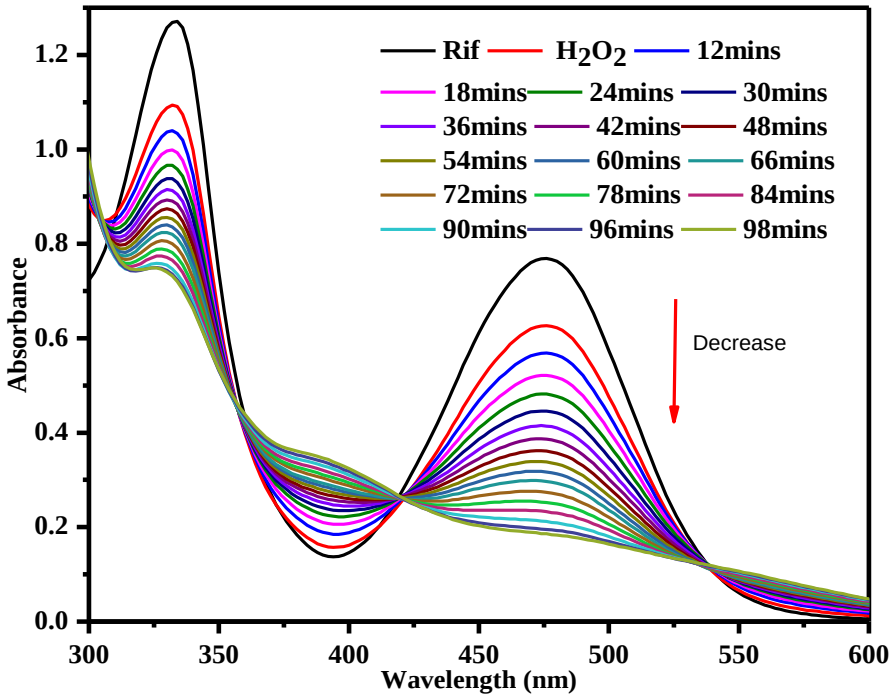

III (D) Degradation of Rifampicin by BpNPs in the presence of H_2O_2 at pH 7

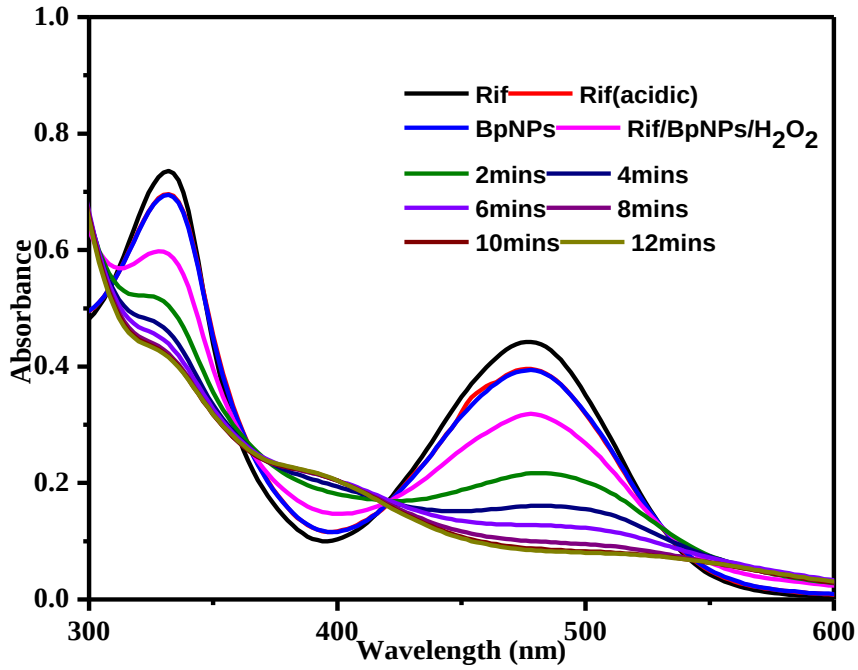

III (E) Degradation of Rifampicin by BpNPs in the presence of H_2O_2 at pH 3

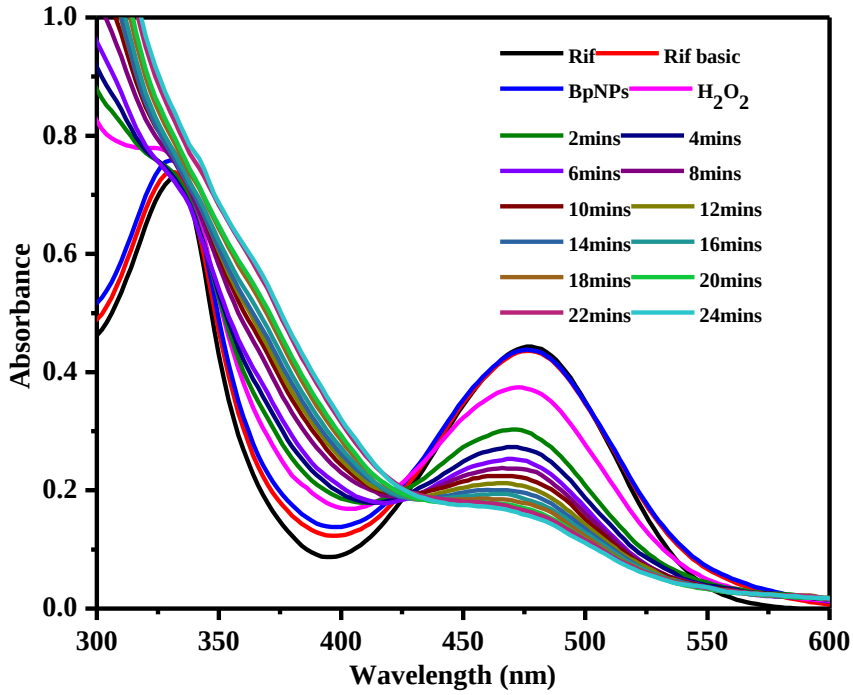

III (F) Degradation of Rifampicin by BpNPs in the presence of H_2O_2 at pH 12

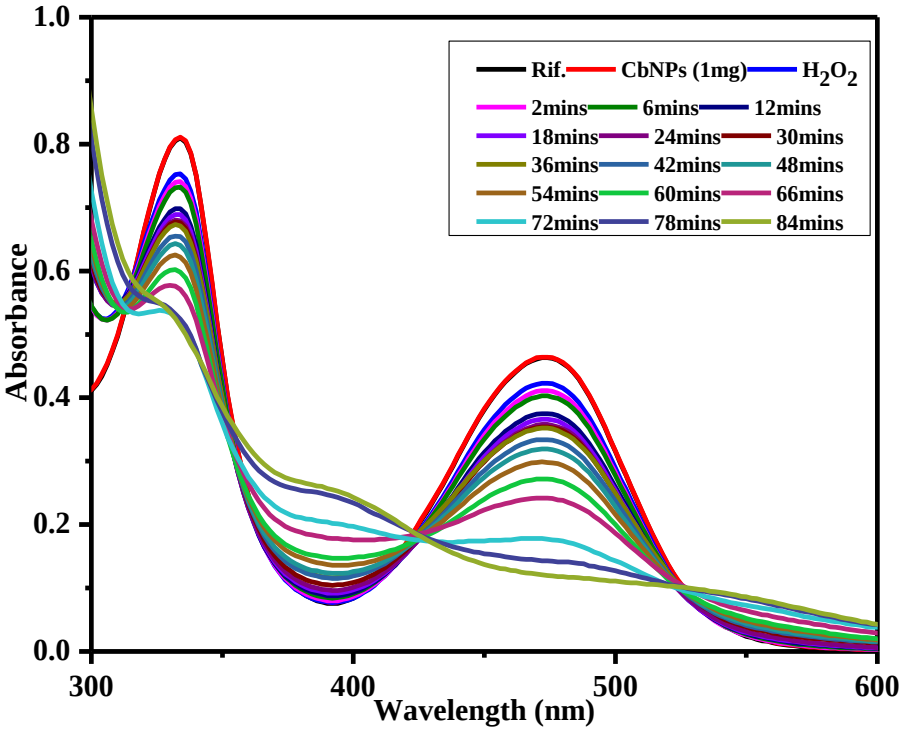

III (G) Degradation of Rifampicin by 10 mg of CbNPs in the presence of H_2O_2

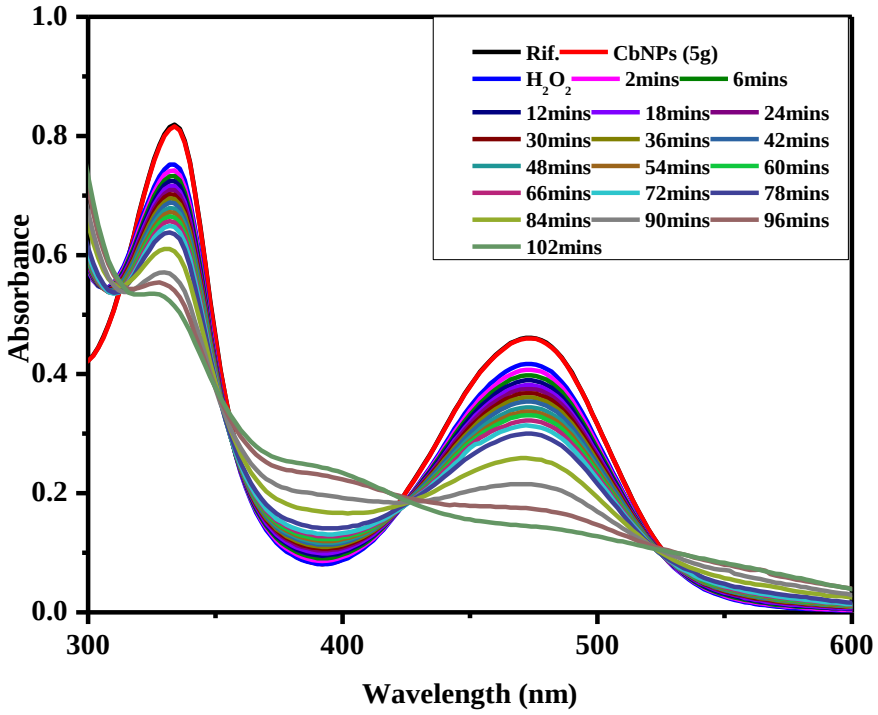

III (H) Degradation of Rifampicin by 5 mg of CbNPs in the presence of H_2O_2

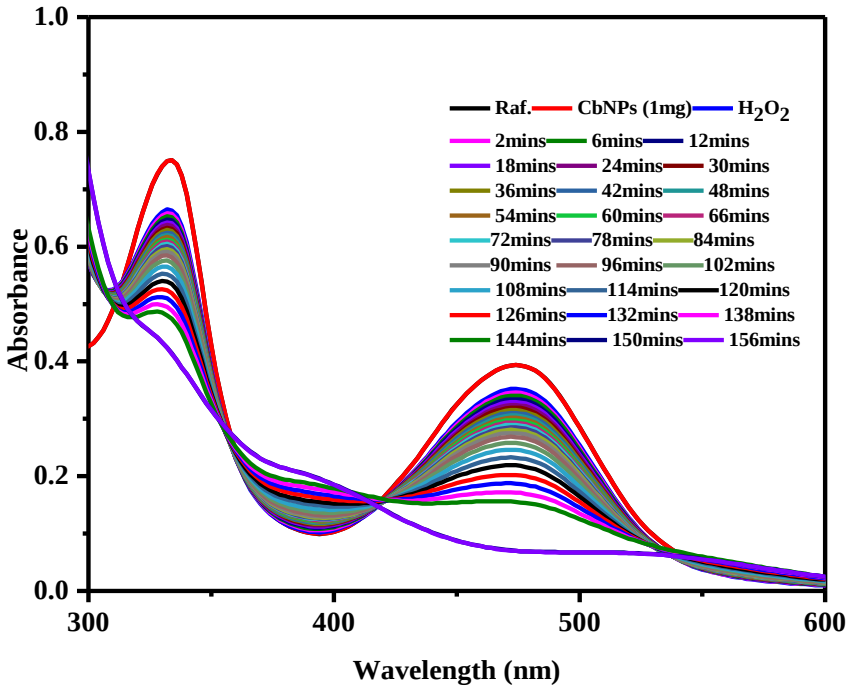

III (I) Degradation of Rifampicin by 1 mg of BpNPs in the presence of H_2O_2

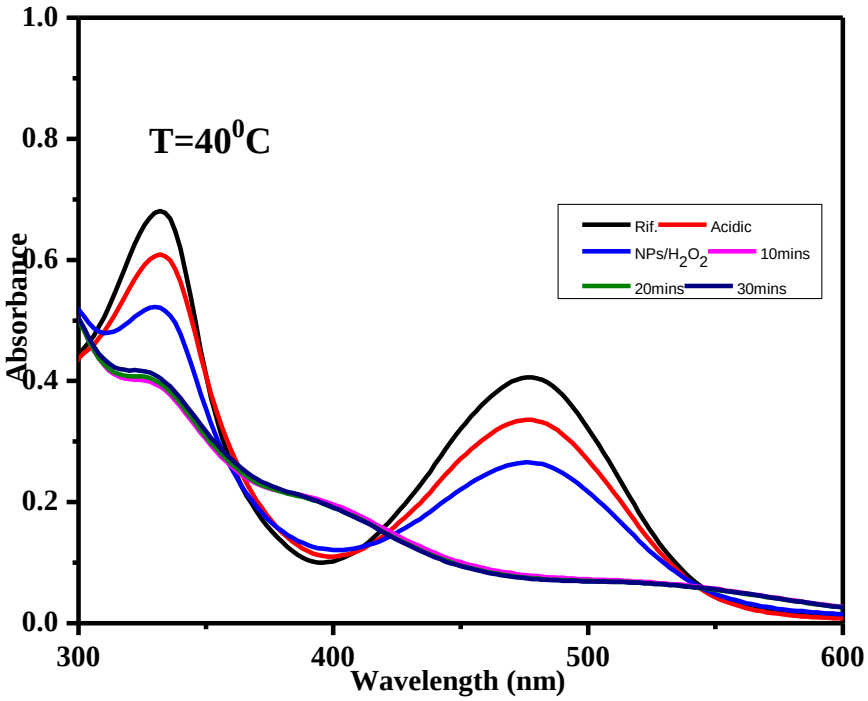

III (J) Degradation of Rifampicin using iron nanoparticles at 40 ℃

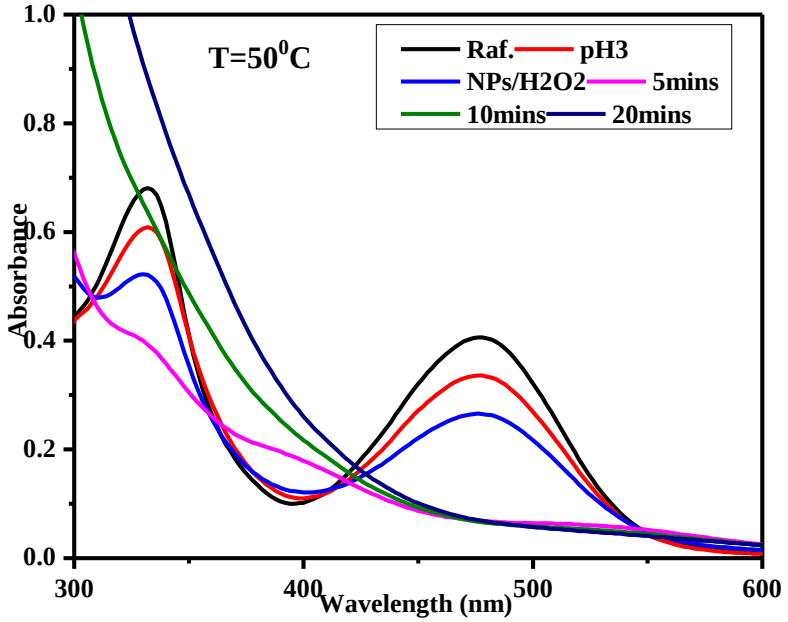

III (K) Degradation of Rifampicin using iron nanoparticles at 50 ℃

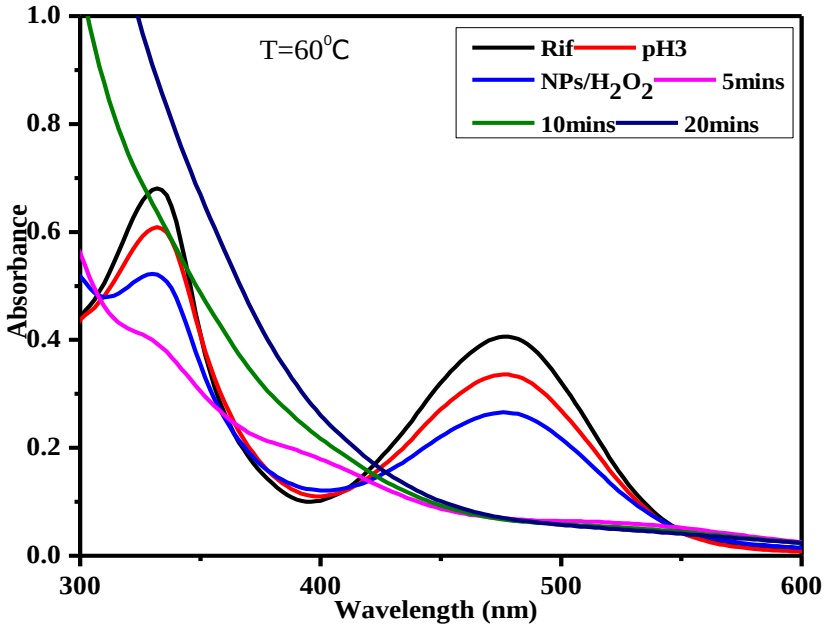

III (L) Degradation of Rifampicin using iron nanoparticles at 60 ℃

Appendix IV: Degradation of Methylene blue by CbNPs and H_2O_2

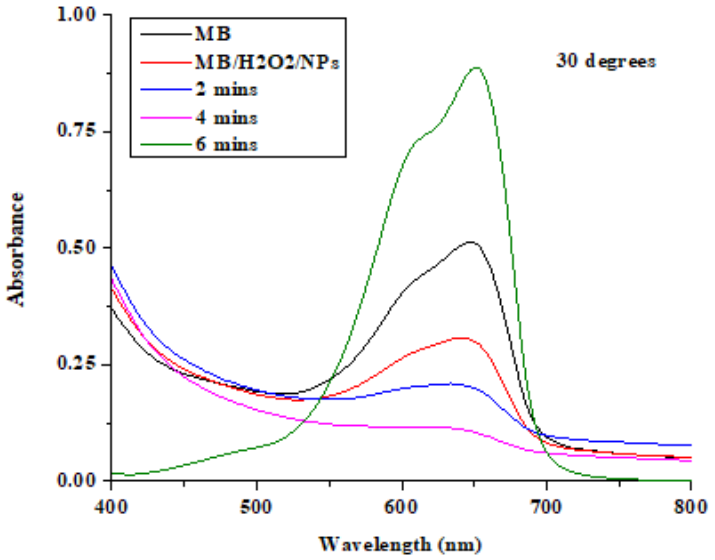

IV (A) Degradation of Methylene blue using *C. bonariensis* iron nanoparticles at 30℃

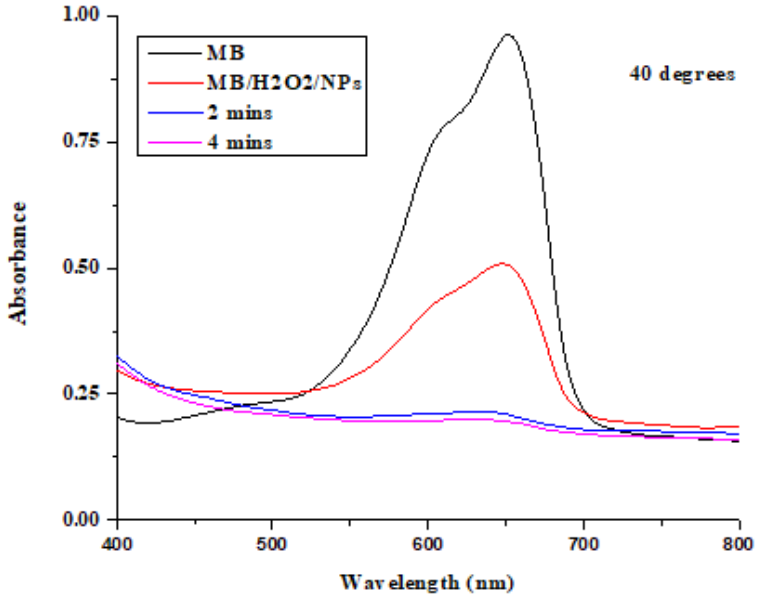

IV (B) Degradation of Methylene blue using *C. bonariensis* iron nanoparticles at 40℃

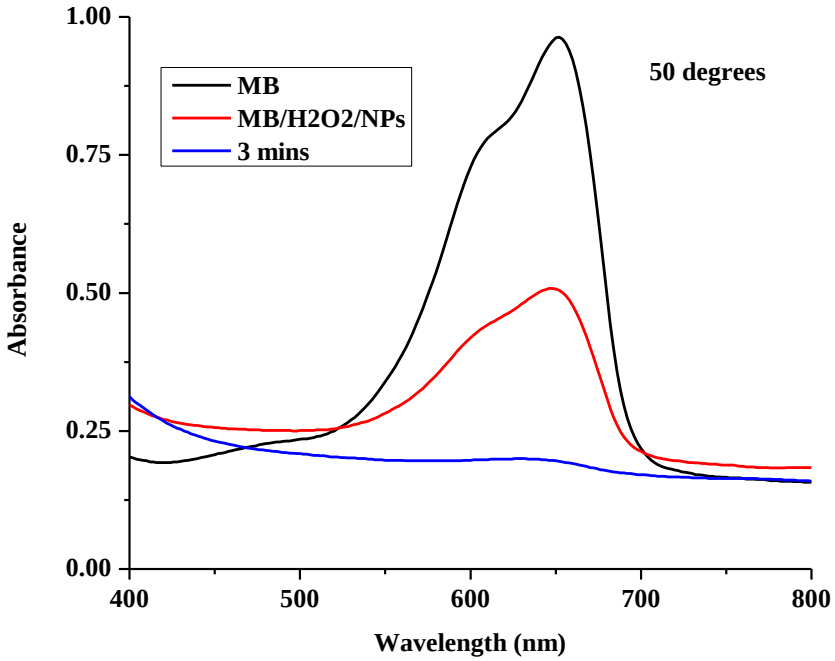

IV (C) Degradation of Methylene blue using *C. bonariensis* iron nanoparticles at 50 ℃

Appendix V: First–order Kinetics Plot of Rifampicin Degradation

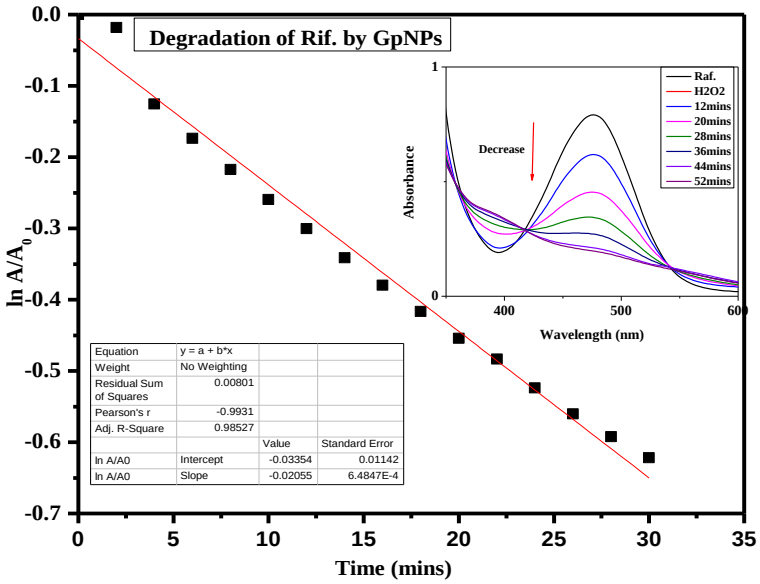

V (A) First–order kinetics plot of Rifampicin degradation using GpNPs/ H_2O_2

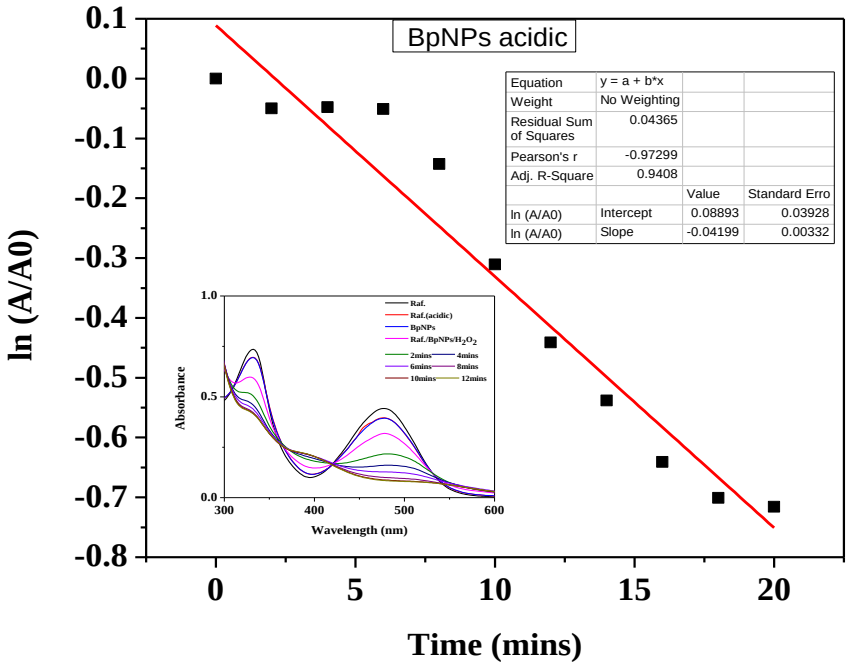

V (B) Kinetics of Rifampicin degradation using BpNPs/pH 3/H2O2

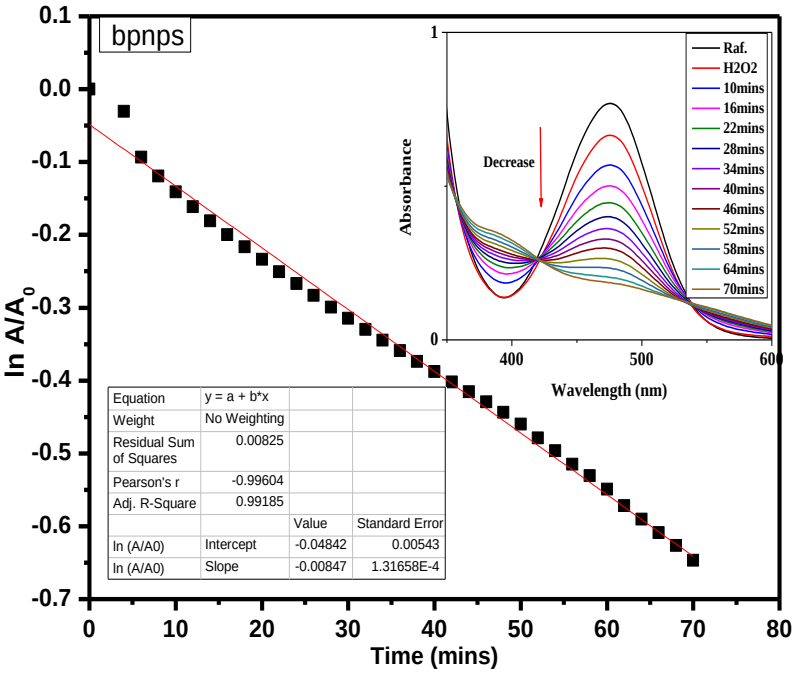

V (C) Kinetics of Rifampicin degradation using BpNPs/H_2O_2

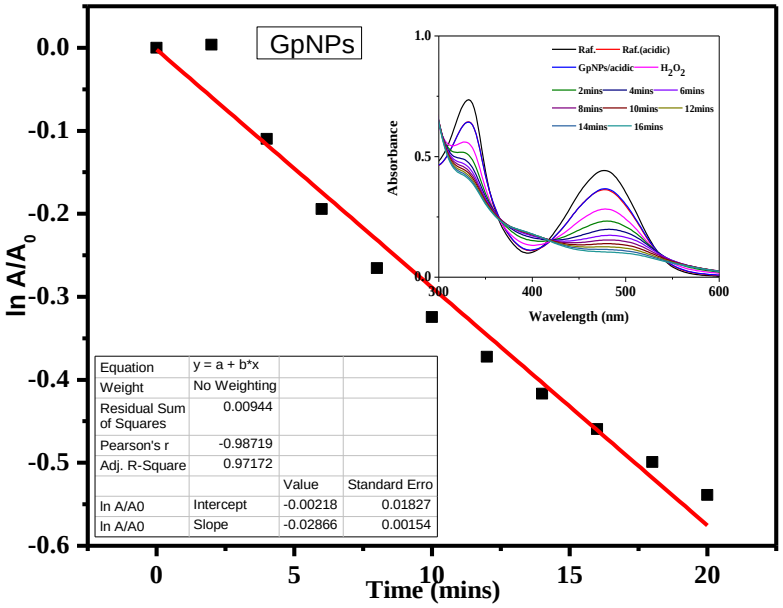

V (D) Kinetics of Rifampicin degradation using GpNPs/pH 3/H_2O_2

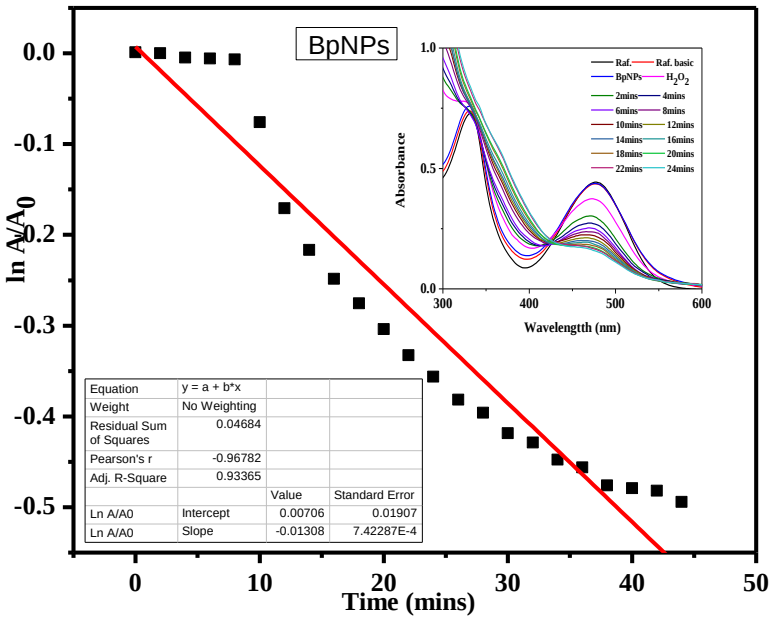

V (E) Kinetics of Rifampicin degradation using BpNPs/pH 12/H_2O_2

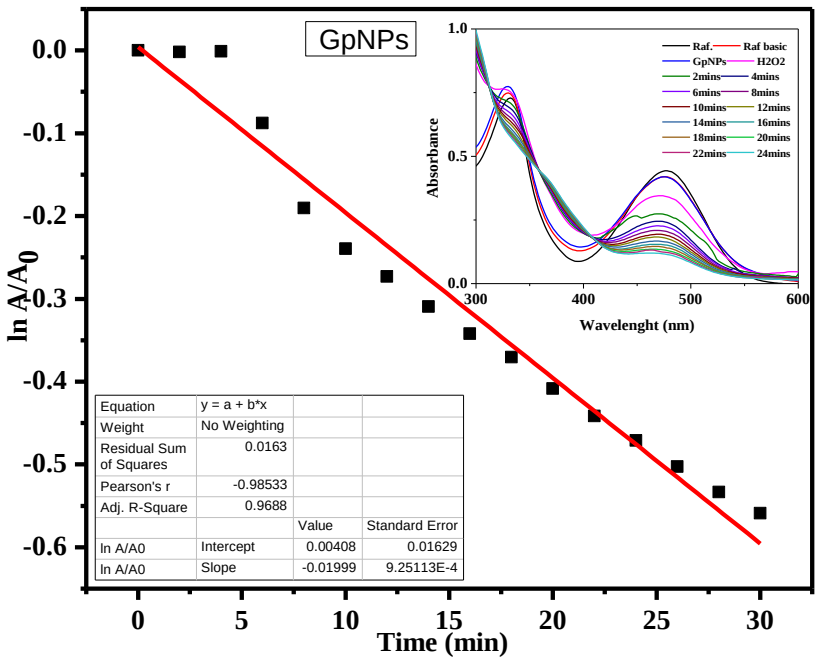

V (F) Kinetics of Rifampicin degradation using GpNPs/pH 3/H_2O_2

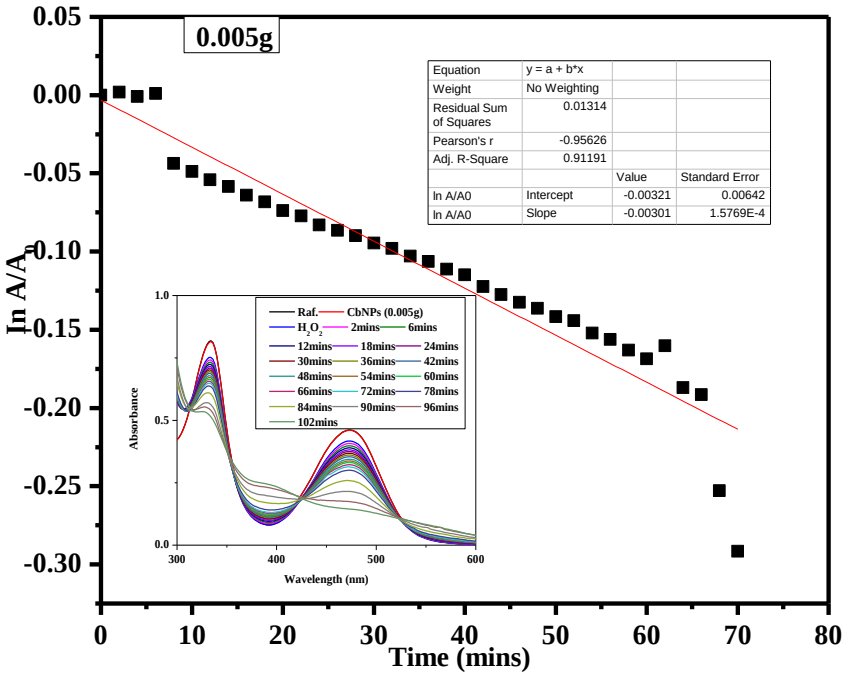

V (G) Kinetics of Rifampicin degradation using 5 mg of CbNPs

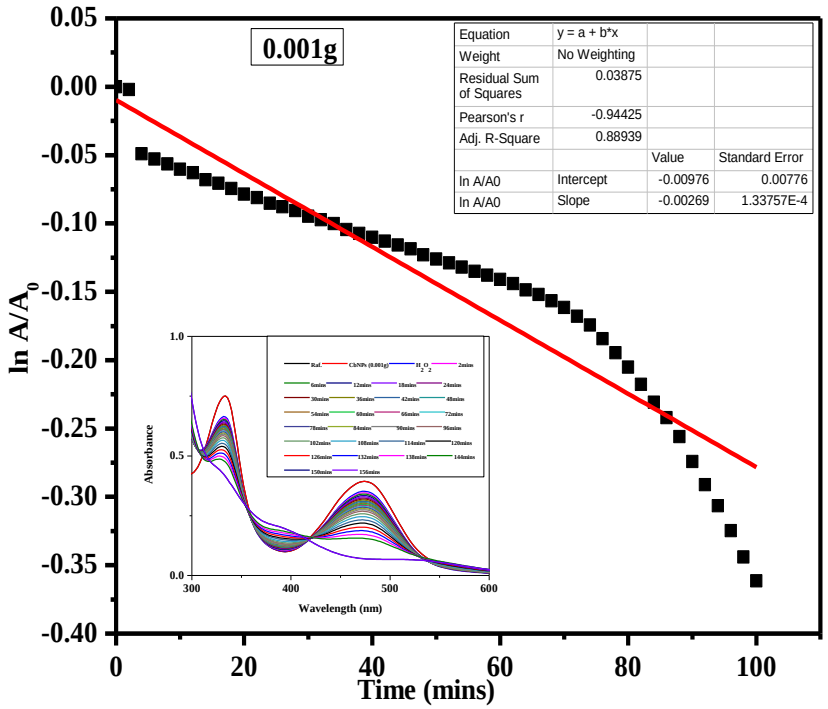

V (H) Kinetics of Rifampicin degradation using 1 mg of CbNPs

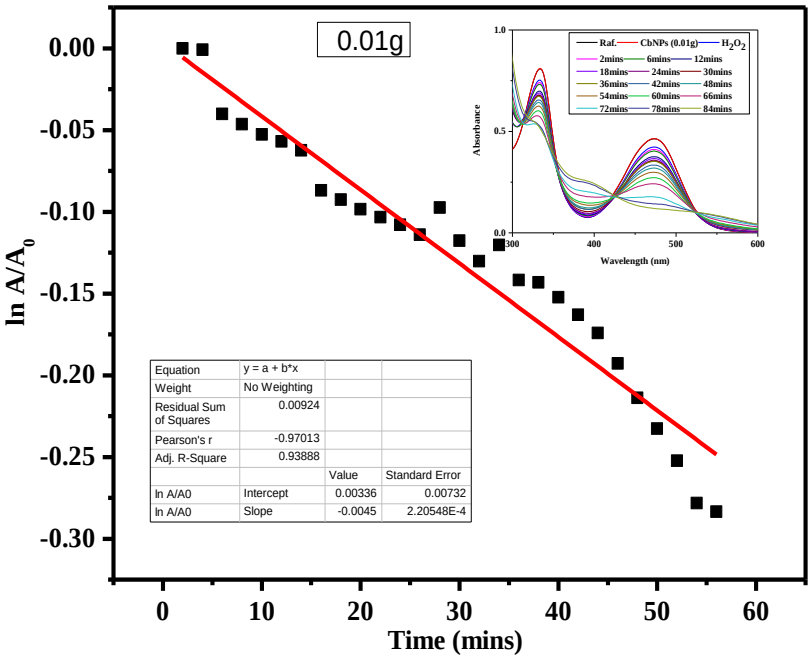

V (I) Kinetics of Rifampicin degradation using 10 mg of CbNPs

Appendix VI: Second–order Kinetics for the Degradation of Rifampicin

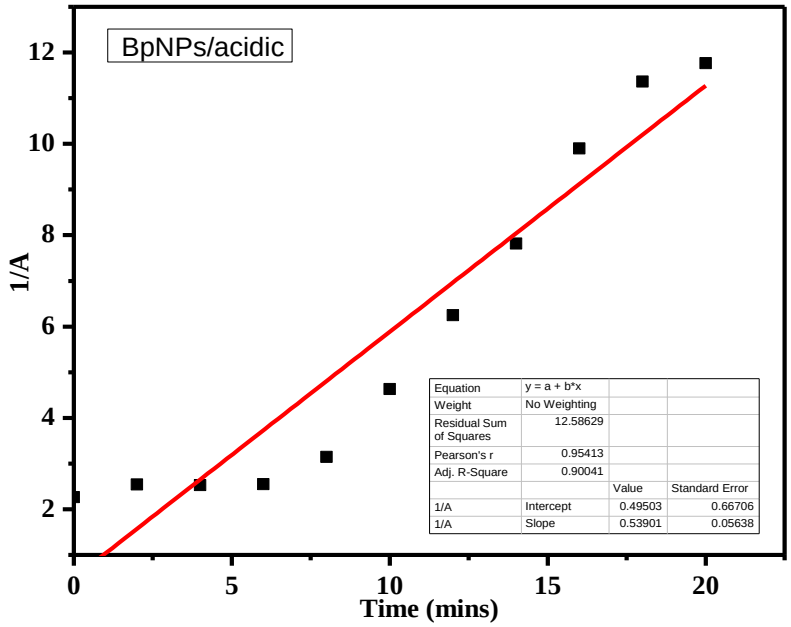

VI (A) Second–order kinetics for the degradation of Rifampicin by BpNPs/H_2O_2 at pH 3

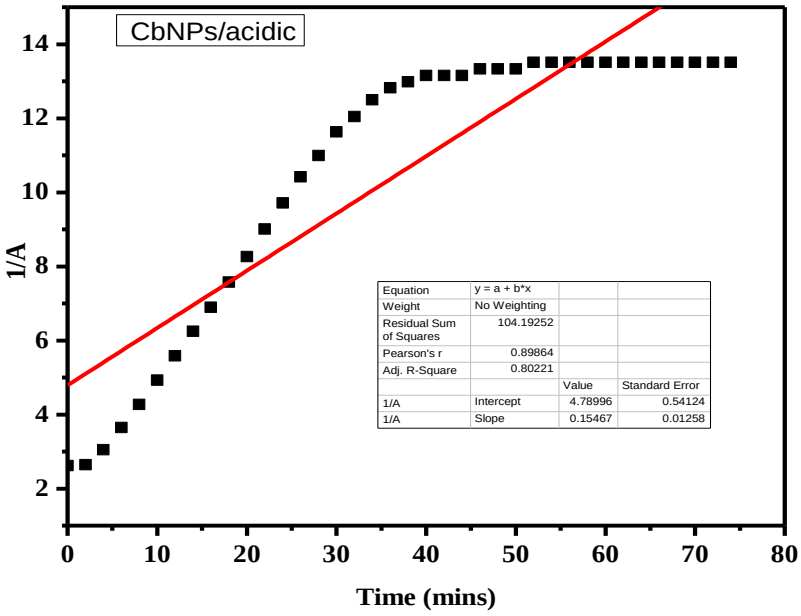

VI (B) Second–order kinetics for the degradation of Rifampicin by CbNPs/H_2O_2 at pH 3

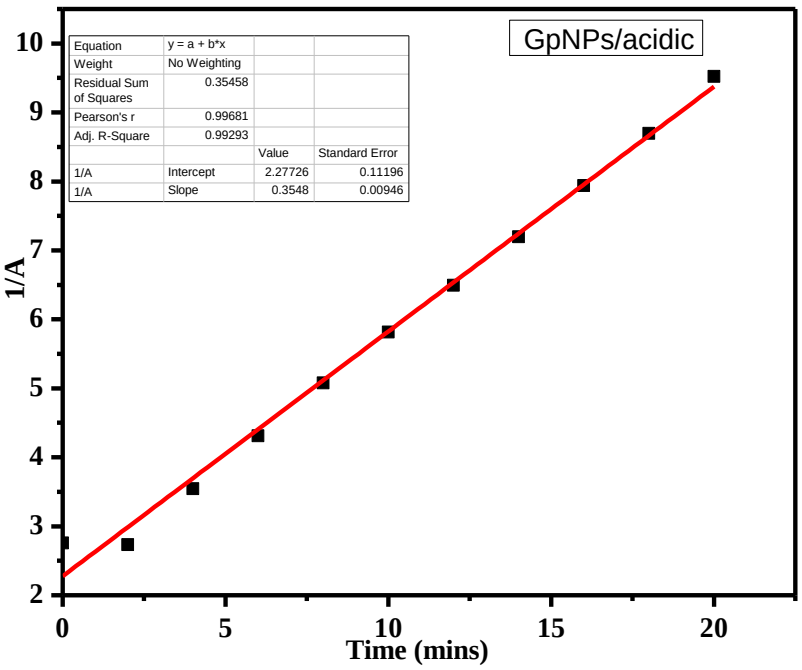

VI (C) Second–order kinetics for the degradation of Rifampicin by GpNPs/H_2O_2 at pH 3

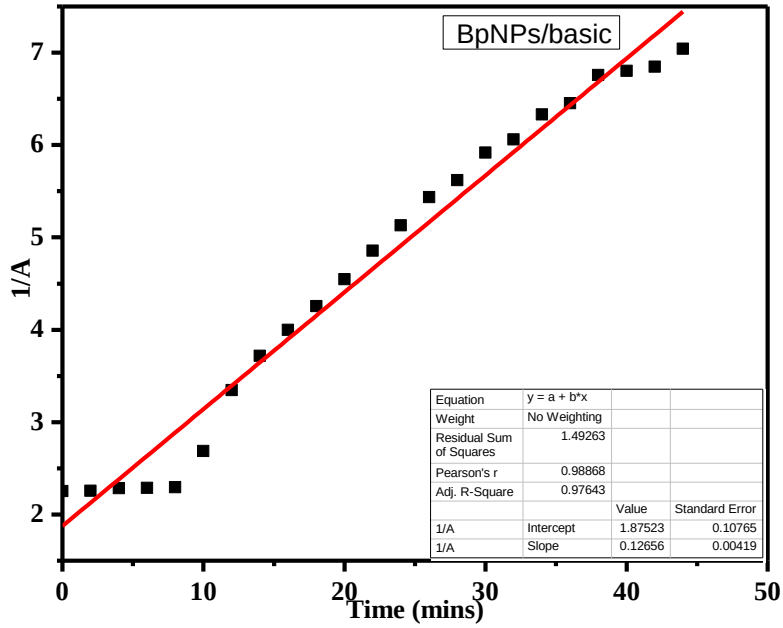

VI (D) Second–order kinetics for the degradation of Rifampicin by BpNPs/H_2O_2 at pH 12

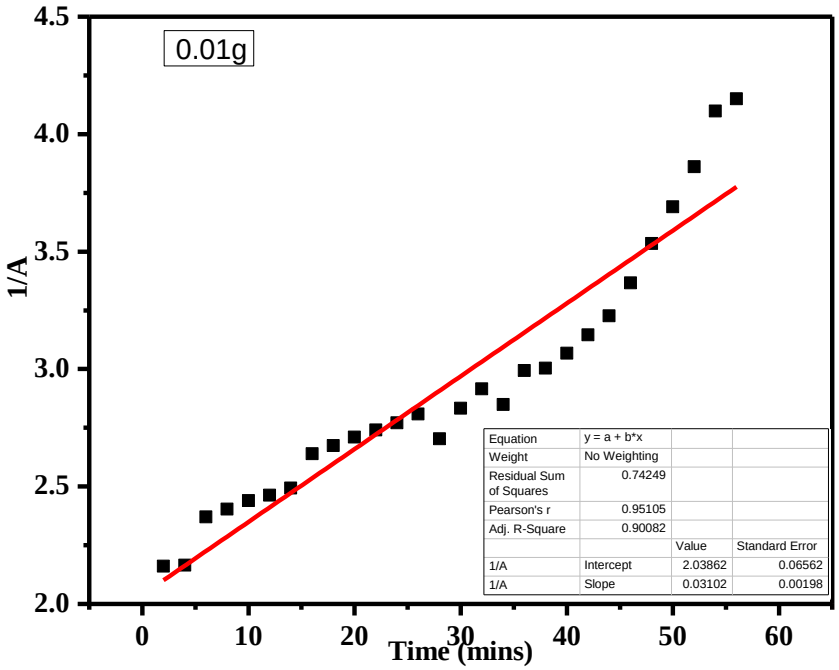

VI (E) Second–order kinetics for the degradation of Rifampicin by 10 mg CbNPs/H_2O_2

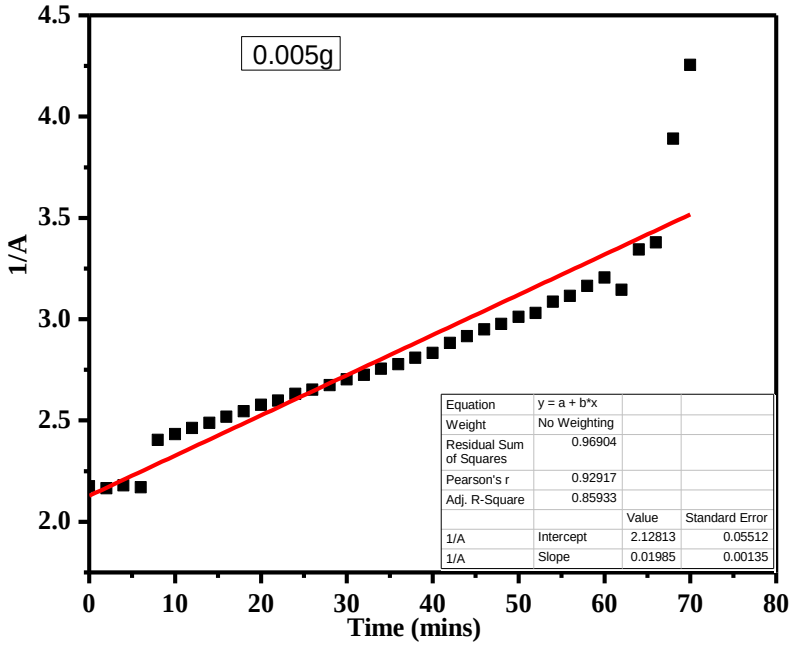

VI (F) Second–order kinetics for the degradation of Rifampicin by 5 mg CbNPs /H_2O_2

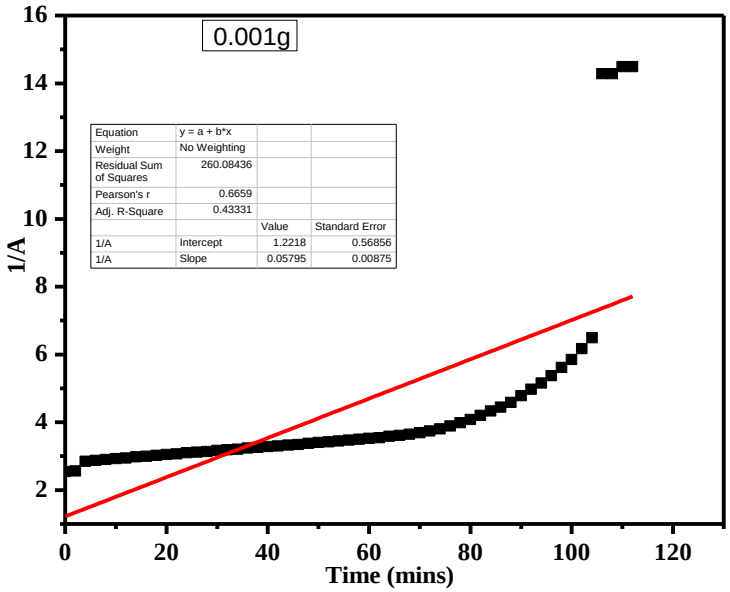

VI (G) Second–order kinetics for the degradation of Rifampicin by 1 mg CbNPs /H_2O_2

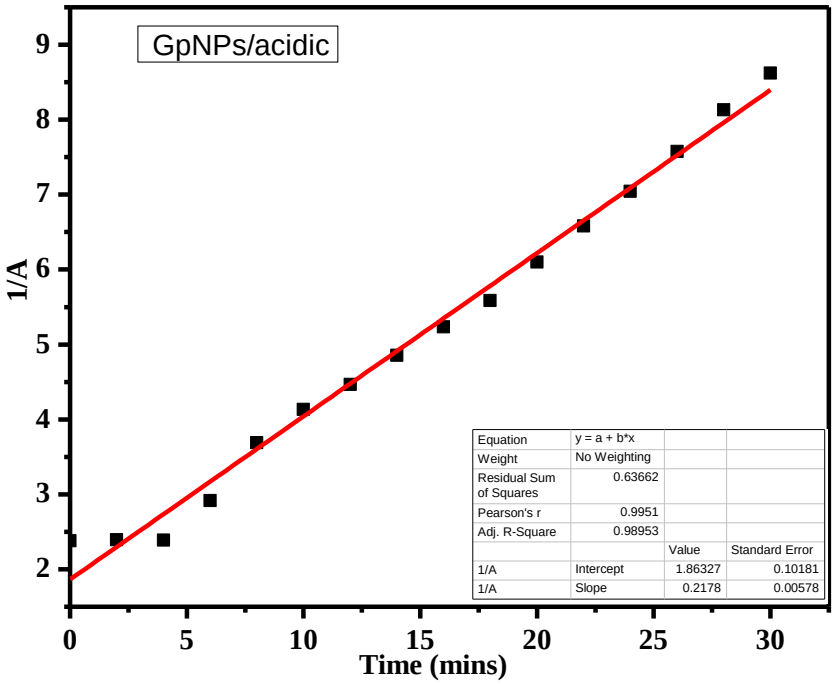

VI (H) Second–order kinetics for the degradation of Rifampicin by GpNPs/H_2O_2 at pH 12

Appendix VII: Antimicrobial Activities of nanoparticles and the Extract

VII (A) Antimicrobial activity of *G. parviflora* iron nanoparticles

Sample ID	Gram positive		Gram negative		Fungus
	S. aureus	*B. subtilis*	*E. coli*	*P. aeruginosa*	*C. albicans*
G. parviflora	11.0±1.0	12.0±2.0	9.3±0.6	8.0±1.0	10.0±2.0
1%INPs	9.3±0.6	11.0±1.0	8.3±0.6	9.7±0.6	10.0±1.0
2% INPs	8.3±1.2	11.0±2.0	7.0±0.0	8.3±1.5	9.3±1.5
4% INPs	8.0±1.0	12.0±2.0	7.3±0.6	8.0±1.0	9.7±2.0
7% INPs	8.0±0.0	11.0±1.0	7.0±0.0	9.3±0.6	8.3±0.6
10% INPs	8.3±0.5	9.7±0.6	7.3±0.6	8.7±1.2	11.7±2.0
15% INPs	9.3±1.2	11.0±1.7	7.3±0.6	8.0±0.0	8.3±0.6
0.1M $FeCl_3$	N.I	N.I	7.0	7.0	N.I
DMSO	N.I	N.I	7.0	N.I	N.I
Amp (10 mg/g)	N.I	7.0	14.0	8.0	N.I
Cp (10 mg/g)	10.0	44.0	40.0	40.0	N.I

VII (B) Antimicrobial activity of *C. bonariensis* leaf extracts iron nanoparticles

Sample ID	Gram positive		Gram negative		Fungus
	S. aureus	*B. subtilis*	*E. coli*	*P. aeruginosa*	*C. albicans*
C. bonariensis	8.7±1.5	11.0±1.0	8.7±0.6	7.7±0.6	9.0±1.0
1% INPs	8.7±0.6	10.3±1.5	8.3±0.6	7.0±0.0	8.3±0.6
2% INPs	8.3±0.6	10.3±1.5	9.0±1.0	7.7±0.6	8.7±1.5
4% INPs	8.0±0.0	10±1.0	7.0±0.0	8.3±0.6	8.7±1.2
7% INPs	8.0±0.6	10.7±1.5	7.0±0.0	7.3±0.6	7.7±1.2
10% INPs	9.0±1.0	8.7±1.5	7.3±0.6	8.7±0.6	8.0±1.0
15% INPs	9.0±1.0	11.0±1.0	9.7±0.6	7.7±0.6	7.0±0.6
0.1M $FeCl_3$	N.I	N.I	7.0	7.0	N.I
DMSO	N.I	N.I	7.0	N,I	N.I
Amp (10 mg/g)	N.I	7.0	14.0	7.0	N.I
Cp (10 mg/g)	10.0	44.0	40.0	40.0	N.I

VII (C) Antimicrobial activity of *B. pilosa* iron nanoparticles

Sample ID	Gram positive		Gram negative		Fungus
	S. aureus	*B.subtilis*	*E. coli*	*P. aeruginosa*	*C. albicans*
B. pilosa	10.0±1.7	9.3±1.5	8.0±1.7	8.3±0.6	9.7±1.5
1% INPs	10.3±0.6	11.0±1.7	8.7±0.6	8.3±0.6	8.3±0.6
2% INPs	9.3±0.6	9.8±0.6	8.3±0.5	9.0±1.0	8.7±1.5
4% INPs	9.3±1.2	12.3±1.8	7.7±0.6	9.7±1.5	7.7±0.6
7% INPs	9.0±1.0	10.0±0.6	9.4±1.8	8.7±1.2	7.0±0.0
10% INPs	8.0±0.0	9.7±1.5	8.0±1.0	9.0±1.0	13.0±1.0
15% INPs	7.0±0.6	9.7±1.5	8.3±0.6	8.3±0.6	8.3±0.6
0.1M $FeCl_3$	N.I	N.I	7.0	7.0	N.I
DMSO	N.I	N.I	7.0	N.I	N.I
Amp (10 mg/g)	N.I	7.0	14.0	7.0	N.I
Cp (10 mg/g)	10.0	44.0	40.0	40.0	N.I

Key: Amp; Ampicillin, Cp; ciprofloxacin, DMSO; dimethylsulfoxide, I nanoparticles; iron nanoparticles, N.I; no inhibition

Appendix VIII: ANOVA for Antimicrobial Activity of the nanoparticles

VIII (A) ANOVA for the Antimicrobial activity of synthesized GPNPs

Source of Variation	***SS***	***df***	***MS***	***F***	***P-value***	***F crit***
Between Groups	46.85	4.00	11.71	13.45	2.16E-06	2.69
Within Groups	26.13	30.00	0.87			
Total	72.98	34.00				

VIII (B) ANOVA for the Antimicrobial activity of CbNPs

Source of Variation	**SS**	**df**	**MS**	**F**	**P-value**	**F crit**
Between Groups	27.31	4.00	6.83	12.36	4.69E-06	2.69
Within Groups	16.57	30.00	0.55			
Total	43.88	34.00				

VIII (C) ANOVA for the Antimicrobial activity ofBpNPs

Source of Variation	**SS**	**df**	**MS**	**F**	**P-value**	**F crit**
Between Groups	14.39	4.00	3.60	2.62	0.055	2.69
Within Groups	41.18	30.00	1.37			
Total	55.56	34.00				

VIII (D) Summary of the ANOVA-Single Factor of Antimicrobial activity GPNPs

Groups	**Count**	**Sum**	**Average**	**Variance**
S. aureus	7.00	62.20	8.89	1.18
B. subtilis	7.00	77.70	11.1	0.60
E. coli	7.00	53.50	7.64	0.73
P. aeruginosa	7.00	60.00	8.57	0.48
C. albicans	7.00	67.30	9.61	1.37

VIII (E) Summary of the ANOVA-Single Factor of Antimicrobial activity of CbNPs

Groups	**Count**	**Sum**	**Average**	**Variance**
S. aureus	7.00	59.7	8.53	0.19
B. subtilis	7.00	72	10.29	0.63
E. coli	7.00	57	8.14	1.14
P. aeruginosa	7.00	54.4	7.77	0.33
C. albicans	7.00	57.4	8.20	0.48

VIII (F) Summary of the ANOVA-Single Factor of Antimicrobial activity of BpNPs

Groups	**Count**	**Sum**	**Average**	**Variance**
S. aureus	7.00	62.90	8.99	1.31
B.subtilis	7.00	71.80	10.26	1.09
E. coli	7.00	58.40	8.34	0.32
P. aeruginosa	7.00	61.30	8.76	0.27
C. albicans	7.00	62.70	8.96	3.87

Appendix IX: Plates for the Antimicrobial Activity of Iron nanoparticles

Plates for the antimicrobial activity of BpNPs (4), CbNPs (5) and GpNPs (6)

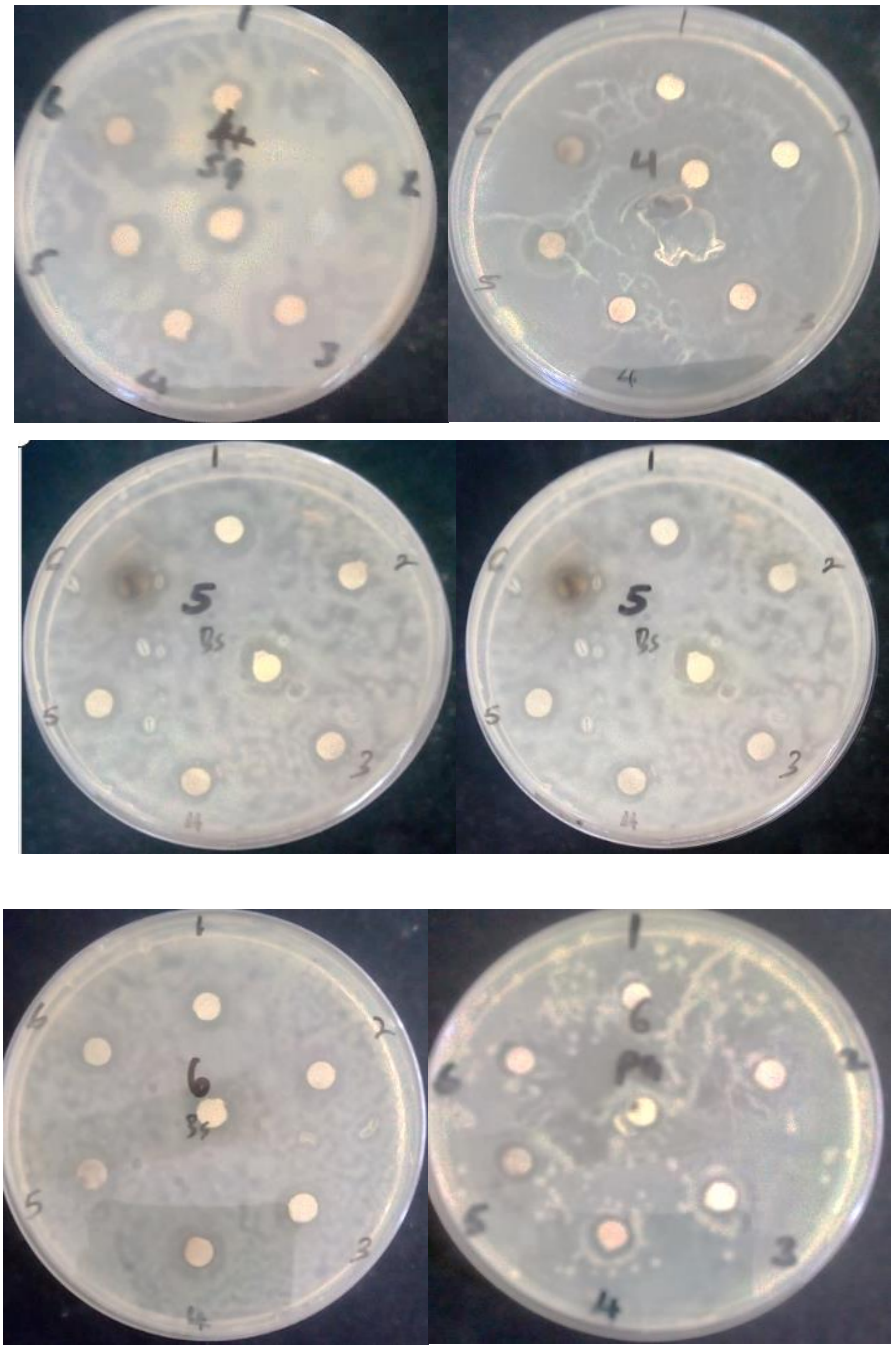

Appendix X: Standard Graphs for Total Phenol and Flavonoid Contents

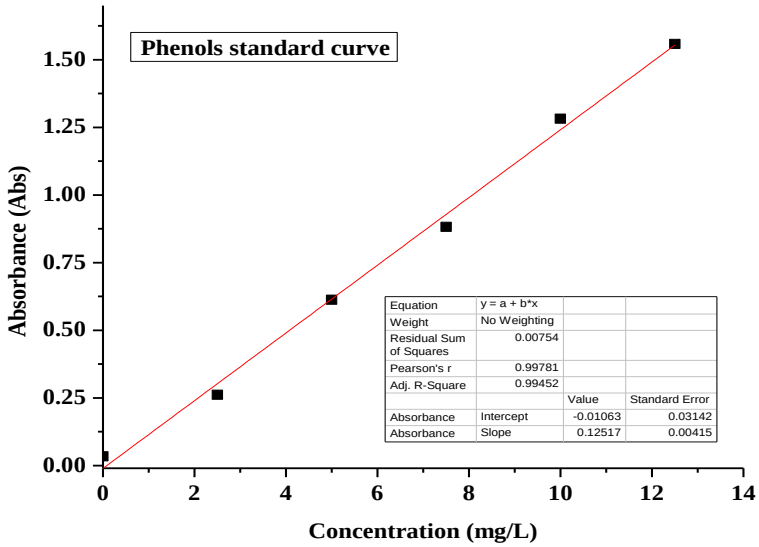

X (A) Standard curve of the Phenol Content

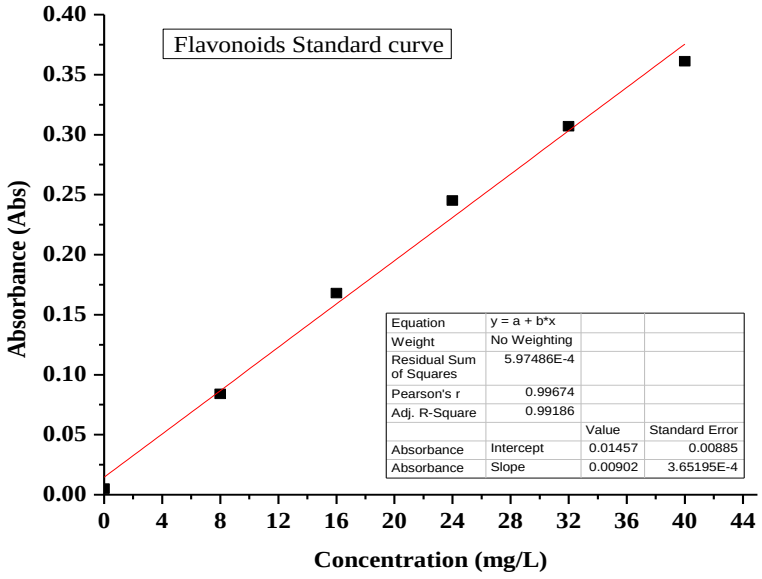

X (B) Standard curve of the Flavonoid Content

Appendix XI: Research Publication I

Research Article

Catalytic degradation of methylene blue by iron nanoparticles synthesized using *Galinsoga parviflora*, *Conyza bonariensis* and *Bidens pilosa* leaf extracts

Sammy Indire Wanakai[1] · Patrick Gachoki Kareru[1] · David Sujee Makhanu[2] · Edwin Shigwenya Madivoli[1] · Ernest Gachui Maina[1] · Augustine Otieno Nyabola[1]

Abstract

Green synthesized metallic nanoparticles are environmentally friendly, bio-compatible, and highly stable. The aim of this study was to synthesize iron nanoparticles (FeNPs) from $FeCl_3$ solution using aqueous leaf extracts of *Galinsoga parviflora* (Gp), *Conyza bonariensis* (Cb) and *Bidens pilosa* (Bp) and use them in degradation of methylene blue dye. The iron nanoparticles were characterized using UV–Vis spectrophotometer, FT-IR spectrophotometer, X-ray Fluorescence (EDXRF), X-ray diffractometer (XRD), and scanning electron microscope (SEM). Phytochemical screening for presence of secondary metabolites revealed presence of phenolics, phytosterols and flavonoids. The total phenolic and flavonoid content in *Galinsoga parviflora*, *Conyza bonariensis* and *Bidens pilosa* leaf extracts were 57.67 ± 1.27, 117.13 ± 0.03, 126.27 ± 0.013 mg Gallic Equivalent/g of Dry Weight (mg GAE/g DW) and 39.00 ± 0.56, 45.50 ± 0.59, 33.13 ± 0.81 mg Rutin Equivalent/g of Dry Weight (mg RE/g DW) respectively. The UV–Vis spectrum of $FeCl_3$ had a shoulder at 320 nm, which disappeared upon addition of *G. parviflora*, *C. bonariensis* and *B. pilosa* extracts confirming formation of iron nanoparticles. Evaluation of iron content of the synthesized nanoparticles revealed that the iron content in *G. parviflora*, *C. bonariensis* and *B. pilosa* extracts was 51, 47 and 44% respectively. XRD data revealed presence of a large amorphous coating that masked iron peaks, though 2 theta values observed have been reported to be of iron oxides. Methylene blue degradation studies revealed that CbNPs, BpNPs and GpNPs synthesized were good biocatalysts as they degraded the dye by 86, 84.3 and 92% respectively. Therefore, green synthesized iron nanoparticles is cost effective and environmentally safe in providing insight in the environmental removal of dyes.

Keywords *Bidens pilosa* · Secondary metabolites · Iron nanoparticles · Biosynthesis · Degradation

1 Introduction

Green synthesized metallic nanoparticles exhibit unique physical, thermal, chemical, and catalytic properties, [1, 2] and have found great application in health care as antiplasmodial [3], anticancer, and antimicrobial [4, 5], synthetic biology and cellular transportation [6]. The most important feature responsible for their wide range use is attributed to their large surface area to volume ratio, stability, biocompatibility and have a high surface energy as well as unique adsorption phenomenon [7-9]. In addition, metal nanoparticles are a few hundred nanometers smaller than comparable large biological molecules such as enzymes, receptors and antibodies [1]. The unique physical and chemical properties of metal nanoparticles may lead to effective interactions between itself, bacterial cell membrane and other biological entities [1, 10]. The antimicrobial activity of nanoparticles is

✉ Sammy Indire Wanakai, wanakaisammy@gmail.com | [1]Chemistry Department, Jomo Kenyatta University of Agriculture and Technology, P.O. Box 62,000-00200, Nairobi, Kenya. [2]Department of Biological & Physical Sciences, Karatina University, P.O. Box 1957-10101, Karatina, Kenya.

SN Applied Sciences (2019) 1:1148 | https://doi.org/10.1007/s42452-019-1203-z

Received: 7 May 2019 / Accepted: 30 August 2019

Published online: 6 September 2019

SN Applied Sciences
A SPRINGER NATURE journal

Appendix XII: Research Publication II

Chemistry Africa
https://doi.org/10.1007/s42250-022-00543-w

ORIGINAL ARTICLE

Kinetics of Rifampicin Antibiotic Degradation Using Green Synthesized Iron Oxide Nanoparticles

Indire Sammy Wanakai[1] · Gachoki Patrick Kareru[1] · Makhanu David Sujee[2] · Shigwenya Edwin Madivoli[1] · Maina Ernest Gachui[1] · Kinoti Pius Kairigo[1,3]

Received: 30 May 2022 / Accepted: 14 November 2022

Abstract

Purpose The presence of antibiotics in water is persistent, bioaccumulative, and harmful to humans and aquatic habitats, so we need to find ways to remove them. This study investigated the kinetics of Rifampicin antibiotic degradation using green synthesized iron oxide nanoparticles.

Methods Iron nanoparticles were synthesized using the leaves of *Galinsoga parviflora* (Gp), *Conyza bonariensis* (Cb), and *Bidens pilosa* (Bp). The effect of temperature, pH, time, and adsorbent dose on the rate of degradation of antibiotic by the nanoparticles and their chemical kinetics was evaluated by employing first and second-order kinetics. The efficiency was determined using the percentage degradation of the antibiotic.

Results The analysis of degradation was based on the absorbance at the wavelength of absorbance of the Rifampicin antibiotic (475 nm), and the nanoparticles were found to degrade the antibiotic. The antibiotic was degraded by the presence of hydrogen peroxide and the nanoparticles; at a pH of 6.5, 3, and 12, the *Conyza bonariensis* (CbNPs) nanoparticles were degraded at 78.12, 86.80, and 87.73% within 58, 20, and 30 min, *Galinsoga perviflora* nanoparticles (GpNPs) at 74.6, 86.8, and 85.9% for 52, 16, and 24 min; and *Bidens pilosa* nanoparticles (BpNPs) by 79.8, 88.7, and 81.0% for 64, 12, and 24 min, respectively. The dosage of the nanoparticles was found to play a minimal role in degradation, as 20 mg, 10 mg, 5 mg, and 1 mg degraded the antibiotic by 65.5, 48.5, 61.5, and 58.4% for 40, 60, 80, and 144 min. Temperature also effected the degradation of the antibiotic; temperatures of 25, 40, 50, and 60°C also revealed a reduced time of degradation from 30 to 5 min. Sunlight radiation also had the highest degradation time of 5 min. The degradation of rifampicin using iron oxide nanoparticles was found to be pseudo-second-order, endothermic, and dependent on the reactant dose used during the study, and variation in reaction conditions led to an increase in the percent degradation observed.

Conclusion Iron nanoparticles synthesized using Gp, Cb, and Bp could be used as a catalyst in the presence of hydrogen peroxide to degrade rifampicin in aqueous media to carbon IV oxide and water.

✉ Indire Sammy Wanakai
wanakaisammy@gmail.com

[1] Chemistry Department, Jomo Kenyatta University of Agriculture and Technology, P.O Box 62,000, Nairobi 00200, Kenya

[2] Department of Biological & Physical Sciences, School of Pure and Applied Sciences, Karatina University, P.O. Box 1957, Karatina 10101, Kenya

[3] Department of Biological and Environmental Science, University of Jyväskylä, P.O. Box 35, 40014 Jyväskylä, Finland

Published online: 23 November 2022

Appendix XIII: Research Publication III

Data in Brief 46 (2023) 108882

Contents lists available at ScienceDirect

Data in Brief

journal homepage: www.elsevier.com/locate/dib

Data Article

Advances in green nanotechnology: Data for green synthesis and characterization of iron nanoparticles synthesized using *Galinsoga parviflora*, *Conyza bonariensis* and *Bidens pilosa* leaf extracts, and their application in degradation of methylene blue dye and rifampicin antibiotic

Sammy Indire Wanakai [a,*], Patrick Gachoki Kareru [a], David Sujee Makhanu [b], Edwin Shigwenya Madivoli [a]

[a] Chemistry Department, Jomo Kenyatta University of Agriculture and Technology, P.O. Box 62, 000-00200, Nairobi, Kenya

[b] Department of Biological & Physical Sciences, Karatina University, P.O. Box 1957-10101, Karatina, Kenya

ARTICLE INFO

Article history:
Received 7 December 2022
Revised 24 December 2022
Accepted 30 December 2022
Available online 11 January 2023

Dataset link: Data for Green Synthesis of Iron Nanoparticles Using Galinsoga parviflora, Conyza bonariensis and Bidens pilosa leaf extracts, and their Application in Degradation of Organic pollutants (Original data)

ABSTRACT

This data article reports contents of the information derived from an efficient, environmentally friendly, and low-cost method of synthesis and recovery of iron nanoparticles using *Galinsoga parviflora*, *Conyza bonariensis* and *Bidens pilosa* aqueous leaf extracts as reducing, stabilizing, and capping agents, and applications of the nanoparticles in degradation of organic dyes and antibiotics. Various spectroscopic and microscopic techniques were used to collect the data. Data is displayed in the form of .raw files, graphs, images, Microsoft Excel sheets, .data point files, and PDF files, along with other formats. Data analysis and interpretation methods have also been presented. Researchers, research students, academicians, and industrialists can benefit greatly from the

Abbreviations: BpNPs, *Bidens pilosa* iron nanoparticles; CbNPs, *Conyza bonariensis* iron nanoparticles; GpNPs, *Galinsoga parviflora* iron nanoparticles.

* Corresponding author.
E-mail address: indire.sammy@students.jkuat.ac.ke (S.I. Wanakai).
Social media: @sammywanakai (S.I. Wanakai)

https://doi.org/10.1016/j.dib.2022.108882